2008

HYDRODYNAMICS OF SMALL BUBBLES IN NON-NEWTONIAN AQUEOUS SOLUTIONS OF XANTHAN GUM

Shahram Amirnia

HYDRODYNAMICS OF SMALL BUBBLES IN NON-NEWTONIAN AQUEOUS SOLUTIONS OF XANTHAN GUM

(Spine Title: Behaviour of Small Bubbles in Xanthan Gum Aqueous Solutions)

(Thesis Format: Monograph)

by

Shahram Amirnia

Graduate Program in Engineering Science
Department of Chemical and Biochemical Engineering

A thesis submitted in partial fulfillment
of the requirements for the degree of
Master of Engineering Science

Faculty of Graduate Studies
The University of Western Ontario
London, Ontario, Canada

THE UNIVERSITY OF WESTERN ONTARIO
FACULTY OF GRADUATE STUDIES

CERTIFICATE OF EXAMINATION

Supervisor

Dr. Argyrios Margaritis

Co-Supervisor

Dr. Maurice A. Bergougnou

Examiners

Dr. Dimitre Karamanev

Dr. George Nakhla

Dr. Greg. A. Kopp

The thesis by

Shahram Amirnia

entitled:

Hydrodynamics of Small Bubbles in non-Newtonian Aqueous Solutions of Xanthan Gum

is accepted in partial fulfilment of the
requirements for the degree of
Master of Engineering Science

Date

Chair of the Thesis Examination Board

Abstract

Free motion of small air bubbles in the volume range of 1-1000 mm^3 (microlitre) has been studied in a column with different concentrations of xanthan gum ranging from 520 to 2580 ppm (w/w). Two high-speed cameras were used to capture the continuous movement of bubbles up to 2000 frames per second. The sizes as well as the rise velocities of bubbles were measured by means of an image analysis software connected to the cameras. A precise method has been developed to create bubbles with high accuracy and controlled specified volumes. One of the main objectives of this work was to investigate the presence of the often-reported discontinuity in the rise velocity versus volume of air bubbles in non-Newtonian fluids. No abrupt velocity change was observed in our studies for the bubble volume range from 1 to 100 microlitre, which has been reported to occur by some other researchers. A thorough rheological study on the working concentrations of xanthan gum has been performed to interpret the observations with the existing hypothesis in literature for velocity-volume discontinuity. To be able to evaluate the results of the rise velocity for xanthan gum solutions in respect to the jump velocity, the same measurements were repeated using two different concentrations of CMC, namely, 0.4% and 0.6% w/w as a second non-Newtonian fluid.

Keywords:

Non-Newtonian fluids; rise velocity; velocity jump discontinuity; xanthan gum; air bubbles; rheology; relaxation time

Acknowledgements

I wish to express my appreciation and thanks to my thesis supervisor, Professor A. Margaritis, for defining this project and his continuous help and supervision during this study and for his financial support through NSERC Discovery Grant No.4388.

Also, I wish to greatly acknowledge Professor M.A. Bergougnou's support in this study by sharing his rich academic and industrial experience.

This work could never have done without the unfailing support of my wife, Neda, who was always there when I needed her, and the heavenly smile of my newborn daughter Melissa, who was always giving me the energy to work harder.

I am indebted to Professor G. Kopp from Civil & Environmental Engineering Department for letting me use his high-speed cameras for an unlimited time during this research. I also owe thanks to Professor J. de Bruyn from Physics Department for letting me use the rheometer in his lab, and for his help and advice. This work would not have been possible without their support.

I would like to extend my thanks and acknowledgements to the department technicians, Souheil Afara and Brian Dennis, for their assistance in the lab work for this study. Also, I would like to thank Joanna Blom for all her help in the graduate office affairs.

Dedication

I would like to dedicate this thesis to my wife, Neda, for her forever love, to my little daughter, Melissa, for her sweet smile, and to my parents, Yadegar and Vaji, for their endless support in my life.

Table of Contents

List of Tables

List of Figures

List of Appendices

Nomenclature

F	force in Equation 2.1, N
A	area in Equation 2.1, m^2
V	velocity in Equation 2.1, m/s
V	particle (or bubble) volume in equations 2.17 and 2.14, m^3
V_B	bubble volume, µl
m	consistency index, $Pa.s^n$
n	power law index
N1	first normal stress difference, Pa
m_1	curve fitting constant (Leider and Bird (1974) equation for relaxation time)
p_1	curve fitting constant (Leider and Bird (1974) equation for relaxation time)
Q	gas flow rate, m^3/s
g	acceleration due to gravity, m/s^2
t_c	time of detachment in equation 2.15, s
V_f	final volume of the bubble, m^3
V_{fb}	volume of the force balance bubble, m^3
r_f	final radius of bubble in Figure 2.8, m
C_D	drag coefficient
Re	Reynolds number
Ar	Archimedes number in equation 2.24
F_B	Buoyancy force, N
F_G	gravity force, N
F_D	total drag force, N
F_t	skin friction force, N
F_n	form drag force, N
d	projected diameter of bubble, m

U, U_t, U_B	terminal velocity of bubble, m/s
L	ring circumference in equation 3.1, cm
G'	elastic modulus, Pa
G''	viscous modulus, Pa
a, b	power-law constants in equation 4.2
d_e	bubble equivalent diameter, cm
d_h	bubble projected (horizontal) diameter, cm
$\bar{d}_h$	bubble average projected diameter, cm

Greek Symbols

τ	shear stress, Pa
μ	viscosity of fluid medium, Pa.s
$\dot{\gamma}$	shear rate, s^{-1}
μ_a	apparent viscosity, Pa.s
τ_{NN}	non-Newtonian shear stress, Pa
$\dot{\gamma}_{NN}$	non-Newtonian shear rate, s^{-1}
μ_0	zero shear viscosity, Pa.s
$\tau_{1/2}$	shear stress that viscosity drops to half of its zero shear viscosity, Pa
α	adjustable parameter in equation 2.6
λ	relaxation time in equation 4.1, s
λ_E	relaxation time in elongational flow used in equation 4.3
τ_0^B	Bingham yield stress, Pa.s
μ_B	plastic viscosity, Pa.s
ρ_l, ρ	liquid density, kg/m^3
ρ_p	particle density, kg/m^3
σ	surface tension, mN/m

1. Introduction

Interest in the study of non-Newtonian fluids has grown over the past few decades due to importance and increasing applications of these fluids in our modern daily life. Of considerable interest is the hydrodynamic study of bubbles, drops, and solid particles, particularly the rise velocity, drag coefficient, and trajectory of these particles in non-Newtonian fluids.

Non-Newtonian fluids have some unique properties that have made them distinguished from Newtonian fluids, or in other words, complicated in comparison to other fluids, and there is still need for further improvements in this area. For instance, one of the important differences between Newtonian and non-Newtonian fluid dynamics is the existence of a discontinuity in rise velocity of air bubbles only in non-Newtonian fluids. To date, there have been several disputes between researchers over the existence of this phenomenon, which is counted as one of the most striking effects associated with motion of bubbles in non-Newtonian fluid (Chhabra, 2007). However, only a part of published papers has reported any abrupt change in velocity-volume curves even using the same material and experimental condition.

One of the objectives of this study is to investigate the existence of this phenomenon in non-Newtonian fluids to be able to provide a clearer idea of existence of this interesting fact in non-Newtonian fluids.

For this purpose, xanthan gum, an exo-cellular polysaccharide produced by the microorganism *Xanthomonas campestris,* has been selected as an important non-

Newtonian shear-thinning fluid to study the behaviour of air bubbles in different aqueous solution concentrations. To our knowledge, there is only one published article in this area (Margaritis et al., 1999), which covers a narrow range of xanthan gum concentrations.

The important properties of xanthan gum, such as its ability to form high viscosity solution at low shear rates and good resistance to shear degradation have made it a material used globally in a variety of industries (food, oil drilling, etc.).

Biopolymers such as xanthan gum, or in general green polymers, are key materials to sustainable development that can maintain our modern lifestyle. In order to develop green polymers using microorganisms, it is very important to understand the complicated process of mass transfer as well as the hydrodynamics of air bubbles in bioreactors. Also, the study of the rheological properties of xanthan gum solutions provides fundamental knowledge which can be applied to the modification of different processes, especially in the food industry.

Since xanthan gum production is carried out through an aerobic fermentation, oxygen transfer from sparged air bubbles to microorganisms becomes a crucial factor in the efficiency of production by these microorganisms in the bioreactor. Bangalore and Bellmer (2006) have shown that micro-bubbles (with the volumes less than $100\,\mu l$) substitution in xanthan gum fermentation enhances the mass transfer coefficient of oxygen ($K_L a$) and increases the production yield by up to 30%, which is another evidence of the importance of the study of small bubbles' behaviour in xanthan gum solutions.

2. Literature Review and Theoretical Development

Bubbles have significant importance in most chemical and biochemical industries where any gas phase interaction inside a liquid phase exists. This interaction may take place in a chemical reactor, a bubble column, a bioreactor, a wastewater treatment vessel, or any other multiphase system. In all cases, the inter-phase mass transfer between bubbles and the surrounding phase plays an important role in the performance of the desired process.

Due to the complex nature of bubble phenomena in multi-bubble systems, a theoretical analysis of these phenomena is not possible unless one has a good knowledge of the single bubble behaviour (Dhole et al., 2007; Chhabra, 2007). Having some background information on the bubbles behaviour from formation to motion is necessary for further research in this area, and the best way to gain this knowledge is to review the previous work of this type in the literature. As well, doing some basic studies on the fluid medium surrounding the bubbles, which is called continuous phase (Clift et al., 1978), and the classification of these fluids as Newtonian and non-Newtonian fluids are essential for better understanding the bubble phenomena.

Other terminology used in this study is also similar to the ones in Clift et al. (1978). For example, bubbles are defined as fluid particles whose dispersed phase is composed of gas, and material forming the particles is expressed as dispersed phase. Solid particles are also defined as material with solid dispersed phase.

In this chapter, all the key and fundamental terms that are important to better describe the results of this work are quantitatively explained by dividing the subject into two distinct categories: fluid behaviour and bubble behaviour. Some basic information about xanthan gum, the non-Newtonian fluid used in this research, is also added at the end.

2.1 Fluid Behaviour

The classification of fluids behaviour can be either by their response to the applied pressure or according to an imposed shear stress on them (Chhabra and Richardson, 1999). Depending on the constancy of volume under pressure, these fluids can be subdivided in two groups: compressible and incompressible fluids. The second classification that we call it as an "engineering classification" is based on the response of fluids to shearing that leads to 'Newtonian' and 'non-Newtonian' fluids, which is of greater practical and engineering utility. Nonetheless, Newtonian fluid behaviour can be counted as an exception for non-Newtonian fluid behaviour that will be further discussed in the following sections.

Even after decades of research in the mechanics of fluids, there is still continuing interest in this area, especially in non-Newtonian fluids due to the importance and complexity of behaviour of these fluids. Therefore, starting with a simple definition for Newtonian fluids, the complex nature of non-Newtonian fluids behaviour will be studied in this chapter.

2.1.1 Newtonian Fluid Behaviour

Newtonian fluids are the simplest class of real fluids that include most of the low molecular weight pure liquids and gases. In a thin layer of a fluid between two big parallel plates at a distance of Δy and an area of A subjected to a force F, as shown in Figure 2.1 the created shear stress will be balanced by frictional forces in the liquid. The moving plate will result in a velocity gradient in the liquid perpendicular to the shear force. The higher the magnitude of the force over area, the bigger the velocity gradient (or shear rate) in the fluid between the plates:

$$\frac{F}{A} \propto \frac{\Delta V}{\Delta y} \tag{2.1}$$

The force on a unit area of the fluid is called shear stress (τ), and the coefficient that needs to be added to equation 2.1 is termed viscosity of the fluid medium (μ):

$$\tau = \mu \dot{\gamma} \tag{2.2}$$

where $\dot{\gamma}$ is shear rate.

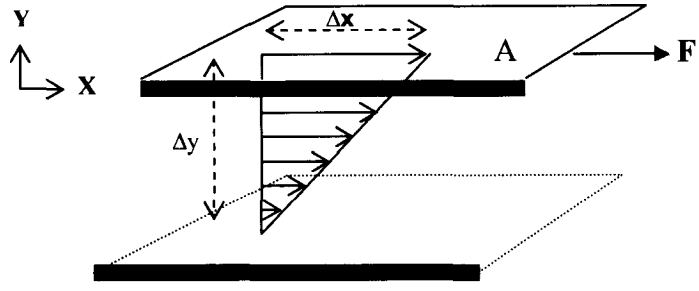

Figure 2.1 Schematic diagram for simple shear flow.

2.1.2 Non-Newtonian Fluid Behaviour

In general, non-Newtonian fluids can be classified in three sub-groups: time-independent, time-dependent, and viscoelastic. This classification is also arbitrary because in the real world, some material can exhibit a combination of these features. However, considering the dominant non-Newtonian characteristics, the classification illustrated in Figure 2.2 is widely accepted in the literature (Chhabra and Richardson, 1999).

Typical examples of material with non-Newtonian behaviour are polymer melts such as polypropylene melt in extrusion, natural polymers like xanthan gum, most of food products like mayonnaise, jellies, yoghurt, biological fluids like blood, multiphase mixtures like emulsions, polymer solutions, and so many other products and material that we encounter in different industries and even in our daily life (Chhabra, 1993).

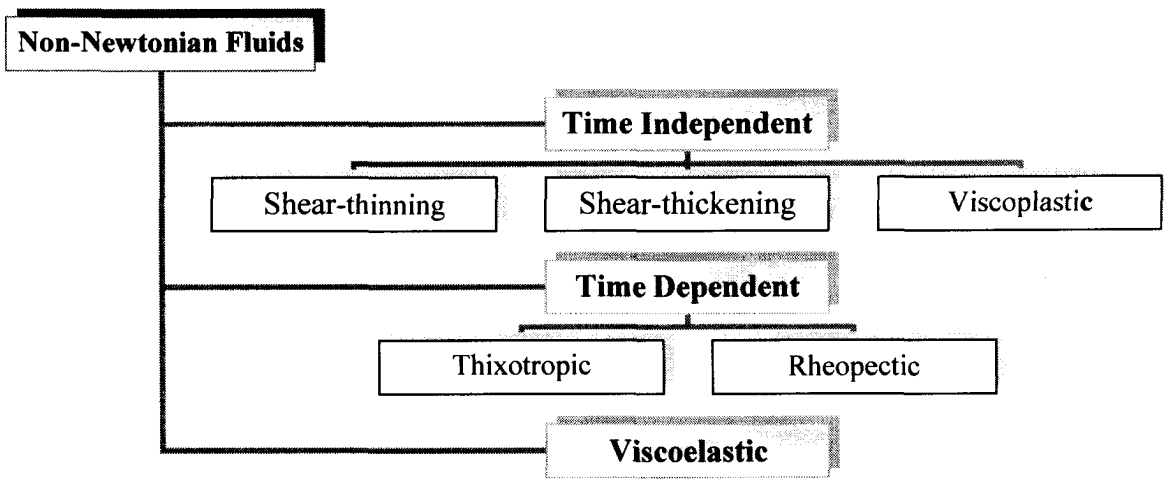

Figure 2.2 Classification of non-Newtonian fluids.

2.1.2.1 Time-Independent Fluid Behaviour

Time-independent fluids are non-Newtonian fluids, behaviour of which is independent of the duration of shearing. In non-Newtonian time-independent fluids, viscosity varies for different values of shear rate. However, shear stress and shear rates are related to each other at every single point on the flow curve by defining an apparent viscosity (μ_a):

$$\tau_{NN} = \mu_a \dot{\gamma}_{NN} \tag{2.3}$$

where τ_{NN} is shear stress, and $\dot{\gamma}_{NN}$ is shear rate, and the subscript NN refers to non-Newtonian fluids.

As it is shown in Figure 2.2, these types of fluids can be divided into three distinct subgroups namely, shear-thinning, shear-thickening, and viscoplastic fluids.

2.1.2.1.1 Shear-thinning and Shear-thickening Fluid behaviour

Shear-thinning or pseudoplastic fluid behaviour is the most common encountered fluid behavior in non-Newtonian fluids (Chhabra and Richardson, 1999), in which, the apparent viscosity decreases with increasing shear rate. This behaviour is the reverse for shear-thickening (dilatant) fluids. Most shear-thinning fluids exhibit a Newtonian fluid behaviour at very high and very low shear rates. Figure 2.3 is a schematic representation for shear-thinning behaviour in a linear flow curve showing that the shear stress-shear rate plot will pass through the origin of the coordinates at low and high limits of shear rate.

2.1.2.1.1.1 A Common Mathematical Model for Shear-thinning and Shear-thickening Fluid Behaviour

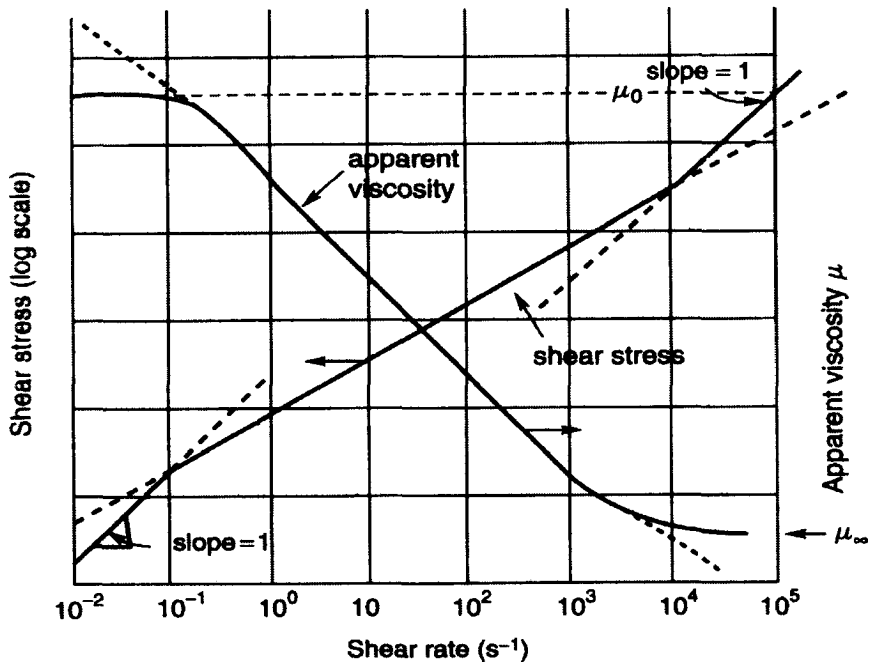

Figure 2.3 Zero shear viscosity and infinite shear viscosity for shear-thinning fluid behaviour (adapted from Chhabra and Richardson (1999) with permission (see Appendix G)).

The apparent viscosity (μ_a) for both shear-thinning and shear-thickening fluids can be approximated by using the power law model which is the simplest and most commonly used mathematical equation for theses fluids:

$$\tau_{NN} = m\dot{\gamma}_{NN}^{\ n} \tag{2.4}$$

Rearranging equations 2.3 and 2.4 gives:

$$\mu_a = m\dot{\gamma}_{NN}^{\ n-1} \tag{2.5}$$

in which, m is named consistency index and n is called power law index.

It is obvious that for Newtonian fluids ($n = 1$) the value of the apparent viscosity would be equal to the consistency index (m). Same thing happens for a shear rate of unity in equation 2.5. We can use the value of m as a single-point comparison for the viscosity of non-Newtonian fluids.

The flow index coefficient (n) is useful in comparing various types of non-Newtonian fluids with each other in terms of their degree of shear-thinning or shear-thickening. For example, in shear-thinning fluids that have a flow index below one ($n < 1$), the lower the value of n, the higher the shear-thinning behaviour. The stronger shear-thickening behaviour is also for higher values of the flow index over one ($n > 1$). All types of non-Newtonian time-independent fluids are illustrated in a single flow curve in Figure 2.4.

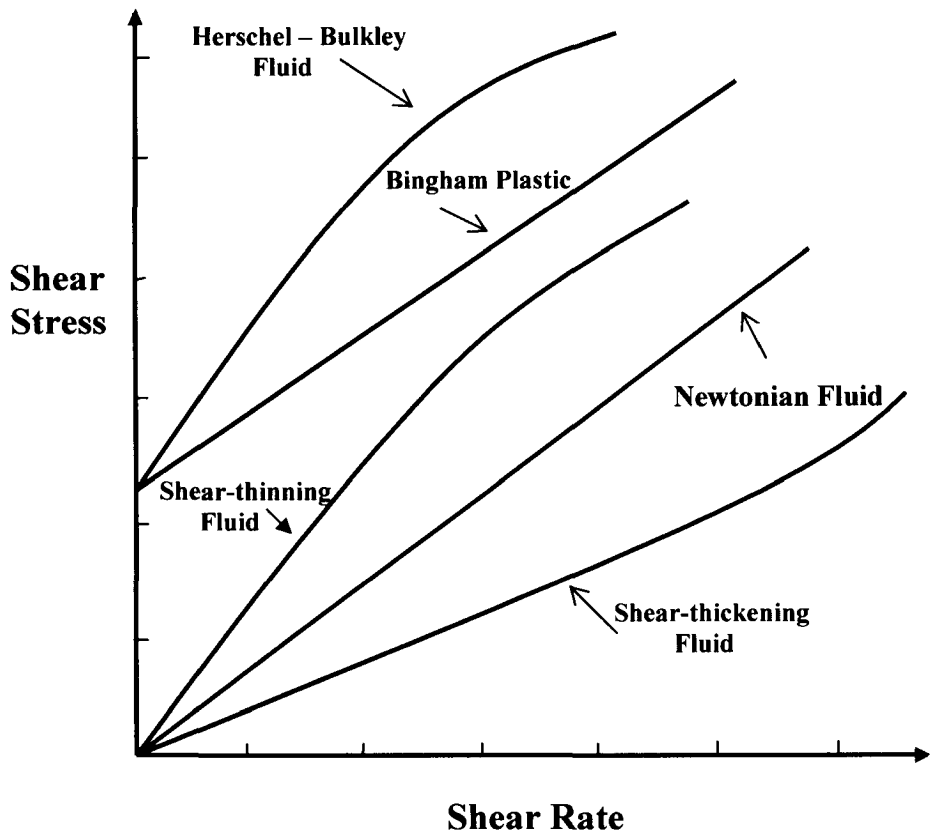

Figure 2.4 Schematic diagram for types of non-Newtonian time-independent fluids.

2.1.2.1.1.2 Mathematical Models for Shear-thinning Fluid Behaviour

As mentioned earlier, the power law model is the simplest approximation for pseudoplastic and dilatant fluid behaviours. However, this model is only applicable in a narrow range of shear rates, and the fitted values of m and n will vary depending on the selected range of shear rate.

For instance, in Figure 2.5 that demonstrates the flow curve for an aqueous polymer solution on a log-log scale, the power law model cannot fit over the entire rage of data for this polymer solution because the plot is not linear; but, it can be divided into two parts, and each part can be represented by a power law model.

This is one of the shortcomings of using power law model in comparison to other viscosity models for shear-thinning fluids. We have taken into account this point in our calculations by substituting the power law model with other suitable models to get more accurate results.

2.1.2.1.1.2.1 Ellis Viscosity Model

The Ellis model is a three-constant equation, in which, the apparent viscosity is given by:

$$\mu = \frac{\mu_0}{1 + (\tau / \tau_{1/2})^{\alpha - 1}} \tag{2.6}$$

where μ_0 is the zero shear viscosity, $\tau_{1/2}$ is the value of shear stress that viscosity has dropped to half of its zero shear viscosity, and α (>1) is an adjustable parameter. This

model is suitable when the deviation from the power law model at low shear rates is significant.

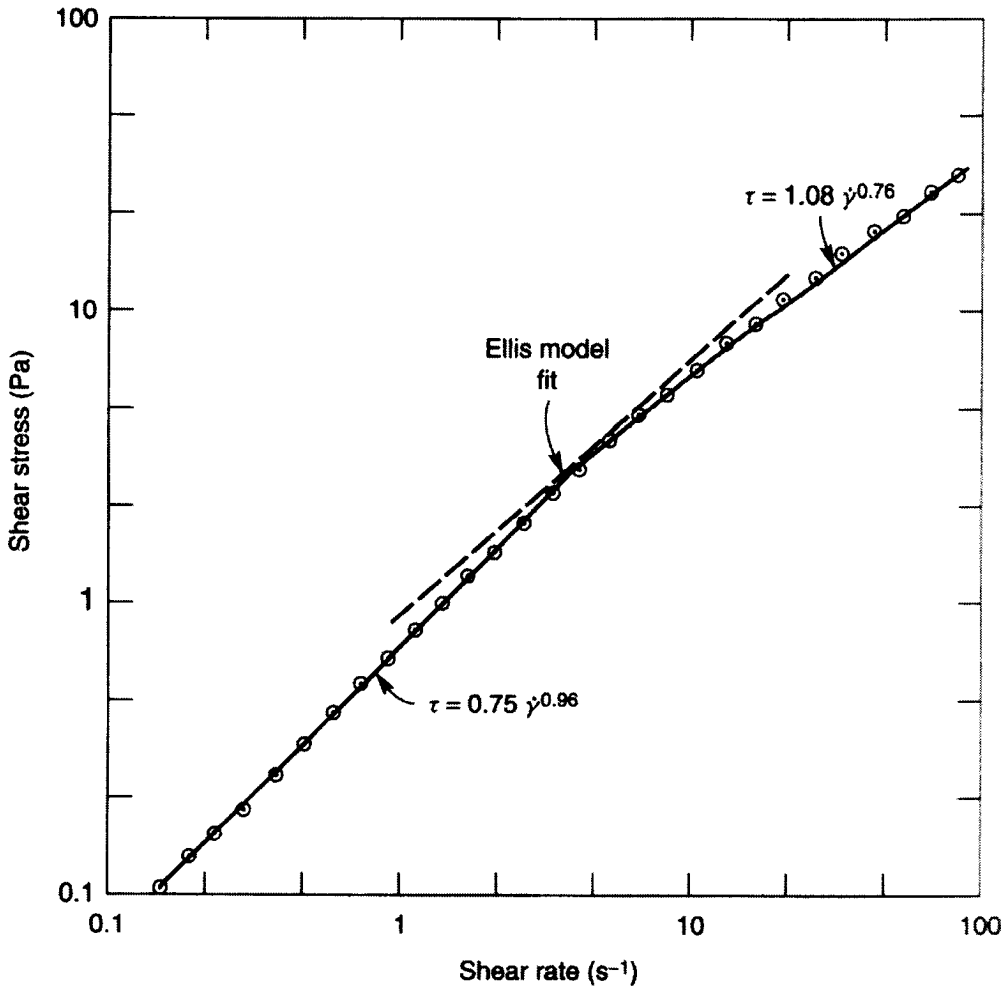

Figure 2.5 Restriction in using power law model over the whole range of shear rates in the flow curve data for a polymer solution. The Ellis model can fit better over the entire data. (cited from Chhabra and Richardson (1999) with permission (see Appendix G)).

2.1.2.1.1.2.2 Carreau Viscosity Model

The Carreau model is a four-constant equation covering a wide range of shear rates taking into account the zero shear viscosity (μ_0) and the infinite viscosity (μ_∞):

$$\frac{\mu-\mu_\infty}{\mu_0-\mu_\infty}=(1+(\lambda\dot{\gamma})^2)^{n-1/2} \tag{2.7}$$

In this equation, n (<1) and λ are two curve-fitting parameters. Attention must be taken that n is not equal to the flow index in the power law model. Also, λ is a time parameter named as the Carreau model relaxation time (Bird et al., 1987).

2.1.2.1.1.2.3 Cross Viscosity Model

This model also gives the Newtonian regions both at low and high shear rates. It is proposed by Cross (1965):

$$\frac{\mu-\mu_\infty}{\mu_0-\mu_\infty}=\frac{1}{1+(K\dot{\gamma})^{1-n}} \tag{2.8}$$

in which, K is a time constant and 'n' is a curve-fitting parameter.

2.1.2.1.2 Viscoplastic Fluid Behaviour

The other type of time-independent fluids that is termed viscoplastic fluid behaviour is shown in Figure 2.4, for which, a yield stress (τ_o) is needed for the fluid to flow. Typical examples of this type of fluids are toothpaste, ketchup, or shaving foam that all need an initial yield stress to move. A viscoplastic fluid with a linear flow curve is called Bingham plastic, and is expressed by the following equation:

$$\tau=\tau_0^B+\mu_B(\dot{\gamma}) \qquad \text{for } |\tau|>|\tau_0^B| \tag{2.9a}$$

$$\dot{\gamma}=0 \qquad \text{for } |\tau|<|\tau_0^B| \tag{2.9b}$$

where τ_0^B is the Bingham yield stress and μ_B is called plastic viscosity.

A viscoplastic fluid possessing a yield stress and a non-linear flow curve is named as Herschel – Bulkley fluid. The Casson model is another mathematical model with two constants to describe the viscoplastic behaviour of a material. Details about this model and comparisons between different models for viscoplastic fluids can be found in Bird et al. (1983).

2.1.2.2 Time dependent Fluid Behaviour

In practice, the viscosity of fluids may depend not only on shear rates, but also on the time that the fluid has been subjected to shearing. These types of non-Newtonian fluids showing a behaviour that varies in time are called time-dependant fluids. Time-dependant fluids can be divided into two sub-groups based on changes in their apparent viscosity with time. If in a fluid the apparent viscosity decreases with increasing the time of shearing, it is called as thixotropic fluid, and if the reverse happens the material is called rheopectic.

To distinguish time-dependent fluid behaviour from time-independent one, the behaviour of these materials can be evaluated by increasing and then decreasing the value of the shear rate. If the resulting flow curves do not match in both directions for the shear rates, the fluid is time-dependant (Figure 2.6).

For a time-independent fluid, shear stress and shear rate are connected by apparent viscosity values for each point no matter what the shearing time is.

2.1.2.3 Viscoelastic Fluid Behaviour

A viscoelastic substance displays fluid-like and solid-like characteristics at the same time. In other words, fluids showing both elastic and viscous behaviour at the same time are called viscoelastic fluids.

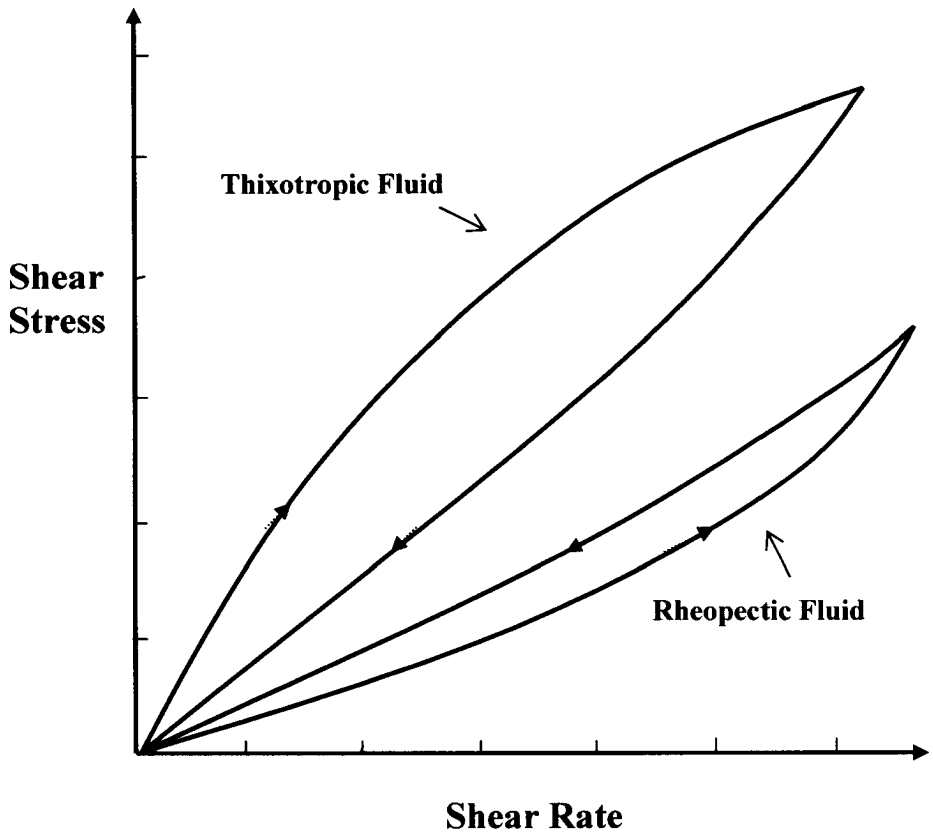

Figure 2.6 Schematic diagram for time-dependant fluid behaviour.

To describe mathematically the viscoelastic behaviour, a combination of elastic and viscous properties has been frequently considered by researchers through spring and dashpot elements (Chhabra and Richardson, 1999; Sperling, 2006).

A dashpot is defined as a container in which the pressure drop at its outlet is proportional to the flow rate due to restriction of flow. It contains a viscous fluid, in which, a plunger moves through in a rate proportional to the stress. A spring represents the elastic component that stretches instantly with a full recovery when the stress is removed.

The spring and dashpot can be put together in different arrangements to develop mathematical models for the behaviour of viscoelastic fluids (Maxwell and Kelvin models). As is illustrated in Figure 2.7, the spring and dashpot are in series for the Maxwell element and parallel in the Kelvin Model. The Maxwell model shows viscous flow behaviour for the deformation in time, and it has a dominant fluid-like response. The Kelvin model shows more solid-like behaviour to deformation in time (more information with new viscoelastic fluid models in Bird et al. (1987)).

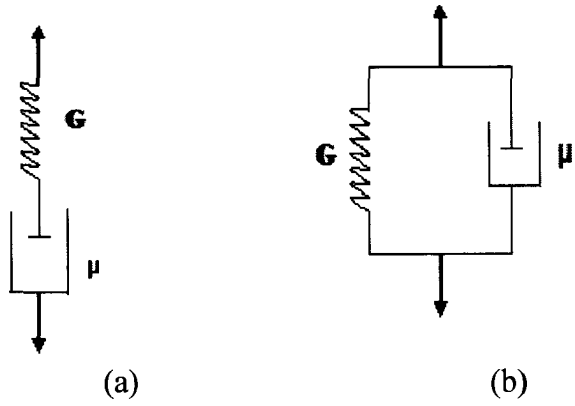

Figure 2.7 Schematic diagram of Maxwell model (a) and Kelvin (Voigt) model (b) re-plotted from Chhabra and Richardson (1999) with permission (see Appendix G).

2.1.2.3.1 Relaxation Time

Generally, relaxation time is a criterion to quantify the viscoelastic behaviour of a fluid. There are different definitions for relaxation time in the literature. In the Maxwell model, the relaxation time is equal to viscosity (μ) over G modulus ($\lambda = \mu / G$). On the molecular scale, the relaxation time of a polymer can be defined as the time required for a certain proportion of the polymer chains to respond to the exerted stresses and relax (Sperling, 2006). Stelter et al. (2002) have defined the relaxation time as a time scale of the stretching of polymer molecules in an elongational flow indicating that the relaxation time measured by the stretching device corresponds to the longest relaxation time for the relaxation time spectra obtained by the rotational viscometer. Besides, Milas et al. (1990) has considered the longest relaxation time as the reciprocal value of a critical shear rate ($\dot{\gamma}$) where the transition from Newtonian behaviour to non-Newtonian behaviour takes place.

Another definition for relaxation time (λ) is the so-called Maxwellian relaxation time that is given by combining the shear stress (τ) and the first normal stress difference (N1) as:

$$\lambda = \frac{N1}{2\tau\dot{\gamma}} \tag{2.10}$$

An alternative definition for λ has also offered by Leider and Bird (1974) assuming that both τ and N1 can be approximated by power-law functions:

$$\lambda = \left(\frac{m_1}{m}\right)^{1/(p_1 - n)} \tag{2.11}$$

in which , the curve fitting constants (m_1, p_1, n, m) can be found by the following equations:

$$N1 = m_1(\dot{\gamma})^{p_1} \tag{2.12}$$

$$\tau = m\dot{\gamma}^n \tag{2.13}$$

A dimensionless number representing the degree of viscoelasticity is called Deborah number defined as fluid response time over process characteristic time. The greater the value of Deborah number, the higher the elasticity of the material (Chhabra and Richardson 1999).

In the present study, relaxation time has been defined based on the longest time that viscoelastic behaviour appears in a solution, and it has been obtained by the frequency sweep test which will be discussed in the results chapter (chapter 4).

2.2 Bubble Behaviour

The study of bubble behaviour is of considerable importance for many industrial operations. Bubble rise velocity, bubble shape and trajectory, bubbles interactions and drag coefficient are some of the important parameters for any multi-bubble system. Bubbles motion has been studied for several decades by many researchers, however; due to the inherent complicated nature of bubble behaviour, there is still need for further investigation in this area.

Recently, a comprehensive review has been presented by Kulkarni and Joshi (2005) on bubble formation and bubble rise velocity in two-phase (gas-liquid) systems, which covers most of the important papers in the bubble phenomena.

2.2.1 Bubble Formation

We have been inspired by the concept of bubble formation at a submerged orifice in a quiescent liquid in making known volume bubbles for some of the solutions that we have worked on in this research. This section contains some of fundamental models for bubble formation followed by some photographic evidences in the coming chapters.

In bubble columns, bubbles are usually formed by forcing (flowing) the dispersed phase (gas phase) inside the liquid through orifices or porous spargers. There has been a lot of interest in modeling and describing bubble formation because of the fundamental importance of this phenomenon. Clift et al. (1978) summarized and compared some proposed models up to that time for bubble formation in liquids. According to Clift and co-workers' study, bubble growth begins in the orifice and ends when the rear of the bubble passes the orifice, or when the buoyancy force overcomes other forces exerted on the bubble within a simple one-stage model.

The main interest in all models for bubble formation is the size or volume of the produced bubble in an orifice in a given gas-liquid system. Among all models, only two of them have been widely accepted by researchers in the literature, which are Davidson-Schuler model and Kumar-Kuloor model (Chhabra and De Kee, 1992). Different regimes of bubble formation have been identified by the Davidson-Schuler model in terms of physical properties of the liquid phase and the flow rate of the gas phase.

According to Davidson-Schuler model, at very low gas flow rates, the drag force can be interpreted by Stokes law leading to the following equation for the produced bubble volume:

$$V = (\frac{4\pi}{3})^{1/4} (\frac{15\mu Q}{2\rho_l g})^{3/4} \tag{2.14}$$

where Q is the gas flow rate.

When the gas flow is sufficiently high, the contribution of the internal forces becomes important for the bubble volume. In the case of high viscosity of the liquid phase, the buoyancy forces will be in balance with the drag force of the liquid. In extremely low gas flow rates, the surface tension appears to be important. Otherwise, surface tension effects are negligible in all models.

Figure 2.8 illustrates the two-stage sequence proposed by Kumar-Kuloor for the bubble formation. The first stage in this model is the growth or expansion stage, which is the difference point between this model and Davidson-Schuler model considering that the bubble stays at the tip of the orifice during the expansion stage.

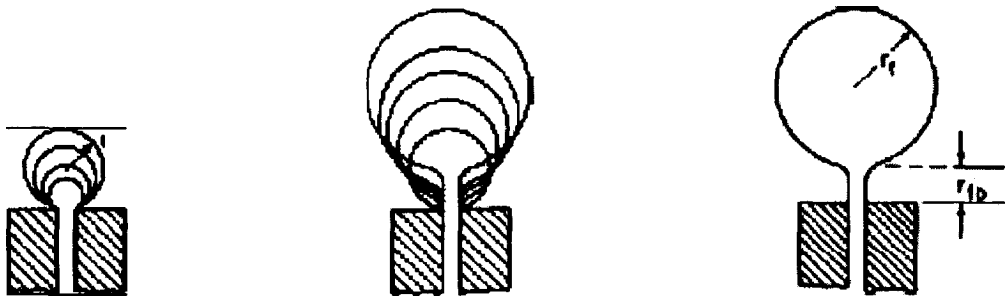

Figure 2.8 Two-stage sequence for bubble formation proposed by Kumar-Kuloor adapted from Chhabra and De Kee (1992) by permission (see Appendix G for the permission).

The second stage is called detachment stage, in which, the bubble moves away from the orifice while keeping expansion through a neck or tongue of gas that is still attached to the orifice. This lift-off from the edge of the orifice happens when there is a net upward force acting on the bubble.

During the first stage when the bubble is expanding, the net force acting on the bubble is zero and the bubble is not moving because the upward force of buoyancy is counterbalanced by the downward forces (drag, surface tension and internal forces).

Kumar and Kuloor have assumed that the second stage of bubble formation occurs when the bubble has travelled a distance equal to its radius at the end of the first stage added by the volume of the air passed the orifice in the time of detachment (t_c):

$$V_f = V_{fb} + Qt_c \tag{2.15}$$

Therefore, knowing the bubble volume at the end of the first stage, one can find the final produced bubble size and volume. This is done by writing a force balance on the bubble, which yields the following equation (Kumar-Kuloor, 1970):

$$V_{fb} = 0.0474\frac{Q^2 V_{fb}^{-2/3}}{g} + 2.42\left(\frac{\mu}{\rho_l}\right)V_{fb}^{-1/3}\left(\frac{Q}{g}\right) \tag{2.16}$$

Variety of equations and mechanisms has been developed by researchers in different gas and liquid conditions, which is out of the scope of this study.

2.2.2 Shape of Bubbles

Bubble shape in Newtonian and non-Newtonian fluids is influenced by different forces exerted on them including gravity, buoyancy, surface tension, viscous forces, and internal forces. Generally, very small bubbles have spherical shapes and larger ones

tend to have ellipsoidal or spherical cap shapes. Clift et al., (1978) has offered a "shape map" based on dimensionless numbers (Reynolds Number vs. Eotvos Number) showing the boundaries between the three principal shape regimes in Newtonian fluids.

Several researchers have studied the shape of bubbles in non-Newtonian fluids and have observed the same shape transitions from spherical to ellipsoidal, and finally to spherical caps (De Kee and Chhabra, 1988; De Kee et al., 1990; Dewsbury et al., 1999).

One of the main differences between the shape of bubbles in Newtonian and non-Newtonian fluids is existence of a tail or cusp on the back-end of bubbles due to negative wake (Hassager, 1979). Cusped-end bubbles have been observed by many other researchers (De Kee et al., 1990; Liu et al., 1995; Rodrigue and De Kee, 1999; Belmonte, 2000; Soto et al., 2006; etc.).

2.2.3 Bubble Coalescence and Break-up

In bubble columns, bubbles are constantly interacting with each other, which may result in coalescence, break-up, or separation along with their upward motion in the liquid media. Bubbles coalescence and break-up rates control the bubble size distribution, and consequently, the interfacial area for gas-liquid mass transfer, which is one of the fundamental factors in the performance of gas-liquid systems. It is not possible to distinguish an individual coalescence and breakage event in a bubble column in which swarms of bubbles are in continuous and even simultaneous breakage and coalescence. For that reason, most of the models offered in the literature

are based on a random binary collision probability and a collision efficiency factor to describe these phenomena and to broaden them to a multi-bubble system.

Bubbles coalescence and breakage are affected by a number of parameters including the size and shape of bubbles, physical properties of the phases; e.g. density, viscosity and surface tension, the presence of surface-active agents, flow patterns and other process variables (Mouza, 2005).

Tavlaridis et al (1970) reported a theory presenting a mechanism for coalescence of two touching bubbles and predicted that the liquid film between the bubbles thins in the collision event until the further thinning of this film leads to the rupture and coalescence of the bubbles. The rate of film drainage and thinning determines the coalescence time and predicts whether coalescence will be achieved. The criterion to determine coalescence efficiency is that the contact time of the coalescing bubbles should be bigger than the time needed to drain the liquid film between them.

This mechanism for bubble coalescence is generally accepted by most of the researchers in the literature and has been used as a basic theory for all investigations in this field (Chhabra and De Kee., 1992; Prince et al., 1990; Lehr et al., 2002).

In three-phase fluidized beds, the large bubbles entering the bed break into small bubbles as they flow upward to reach a stable bubble size when there is an equilibrium between the rate of bubble break-up and coalescence. This can be evaluated by measuring bubble sizes at different distances from the first point they enter the bed.

Tse (2002) investigated small bubble formation via a coalescence-dependent break-up mechanism. He used a photographic method in his experiments and realized that a significant number of very small bubbles are generated in coalescence-mediated

break-up of bubbles due to the formation of an annular wave in the liquid film rapture in the coalescence event.

2.2.4 Small Bubbles (Microbubbles)

Small gas bubbles are important to increase the interfacial area of bubbles and eventually to increase the mass transfer between phases. Small bubbles are also important for different environmental processes, particularly for water and wastewater treatment (Burns et al, 1997). Controlling the size of bubbles in these processes is crucial due to the increased bubble density in a constant flow rate as well as the enhanced surface area to volume ratio.

In some chemical and biochemical processes, making small size bubbles and dispersion of the gaseous phase in liquid phase is done by means of a mixer in a stirred vessel, which leads to a mechanistic breakage of bubbles.

It is clear that uniform dispersion and narrow bubble size distribution is desirable in multi-bubble systems, particularly in bioreactors to enhance the mass transfer coefficient ($K_L a$).

2.2.5 Bubble Jump Velocity

The existence of a jump in velocity-volume curves for small bubbles in non-Newtonian fluids is an interesting phenomenon, and is the subject of a dispute between researchers in the literature. Quite a few of researchers have encountered this phenomenon in some non-Newtonian aqueous solutions (Figure 2.9).

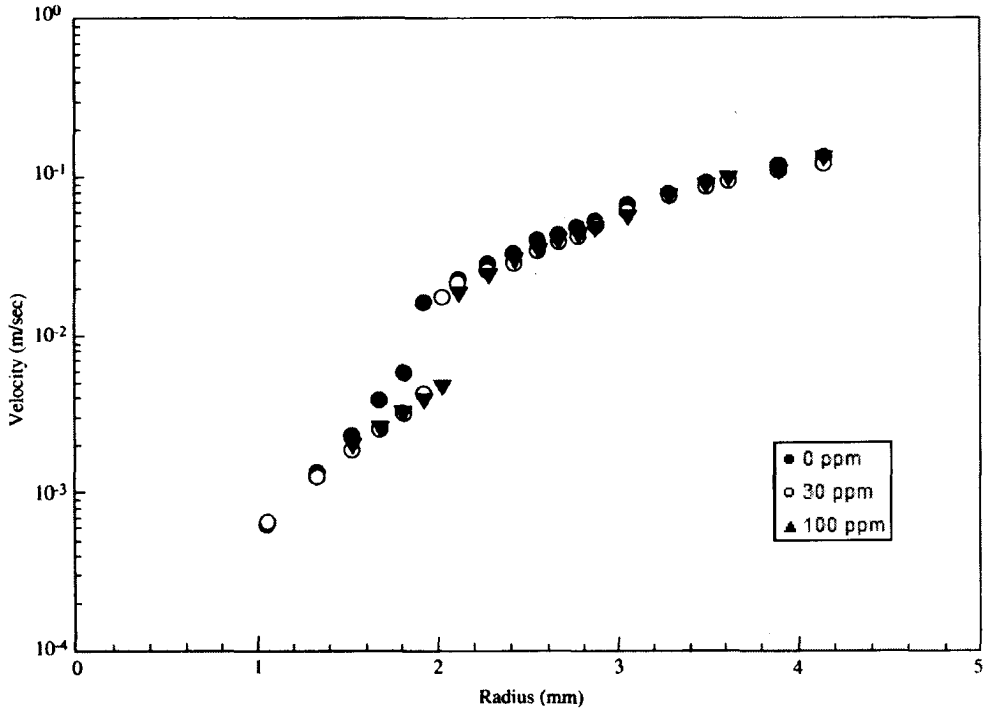

Figure 2.9 Bubble rise velocity versus bubble radius for 0.25% polyacrylamide solution at three concentrations of SDS adapted from De Kee and Chhabra, (2002) with permission (See Appendix G).

However, some of them have not reported any abrupt change in the rise velocity of bubbles in non-Newtonian fluids, and few of them have denied clearly the existence of such phenomenon. Furthermore, among the authors that have reported the discontinuity in the rise velocity of bubbles, there is still disagreement with regard to the origin of this phenomenon.

The first observation of this phenomenon in the rise velocity of bubbles was reported by Astarita and Apuzzo (1965) and Leal et al. (1971). Then, it was extensively

explained by Rodrigue et al. (1999), Chhabra and De Kee (2002), and Herrera-Velarde et al. (2003) using photographic techniques.

More recently, Chhabra (2007) has called the discontinuity in rise velocity of bubbles one of the most striking and fascinating effects associated with bubble motion in non-Newtonian fluids. Although, Chhabra and De Kee (1992) has put emphasis on no-jump in velocity-volume curves for the bubbles in non-Newtonian fluids based on their observations.

Thus far, to our knowledge, nobody has confirmed such a sudden transition in the rise velocity of bubbles in the rheologically complex solutions of xanthan gum. Therefore, it is important to investigate this phenomenon in xanthan gum solutions to be able to provide a clearer idea of the existence of this interesting fact in non-Newtonian fluids, which can be counted as one of the noticeable differences between Newtonian and non-Newtonian fluid dynamics.

There are a couple of hypotheses in the open literature to describe the jump discontinuity. In this study, the results obtained for the rise velocity of bubbles in xanthan gum and CMC solutions have been used to evaluate the consistency of these theories with the experimental data:

- Astarita and Appuzo (1965): Abrupt change in the velocity-volume curve is due to a transition from Stokes to Hadamard regimes because of viscoelsticity.
- Rodrigue and De Kee (1999): Elastic and surface tension gradient forces must be present simultaneously for a jump to occur.

- Herrera et. al. (2003): Appearance of the negative wake behind the rising bubble which is only for bubble sizes above the critical volume is the main reason for the velocity jump.
- Pilz and Brenn (2007): Relaxation of stresses in elongational flow plays an important role in the physics of the jump.

The recent works by Pilz and Brenn (2007), and Herrera et al. (2003) confirm that the jump can happen even without the presence of surfactants. Our focus in this study is to compare the experimental results with some of the mentioned theories using the rheological measurements for xanthan gum and CMC solutions.

Some of the major works and comments on the jump velocity of bubbles with a brief description on the material used and the conclusions made have been summarized in Table 2.1.

2.2.6 Bubble Drag coefficient

It had long been established that three types of forces are applying on a solid particle or gas liquid through a fluid: gravity, buoyancy, and drag. For bubbles, the gravity force (F_G) is very small because of the low density of gases:

$$F_G = \rho_P g V \tag{2.17}$$

in which, ρ_P = particle density (kg/m^3); g = acceleration due to gravity (m/s^2); V = particle volume (m^3).

Table 2.1 Summary of major investigations on the velocity discontinuity of the bubbles in non-Newtonian fluids.

Investigator	Test Fluid and details	Velocity-Volume Discontinuity Observation	Remarks
Astarita and Apuzzo (1965)	Aqueous solutions of Carbopol, CMC, ET497, and J-100 (a commercial additive)	Yes. (For ET 497 and J-100 solutions that are highly elastic). No abrupt change in velocity of bubbles in purely viscous solutions of carbopol and slightly elastic solutions of CMC.	Jump velocity is due to a transition in the boundary condition from no-slip for small bubbles in the Stokes regime to free surface conditions for larger bubbles in the Hadamand-Ryligynski regime.
Calderbank et al. (1970)	Carbon dioxide bubbles in aqueous Polyox	Yes. (Abrupt increase in velocity observed by a factor of 4 at a critical bubble size d_e = 0.27 cm).	The bubble rear undergoes a shape change at the critical bubble volume.
Leal et al. (1971)	Glass spheres and air bubbles in polyacrylamide solutions	Yes. (Velocity jump observed in the gas bubble, but no velocity discontinuity for the glass spheres).	Evidence for the hypothesis of Astarita & Apuzzo (1965).
Liu et al. (1995)	Aqueous solutions of Polyox	Yes. (A two-dimensional cusped tail with a broad edge in one view appears around the critical capillary number ($Ca = U\mu_0 / \sigma$) when the jump occurs).	The jump in the velocity is due to the reduction in the drag caused by the appearance of a cusp tail in the bubbles.
De Kee et al. (1986)	CMC and PAA solutions	No. (No velocity discontinuity observed).	Similar viscosity curves for CMC and PAA solutions in this work.
De Kee and Chhabra (1988)	Air, nitrogen, and carbon dioxide bubbles in CMC, PAA (Separan AP30), PAA with surfactant (sorbitan monolaurate)	No. (No discontinuity observed).	Shape of the bubbles did not depend on the type of gas.

Table 2.1 (Cont'd)			
Rodrigue et al. (1996)	CMC, Gellan gum, Polyethylene oxide (PEO), PAA in presence of surfactant (SDS)	Yes. (Jump observed for PAA solutions).	Surfactants and elastic forces presence is necessary for modifying the surface and generating a sudden jump in the bubble rise velocity.
De Kee et al. (2002)	Mathematical analysis for the free-surface problem	Yes. (Jump discontinuity is most likely due to a discontinuity in the surface forces).	The existence of a cusp end is a necessary but not sufficient condition for the occurrence of a jump discontinuity.
Herrera et al. (2003)	Polyacryleamide (PAA) solutions without the presence of surfactant using particle image velocimetry (PIV) technique	Yes. (The critical volume of the bubbles at which the jump occurred decreased as the concentration of polymer increased).	A negative flow field around the bubbles appears only after the critical volume.
Funfschilling and Li (2006)	Nitrogen (N_2) bubbles in CMC and PAA solutions.	No. (No discontinuity observed even in the similar bubble volumes at the work of Astarita and Apuzzo (1965)).	Bubble volumes between 20 to 1000 microlitre.
Soto et al. (2006)	HASE-type associative polymer solutions exhibiting both shear-thickening/shear-thinning and also Newtonian behaviour.	Yes. (But, it is much more like a steep change in velocity than a sudden jump).	The appearance of the discontinuity results from a balance between elastic and surface tension forces. Dimensionless number $N1.d/\sigma \approx 0.25$ is the jump occurrence condition.
Pillapakkam S.B. et al. (2007)	The role of viscoleastic parameters in jump velocity investigated by using direct numerical simulations (DNS)	Yes. (Simulations are in agreement with experimental data. The magnitude of the jump varies significantly with the concentration of solution).	Simulations show that the shape of bubbles and their wake structure changes fundamentally at a critical volume at which there is a sharp increase in the terminal velocity.
Malaga and Rallison (2007)	Numerical calculations for bubble deformation	No. (No jump discontinuity found).	The shape of a rising bubble in a polymer solution studied.
Pilz and Brenn (2007)	Praestol 2500 (a linear polyacrylamide), polyethylene oxide (PEO), and Praestol 2540 in de-ionized water and also in solutions of glycerol in de-ionized water	Yes. (No discontinuity observed at low solution concentrations).	The relaxation time in elongational flow is important in potential of a solution to exhibit a discontinuity in rise velocity of bubbles.

Any immersed object in a fluid is subjected to an upward force from the fluid which is called Buoyancy force (F_B). This force is proportional to density of the fluid and the volume of the object. So, for a bubble inside a liquid, the buoyancy force is of a great magnitude in comparison to the gravity force:

$$F_B = \rho g V \tag{2.18}$$

where ρ is the liquid density (kg/m^3).

A moving object experiences another force by the surrounding fluid which is called drag force, F_D (Figure 2.10). This force has two components: the viscous drag and the form drag. Viscous drag is the skin friction of fluid molecules with the moving object, and form drag is due to the pressure distribution around the body which is dependant on the form or shape of the object in the fluid.

The contributions from both viscous and form drag to the total drag force on a moving body in a fluid or on an immersed body in a free stream can change depending on some conditions such as Reynolds number and the shape of the object. For instance, at low Reynolds numbers, the skin drag contribution to the total drag force on a sphere is more than of high Reynolds number when the separation of the boundary layer takes place.

$$F_D = F_t + F_n \tag{2.19}$$

where: F_D is the total drag force; F_t = skin friction force; and F_n = form drag force.

A dimensionless analysis for a sphere with diameter d moving at constant velocity in a power-law fluid would show that the drag coefficient (C_D) be expressed by the Reynolds number and the power law index (n) (Chhabra and Richardson, 1999):

$$C_D = f(\mathrm{Re}, n) \tag{2.20}$$

for which:

$$C_D = \frac{F_D}{(\frac{1}{2}\rho U^2)(\pi d^2/4)} \tag{2.21}$$

$$\mathrm{Re} = \frac{\rho U^{2-n} d^n}{m} \tag{2.22}$$

in which, d is the projected diameter of the bubble on a horizontal plane and U is the terminal velocity of the particle.

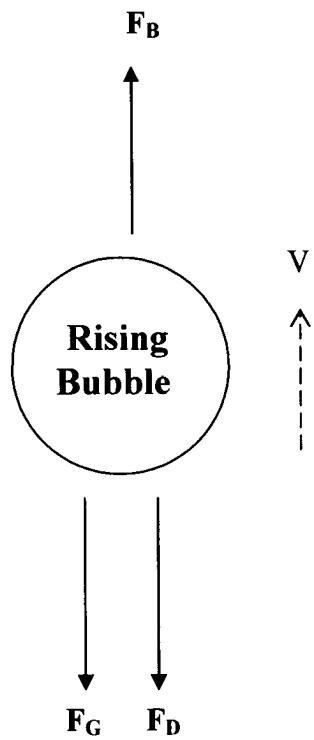

Figure 2.10 Schematic of forces acting on a rising bubble with a velocity of V.

The form of the Reynolds number for the calculation of the drag coefficient in this study will be according to equation 2.22 assuming power law behaviour for xanthan gum solutions in a specified range of shear rates.

There has been many studies on describing the motion of gas or solid particles in liquids using dimensionless groups of Reynolds number(Re) and drag coefficient (C_D). Turton and Levenspiel (1986) and Clift et al. (1978) studied falling spheres in various Newtonian fluids. They offered different correlations for the drag coefficient for a wide range of Reynolds number, from which, the following expression by Turton and Levenspiel (1986) is among the best for high precision:

$$C_D = \frac{24}{\mathrm{Re}}(1 + 0.173\,\mathrm{Re}^{0.657}) + \frac{0.413}{1 + 16300\,\mathrm{Re}^{-1.09}} \tag{2.23}$$

Karamanev (1996) proposed a generalized correlation based on Archimedes number (Ar) for a precise calculation of drag coefficient for falling and rising particles independent of their rise velocity:

$$C_D = \frac{432}{Ar}(1 + 0.0470\,Ar^{2/3}) + \frac{0.517}{1 + 154\,Ar^{-1/3}} \tag{2.24}$$

and,

$$Ar = d_e^{\,3} g \rho_f (\rho_f - \rho_p)/\mu^2 \tag{2.25}$$

in which, ρ_f is the density of continuous phase, ρ_p is the density of dispersed phase, μ is the viscosity of the fluid, and d_e is the projected diameter of the particle.

Substituting equations 2.17, 2.18, and 2.21 in equation 2.19, yields the following equation for the drag coefficient used by Karamanev (1994):

$$C_D = \frac{4 g \Delta\rho d_e^{\,3}}{3 \rho d_h^{\,2} U^2} \tag{2.26}$$

In the latter equation, the volume of the particle is calculated based on the equivalent diameter with the following equation:

$$V = \frac{\pi d_e^{\,3}}{6} \tag{2.27}$$

The equivalent diameter, d_e, is the diameter that a bubble would have if it had spherical shape. The accuracy of equation 2.26 for the calculation of drag coefficient, which is based on equivalent and horizontal diameters (d_e, d_h, and d_e/d_h), has been discussed by Karamenv et al. (2005) and Dziubinski et al. (2003).

Margaritis et al. (1999) studied the rise of gas bubbles in polysaccharide aqueous solutions and proposed a universal drag curve modifying the equation 2.23:

$$\mathrm{Re} < 60 \qquad C_D = \frac{16}{\mathrm{Re}}(1 + 0.173\,\mathrm{Re}^{0.657}) + \frac{0.413}{1 + 16300\,\mathrm{Re}^{-1.09}} \tag{2.28a}$$

$$\mathrm{Re} > 60 \qquad C_D = 0.95 \tag{2.28b}$$

Dewsbury et al. (1999) also found the similar results for C_D in aqueous CMC solutions as Margarits et al. (1999).

2.3 Xanthan Gum

Xanthan gum is a microbial polysaccharide produced in a bioreactor by the microorganism *Xanthomonas campestris*. Xanthan gum solutions have extensive applications in food, cosmetics, pharmaceutical, oil drilling, and other industries with even larger future potential (Margaritis and Pace, 1986). Shear-thinning behaviour with high viscosities, drag reduction properties, emulsion stabilizing and thickening

properties are some of the unique specifications of microbiologically produced xanthan gum (Margaritis and Zaijic, 1978).

The molecular structure of xanthan gum contains pentasaccharide repeating units of D-Glucose, D-Mannose, D-Glucuronic acid, Acetyl linked Pyruvic acid, and d-Acetyl groups as shown in Figure 2.11 (Bewersdroff, 1988).

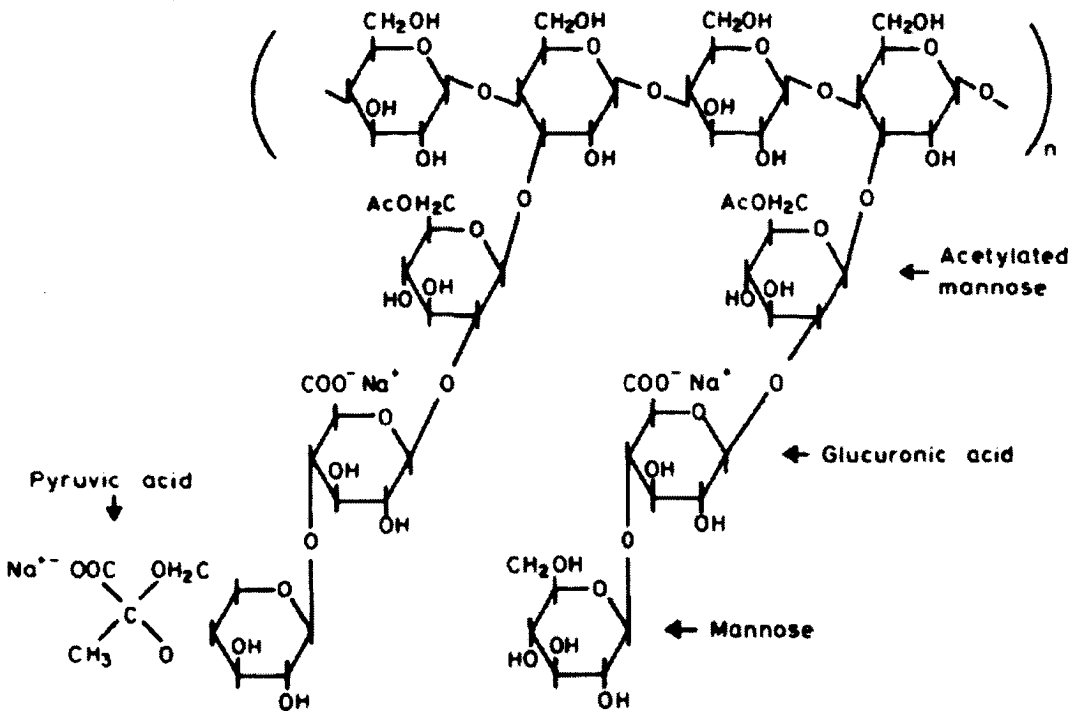

Figure 2.11 Molecule structure of xanthan gum (Bewersdroff, 1988).

Polymers are long chain of monomers or small molecules, with very high molecular weight, often up to a couple of millions of g/mol. Biopolymers such as xanthan gum are also similar to synthetic polymers that have a mixture of several molecular species,

but with the main difference that xanthan is produced by means of microorganisms rather than by catalysts.

Xanthan gum solutions are distinguished from the other microbial polysaccharides because of their distinctive rheological properties. Owing to increasing global demand for xanthan gum due to its excellent properties, it has become an important issue for studying by the researchers in both academia and industry.

For instance, the production and properties of xanthan gum have been reviewed by Garcia-Ochoa et al. (2000) focusing on the various aspects of production such as kinetic of growth of microorganisms. Performances of a bubble column and a stirred tank fermentor have been compared by Pons et al. (1990), and the effect of different carbon sources on the production of xanthan gum has been investigated by Leela and Sharma (2000).

The present study is also a step in increasing the knowledge about this material including rheological properties as well as the bubbles behaviour in its aqueous solutions which is crucial for the production of xanthan gum in a bioreactor.

3. Experimental Setup and Procedure

3.1 Experimental Setup

To study the motion of air bubbles in xanthan gum solutions, the experimental setup presented in Figures 3.1a and 3.1b was used. The setup consisted of a transparent column and a bubble release system equipped with microsyringes to make bubbles with certain volumes. Two high-speed cameras mounted at different levels were used to monitor and record the motion of the bubbles. The recorded video files were analyzed by image processing software, MiDAS, to determine the path of movement, velocity and geometric parameters of the released bubbles.

The schematic diagram of the setup in Figure 3.2 gives a general view of all of the components in this experimental device. It also contains the typical shapes of the bubbles encountered in this study.

3.1.1 Column

The column used for this research was a rectangular Acrylic column with dimensions of $27\,cm \times 30\,cm \times 240\,cm$, and wall thickness of about $1\,cm$. Although in all of the experiments around a half of the height of the column was filled with the solutions, the size and the working volume of the column was big enough in comparison to the size

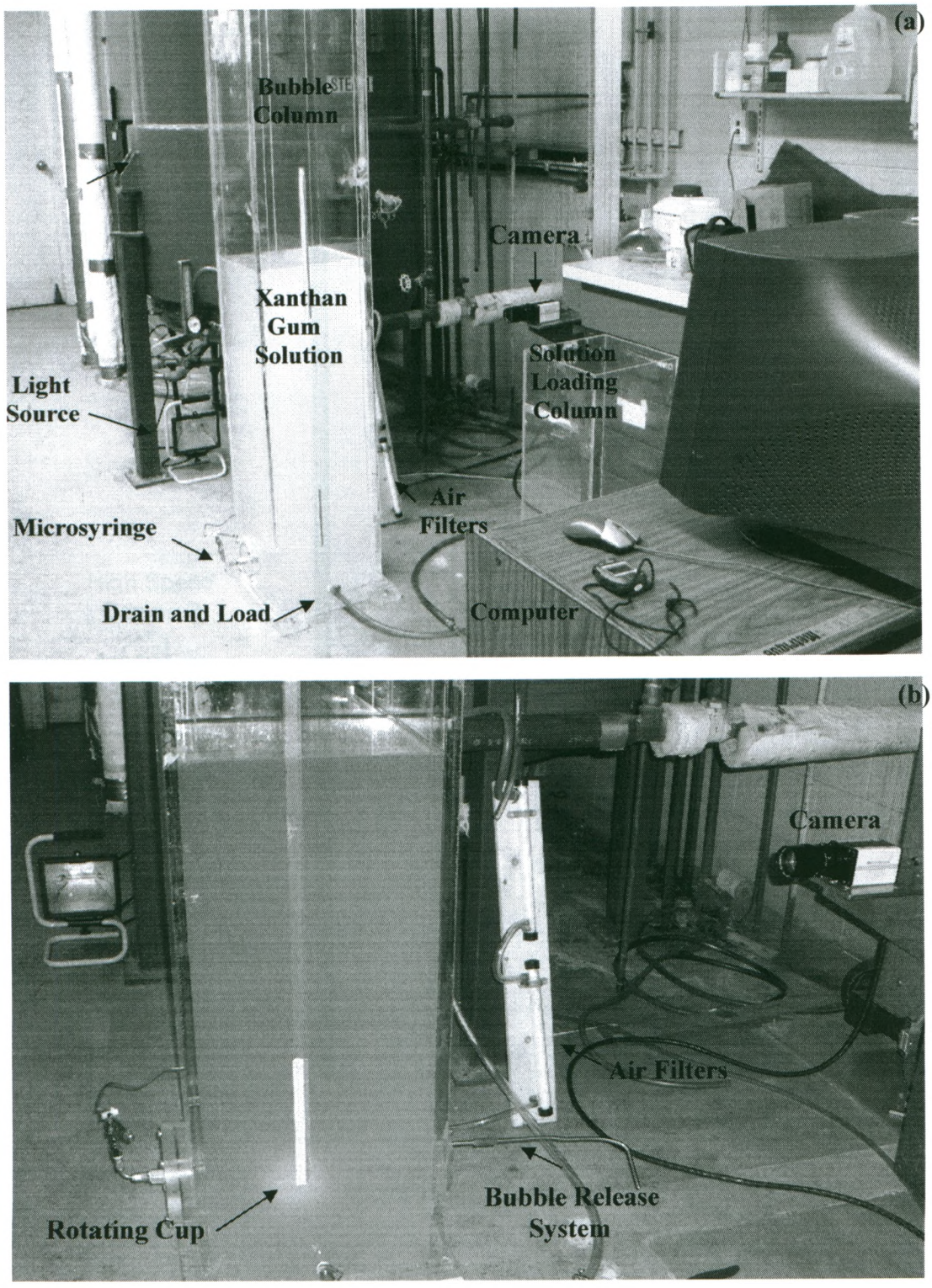

Figure 3.1 (a), (b) Experimental setup for the study of motion of air bubbles.

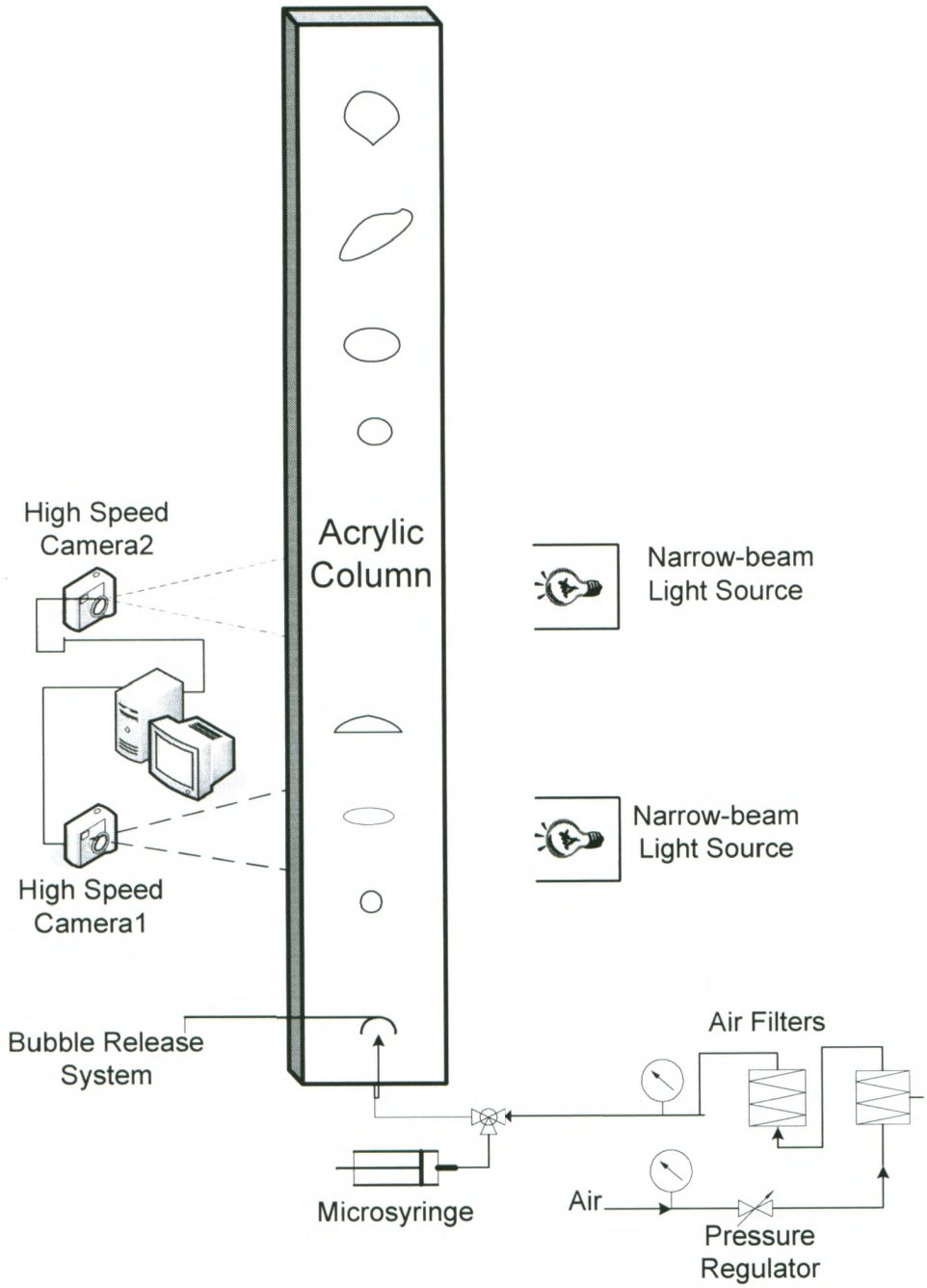

Figure 3.2 Schematic diagram of the experimental setup (not to scale).

of the bubbles to avoid any end effects and wall effects in the motion of the studied air bubbles. To load the prepared xanthan or CMC solutions to the column, a smaller column and a peristaltic pump were used. Loading or unloading the column with liquid was done through the drain hole located at the lowest part of the column.

After each set of experiments, the column was drained and washed thoroughly by a brush and flow of hot water on the walls of the column. Then, the column was leveled with tap water for a whole day long, and rinsed with distilled water. Depending on the concentration of xanthan gum, the cleaning procedure was repeated.

3.1.2 High-Speed Cameras

Two Redlake *Motion*Scope high-speed imaging cameras with recording speed ability up to 500 and 8000 frames per second (fps) were used. The working frame rate in this study was between 500 to 2000 fps due to reduced resolution of the pictures in higher frame speeds.

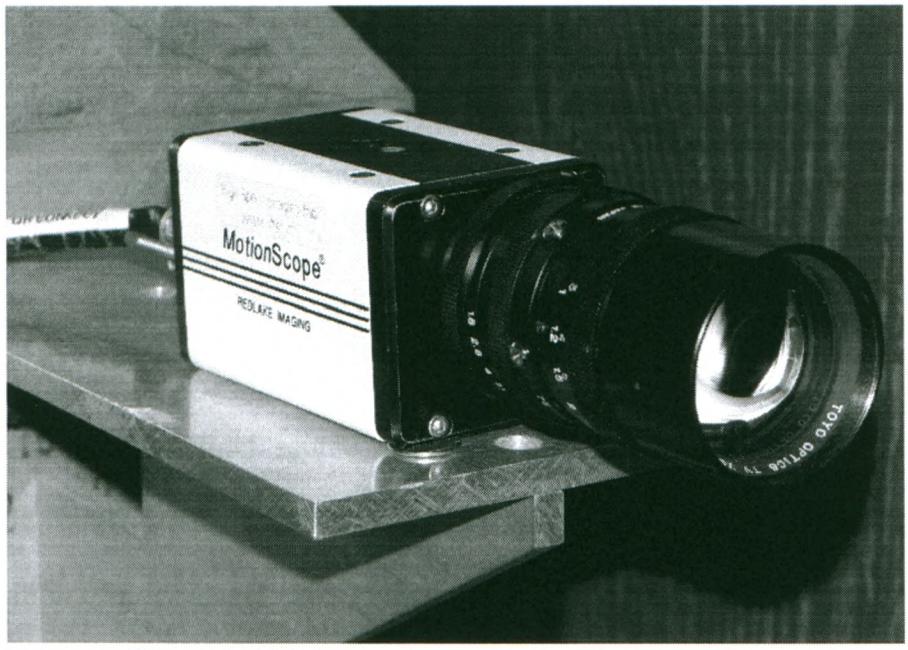

Figure 3.3 High-speed camera used in this study.

The cameras were connected to a PC equipped with MiDAS data analysis tool for video processing. To give better zoom ability to the cameras, a Toyo Optics zoom lens (12.5 mm – 75 mm f1.8) was connected to each of them. The lens made it possible to zoom on the small bubbles in a very narrow field of focus and to detect them in high concentrations of xanthan gum when the bubbles were not visible by the naked eye due to opacity of solution. Figure 3.3 is a picture of high-speed camera with the lens connected to it. The vertical position of the cameras will be discussed in the results and discussion section (chapter 4). .

3.1.3 Bubble Release System

The bubble release system consisted of an immersed Teflon cup located in the center of the column at the bottom. A piece of rod was attached to the Teflon cup through a hole in one of the portholes of the column to enable fully rotation of the cup from outside the column. The rod was constructed from stainless steel to ensure that no corrosion would occur, and it was sealed in the column's porthole by a piece of silicon rubber to avoid leakage of the solutions out of the column.

3.1.4 Light Sources

Using an appropriate light source was very important in getting clear images of bubbles in xanthan gum solutions that have poor transparency. Depending on the concentration of xanthan solution, three types of light sources were used in this study (Figure 3.4). For the highest concentration of xanthan gum, which was 0.2580 %w/w

(2580 ppm), a 500 watt narrow beam light was used. Working with higher concentrations than 2580 ppm was not possible because of the opacity of the solutions. The drawback of the high-watt lamp was that the heat produced by it was raising the temperature of the facing wall of the column. To reduce this problem, the light was turned on only at the short time of the recording images by the camera. The narrow beam light made it possible to track the small bubbles inside the column despite the opacity of the high concentration solutions.

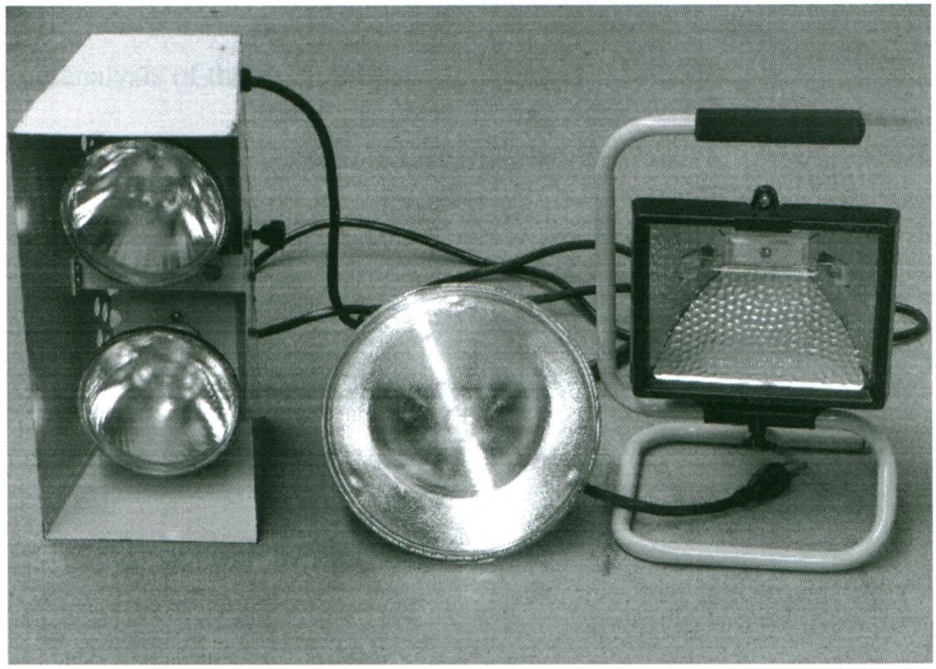

Figure 3.4 Different types of light sources used in photographing of bubbles.

As for the location of the light sources, it was found that in all of the working xanthan solutions, the best place was the opposite side of the column where the camera was located. This means that the camera was face to face with the lamp through the column. Therefore, the lower the concentration of the xanthan gum solutions, the higher the contrast of the bubble images. For CMC solutions that were transparent

unlike xanthan gum solutions, the best place for the light source was the same side where the camera was located.

3.1.5 Motion Analysis Software (MiDAS)

Controlling the high speed cameras and managing the recorded video files from the motion of air bubbles was done through a software called MiDAS which was installed on a PC connected to the cameras. MiDAS consists of base software that allows the user to record, play, view, save and load image sequences, and a module that provides the motion analysis of the captured events. The details for the analysis module that has been used extensively in this study are given in the following sections.

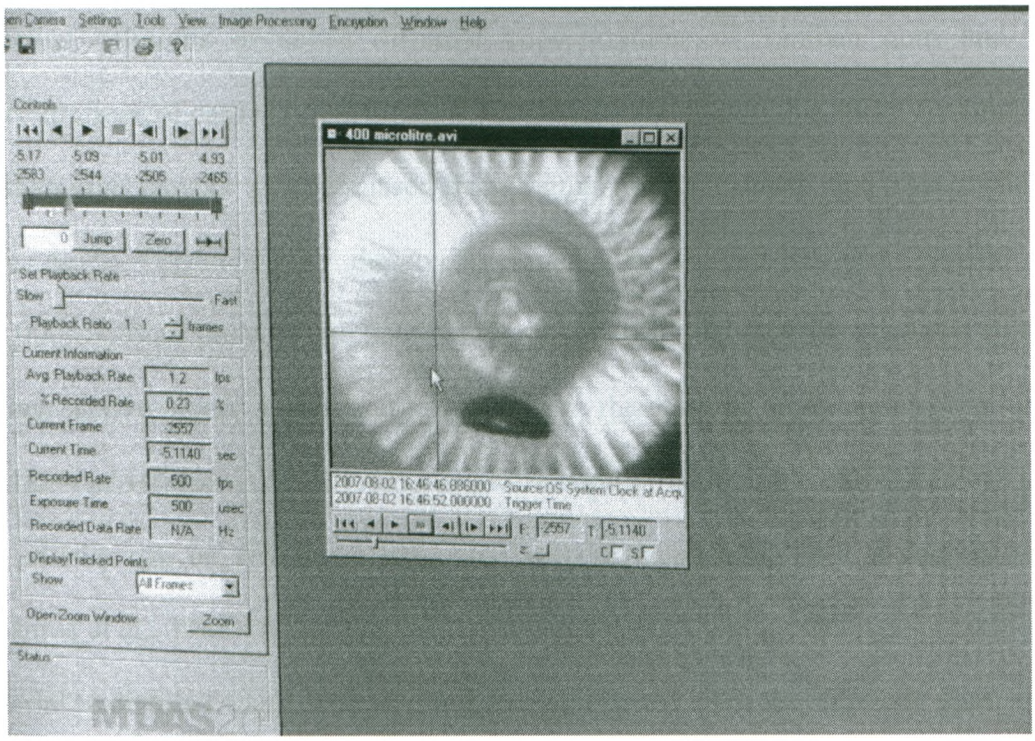

Figure 3.5 A typical recorded scene from bubbles motion in xanthan gum solutions.

When MiDAS was in record mode, the cameras were instructed by MiDAS on how and when to acquire pictures by keeping track of time and location of frames and acquired information. Figure 3.5 is a sample frame of recorded files for bubbles in 1050 ppm xanthan gum solution.

MiDAS also includes various techniques for manipulating the images and improving their quality and contrast. These techniques were useful in better viewing of the images and also in helping to improve accuracy of tracking and motion analysis of the bubbles.

3.1.6 Materials Used

Aqueous solutions of seven different concentrations of xanthan gum and two concentrations of carboxymethylcellulose (CMC) were used in this study. Commercial xanthan gum powder was purchased from Sigma-Aldrich Canada, and CMC obtained from Acros Organics with the average molecular weight between 250,000 and 700,000. Sodium dodecyl sulphate (SDS) supplied by EM Science was also used as surface active agent (surfactant) to perform rheological measurements in some solutions of xanthan gum. All materials were kept in room temperature. Xanthan gum dry powder can be kept for a long time without degradation in a sealed container (Cadmus et al., 1982). All of the solutions were made by adding weighed quantities of material to distilled water. The working temperature for all of the solutions used in this study was $22.5\,^{\circ}C$.

3.2 Experimental Procedure

3.2.1 Aqueous Solution Preparation

Xanthan gum solution preparation was done in a 10-litre stirred tank equipped with two sets of 4-blade flat plate turbine impeller as shown in Figure 3.6. Xanthan powder is soluble in cold or hot water. Lumps that take longer time to dissolve are produced if xanthan gum powder is added up to water once. Thus, after adjusting the mixer at around 200 rpm, xanthan powder was added to distilled water at a very low rate through the top of the vortex to avoid lump formation (Nussinovitch, 1997).

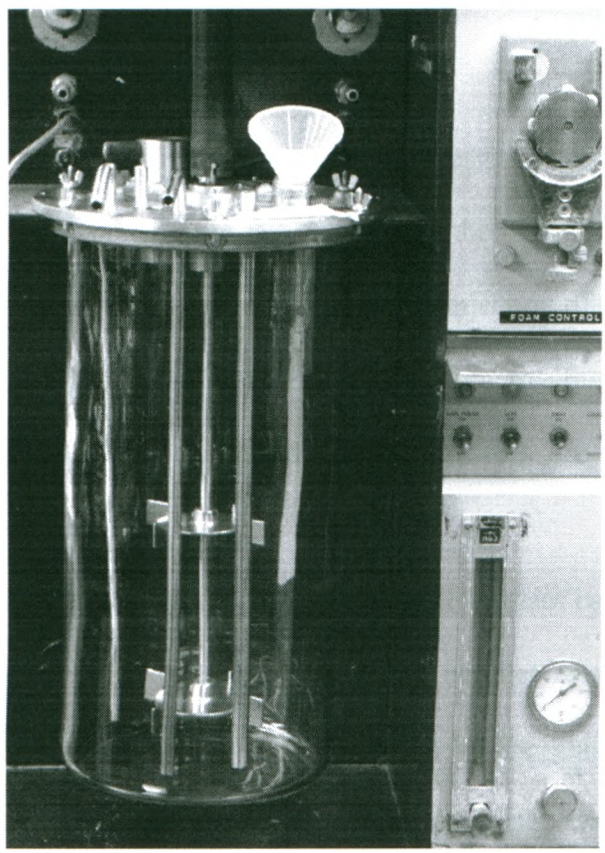

Figure 3.6 10-litter stirred vessel for dissolving xanthan powder in distilled water before transferring the solution to the bubble column.

Each batch of prepared solution was transferred to the bubble column slowly with a pump from the bottom of the column to decrease the entrainment of small bubbles in the solution. Some time was needed to allow the small bubbles created by the high-shear mixer to come out of the column after transferring all batches of the solutions to the column.

The final concentration of the prepared solutions was corrected by measuring the total volume in the column considering the density of the solutions and sum up of the weights of xanthan consumed in all of the batches in the stirred tank.

3.2.2 Bubble generation

Low pressure air in the lab which is basically oil-free was used to generate bubbles with different volumes in the column. To ensure that the bubbles are completely free of oil, two fiberglass filters in series were used before injection of air into the column. An air pressure regulator was also connected to the air line to adjust the pressure of the inlet air to the column to a value equal to the hydrostatic pressure of the solution at the tip of the glassware orifice.

The orifice was made by glasswork on a 0.3 mm diameter glass capillary tube to make a smaller diameter glass orifice capable of creating bubbles as small as around one microlitre. The size of the smallest bubble created by the glass orifices has been determined using photographic techniques that will be described in the later sections.

By means of three different sizes of micro-syringes (50μl, 100μl, 200μl) with high accuracy provided by the Hamilton Company, known air bubbles volumes were injected into the column. The syringes were of the gastight type withstanding pressures up to 1000 psig without any leakage.

To make sure of the accuracy of the volume of the bubbles measured by the syringes, it was very important to ensure that all the connections and tubing were selected from metal or glass, which had not changing inside volumes under pressure.

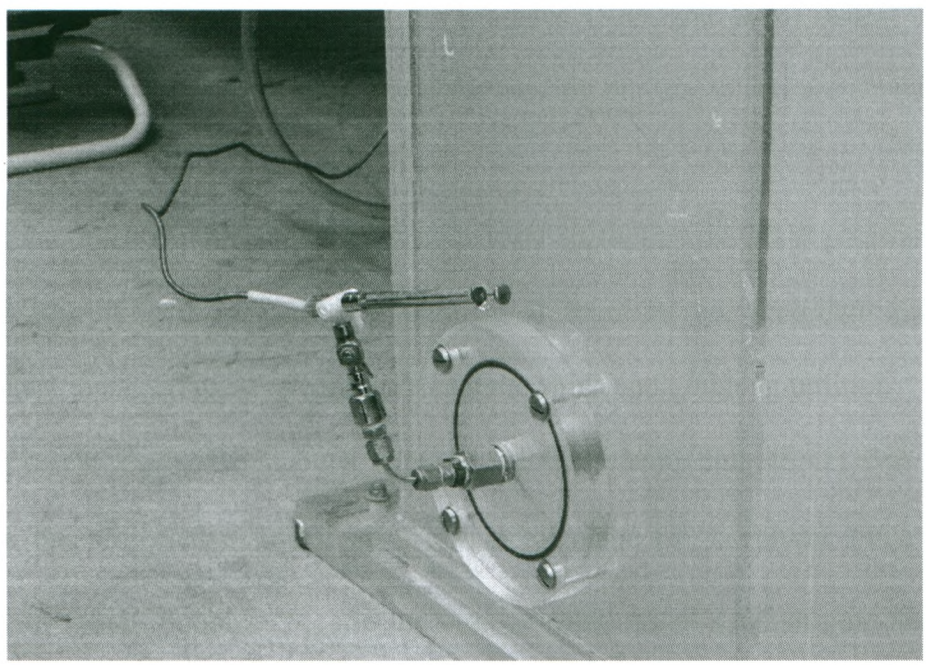

Figure 3.7 Method of connecting microsyringes to the air supply and to the column.

Also, the shorter the tubing (after the syringe) the better results in volume measurements. As it is shown in Figure 3.7, the only non-metal part after the syringe was the 3-way valve that was made from non-flexible stiff plastic.

The desired volume of air was injected through the orifice under the capsized Teflon cup. Coalescence of the injected bubbles under the cap was the key point for making different bubble volumes.

3.2.3 Image Processing

MiDAS 2.0, imaging software licensed by Xcitex Inc., was used to analyze the video files captured by the high-speed cameras. MiDAS contains two modules for image processing called Spreadsheet Analysis modules (SA1 and SA2). These modules support manual or automatic tracking of the moving objects, which are air bubbles in this research.

In each module, the results of image analysis including the X-Y position of the selected objects with related time and frame numbers are recorded into Excel spreadsheet that enables us to benefit from its formula and graphing utilities.

In the present study, the manual spreadsheet analysis module (SA1) was used to measure the projected diameter on a horizontal plane (d_h), volume (V_B) and the velocity of the air bubbles (U_B) in the various solutions of xanthan gum and CMC. This module allows the operator to manually select and identify the studied points or objects within the desired frames of the images after the videos are recorded.

Figure 3.8 shows a typical use of the Spreadsheet Analysis module for the determination of the projected diameter of the bubble as well as for the path of movement of the bubble in the selected frames that were precisely tracked. By selecting a new task in SA1module, an Excel spreadsheet along with the Excel toolbar

popped up at the top of the screen. Every spreadsheet was linked to a video playback that could be saved either separately or together in the computer.

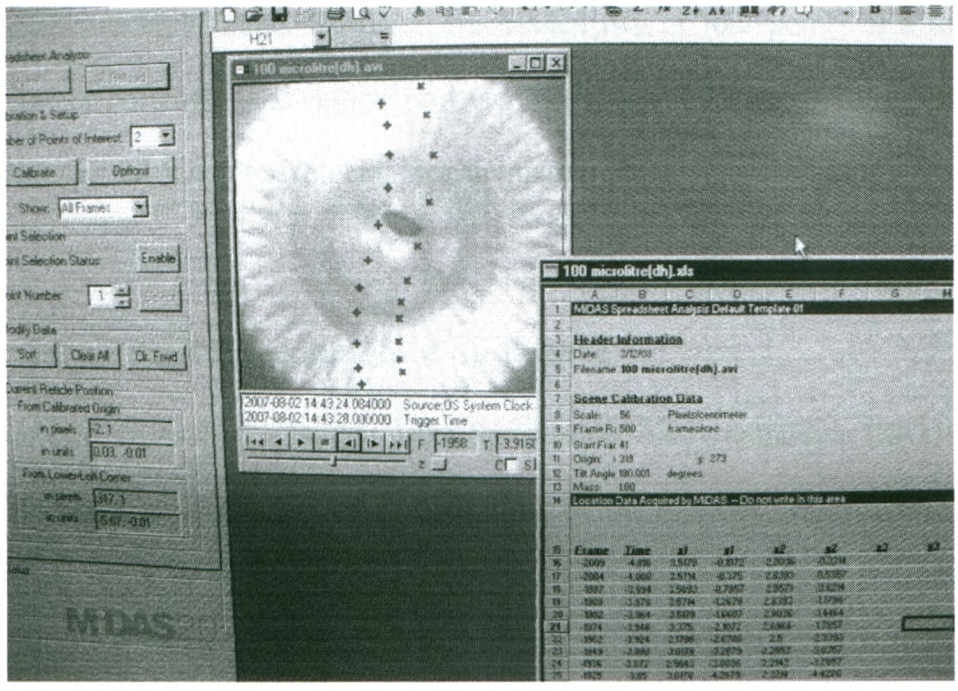

Figure 3.8 Spreadsheet Analysis Module for tracking the bubbles in xanthan solutions.

There were a couple of other options that allowed the user to customize the selection and displaying settings, which must have been set before any image processing. For instance, to be able to have a fast tracking of the points or features, it was better to use the single-step selection mode. To precise placements of the points on the images, two-step selection was a better option to use. We used the latter along with the zoom window option to accurately identify the edges of the bubbles with the precision of a

pixel for their volumes and diameter determinations. A two-step selection could be a combination of left and right click on the mouse.

Before enabling the tracking feature, MiDAS must have been instructed as to the number of points of interest per frame to be tracked. MiDAS has the ability to track up to 64 points in each frame. However, we needed two or four points in a frame to determine the horizontal and vertical projected diameters of the bubbles. Just one point per frame was sufficient for velocity measurements.

3.2.3.1 Calibrating Camera Images of Air Bubbles

The first step in tracking a bubble using Spreadsheet Analysis module (SA1) was to define the real dimensions of the recorded scene for the software. MiDAS used this to convert any object in the image, which consisted of pixels, to the actual dimensions.

For this purpose, in each set of experiments, after adjusting the lens of the cameras in the desired field of view in the bubble column, a ruler was placed exactly in the middle of the column where the bubbles were rising up. Then, an image of the ruler was made and used as the reference point for calibrating the scene. The same procedure for the calibration was repeated only after changing the view length of the cameras by readjusting the lens. By defining two points with known distance as set points, it was possible to set the scale factor defined as pixels per measurement unit (e.g. pixels/cm).

Next step in calibrating the scene was to remove any residual tilt in the camera relative to the field of view by clicking on two sides of a horizontal object in the playback window. After calibrating the scale factor and the tilt, the size of any object in the

scene could be automatically calculated by MiDAS using the number of pixels that are covered by the object and the defined conversion factor.

To identify the position of a bubble in the scene, an origin point (0, 0) has been defined as the origin for X-Y coordinates at the right bottom corner of scene. All of the absolute movements of the bubbles have been calculated relative to this point.

3.2.3.2 Air Bubble Terminal Velocity Measurements

The rise velocity of the bubbles in xanthan and CMC solutions was determined by doing a basic analysis using MiDAS in the playback mode for the recorded scenes of bubble movement. The general concept of velocity measurement was to use the high speed cameras to precisely determine the time that the bubbles travel a specified distance.

One of the advantages of using a high speed camera instead of a normal digital camera was the number of frames that this type of cameras can take in each second, which allows an exact determination of the elapsed time for velocity measurements. For example, if recording were performed in 500 fps, the time travel for each frame would be 0.002 seconds. So, the amount of frames covered by a bubble in the video playback for a known distance in the field of focus of the camera will give the precise time and rise velocity of the bubbles.

In order to obtain more accurate results for the rise velocity of bubbles, two high-speed cameras were used at different heights of the column. This was done after a primary measurement at two levels of 50 cm and 90 cm above the bubbles release point and making sure that the bubbles had reached to a terminal velocity at the level

of 50 cm (the results are reported in the next chapter). The first point for the cameras (50 cm) was selected high enough to avoid any probable disturbance effect of the rotating Teflon cup in the bubble generation system.

A log sheet was designed for data collection after each video was taken for the bubbles (Appendix H). This log sheet contains the time data at the beginning and end of the path of movement of the bubbles at a precision of 0.002 second, from which, the rise velocity can be calculated based on the particular field of focus of the camera in the experiment.

A second approach was also used for the velocity measurements by means of the MiDAS data analysis feature, and the results were compared. However, the final results were reported based on image analysis which covered several points in the field of view instead of considering only the end points.

Before performing the velocity measurements in each set of experiments, precautions must be taken to ensure that the liquid is quiescent before releasing the bubbles. For this purpose, the injection period for the bubbles was taken long enough to avoid any effect of trajectory memory on the successive released bubbles.

3.2.3.3 Bubble Volume and Projected Diameter Measurement

As described previously, the volume of the bubbles has been measured using different types of microsyringes to inject air into the column. This approach has drawbacks that are discussed in the next chapter. However, to reduce the error of measurements, a pressure regulator provided a pressure equal to the hydrostatic level of the liquid inside the column. To set the pressure in the regulator, either the level of liquid was

used to calculate the pressure head, or the regulator pressure was adjusted up to the pressure necessary to release the first bubble.

Also, a second approach was used for bubbles volume measurements, which was more suitable in case of CMC because of the transparency of the solutions. The number of coalesced same size small bubbles under the Teflon cup was the bottom line for this method. To create small and same size bubbles, the pressure of inlet air to the column was adjusted a little bit more than the previous volume measurement approach in a way that small bubbles begin making chains with a long time intervals around 10 seconds between two successive bubbles.

Labeling the volume of the first bubble in the bubble chain as "unit volume", the volume of the rest of the bubbles would be a multiple of this unit volume. In case of working on a transparent solution like CMC, the number of the bubbles can be visually counted. But, for solutions like xanthan gum solutions which were not transparent, the time interval between the successive bubbles can be the yardstick for calculating the total volume.

The only point in this method for bubble volume measurement was that the size of orifice for making the bubbles must be small enough to make spherical bubbles. Then, the "unit volume" could be precisely calculated using photographic techniques. A known value for the "unit volume" meant that the volumes for the rest of the bubbles have been exactly determined (known multiples of the unit volume). This approach was only applied for a concentration of 780 ppm for xanthan gum and all CMC solutions.

The projected diameter of the bubbles was determined by using the image analysis mode in MiDAS. Using a two-point selection option in MiDAS, as discussed before, the diameter of the bubbles was calculated by the software based on the scale factor and the number of pixels covered by the bubble. For the bubbles with zigzag trajectory and moving interfaces, an average projected diameter was obtained by considering the minimum and maximum calculated diameters in the whole field of focus of the camera.

3.2.4 Physical Property Measurement of Solutions

3.2.4.1 Density

The density of all solutions was measured by a constant volume pycnometer at the working temperature of 22.5 $°C$. The pycnometer has a lid with a capillary tube inside it to provide equal volumes for all of the samples, which was 10 ml as shown by the marking on it.

The volume measurement containers used in laboratories including this pycnometer measure the volume with an error which is normally around $\pm$ 5% of the real volume of the liquid. For this reason, the exact volume of the pycnometer was determined with distilled water at 22.5 $°C$ and using its exact density from Perry's Handbook (7^{th} edition, 1997):

- Distilled water net weight in the pycnometer: 10.4090 g

- Distilled water density at 22.5 $°C$ (Perry's Handbook, 1997): 997.656 kg / m^3

- Real volume of the pycnometer = $\frac{10.4090}{997.656/1000}$ = 10.4335 ml

To get accurate results with this pycnometer, one must avoid the entrainment of tiny bubbles when filling out the pycnometer. In addition, the sample's temperature may change when holding the body of the pycnometer in hands (because of the small amount of the sample). So, the throat of the pycnometer must be grasped while cleaning the excess of the sample poured out of the capillary. The result of the density measurements are summarized in the later sections.

3.2.4.2 Surface Tension

A Fisher Autotensiomat operating on the principle of du Nouy ring was used for surface tension measurements. In this tensiometer (Figure 3.9), a transducer provides signals that are proportional to the force applied to the immersed ring in the sample liquid. The equipment uses a simple linear equation to measure the surface or internal tensions based on the force exerted on the balance beam, which is converted to an analog signal by a transducer.

$$\sigma = \frac{F}{2L} \tag{3.1}$$

in which,

σ = surface tension (mN/m).

L = ring circumference (cm), which is 6 cm in the Fisher tensiometer used.

$F = m.g$ = force applied to the ring (N).

3.2.4.2.1 Installation and Preparation

The equipment, as illustrated in Figure 3.9 consists of two parts: a control module and a sample module. The control module contains operating controls such as zero and full scale adjustments, elevator direction and override switches, and surface tension indicator, and etc. (Figure 3.9a). The sample module contains motor driven elevator platform, sample vessel (jacketed), balance beam, suspension loops to which the ring and stirrup are connected, and other carriage supports and locks (Figure 3.9b).

The installation of the equipment consists in simply connecting the control and sample modules by elevator and strain/gage cables on the rear panel of each module and in supplying power to the system. The power and meter switches must be in the off position before installation and also before the calibration procedure.

Prior to any surface tension measurement, it is very important to clean the glassware vessel and the platinum-iridium ring to avoid any error in the results due to effect of other samples. It is recommended by Fischer to flame the ring to white heat after rinsing it in benzene and acetone and then to wash it thoroughly in distilled water. In this research, because of usage of surfactants (SDS) in some samples, a double cleaning method has been applied.

The cleaning procedure for the glassware depending in the testing sample is different. For xanthan gum and CMC solutions, a through rinse of the sample vessel with hot water and then with distilled water because of high solubility of these solutions in water was sufficient.

3.2.4.2.2 Calibration and Measurement

Full-scale calibration of the tensiometer was done by a one gram weight and the direct reading of the calibration reference line, which is marked at 81.6 dynes/cm (or mN/m) on the meter. Lower scale measurement is possible by using fractional divisions of a 1-gram weight as calibration weights for the full-scale.

For 1-gram calibration, the stirrup and cleaned platinum-iridium ring must be hanged from the related suspension loop (the first suspension loop on the tip of the balance beam).

By placing and removing the weight on the stirrup pan and adjusting the meter at 81.6 and zero dynes/cm, respectively, the final calibration was obtained providing the meter indicated exactly 81.6 and zero dynes/cm when the weight was alternately placed.

Surface tension measurement was made by pouring the sample in the glass vessel and adjusting the temperature by means of the circulating bath through the jacket of the vessel. After raising the elevator platform on which the sample vessel was located, the ring had to be submerged in the sample by lowering the transducer-balance assembly. By turning the elevator direction switch to "down", the platform descended at the selected speed at a constant rate (maximum 1 inch/min).

When the ring approached the liquid surface, the meter readout started increasing until reaching a maximum peak which corresponded to the surface tension of the liquid. After this peak, the meter readout decreased gradually up to the point where the ring breaks the surface.

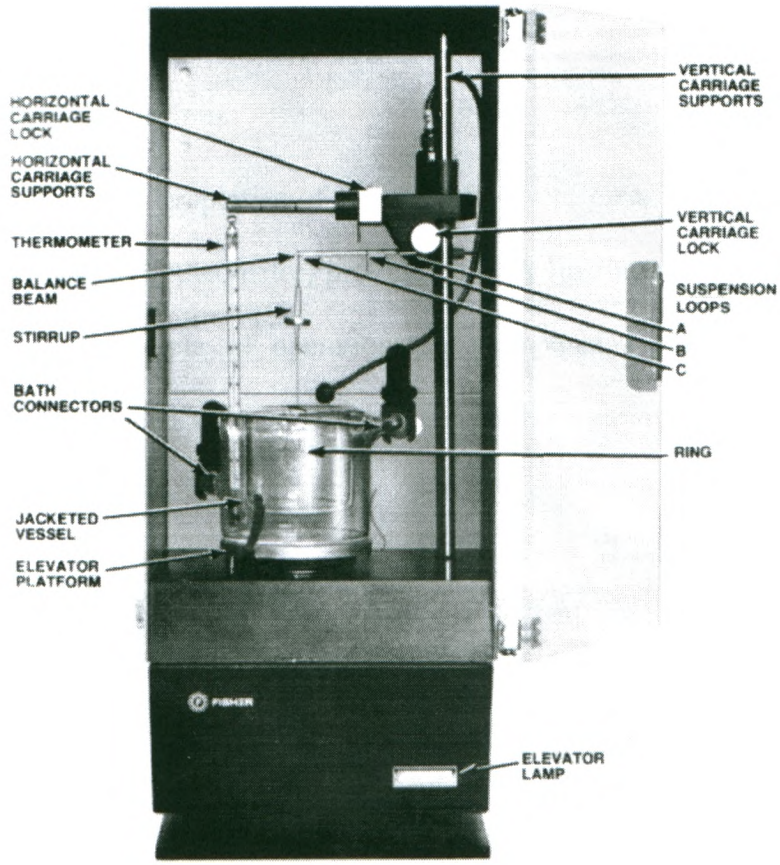

(a)

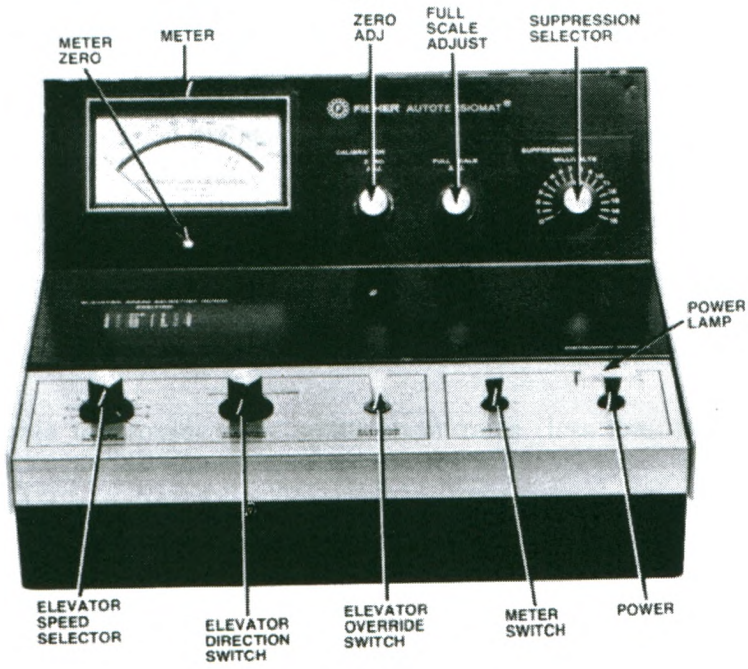

(b)

Figure 3.9 Fisher Autotensiomat (a) Control module, (b) Sample module.

3.2.4.3 Rheology of Solutions

The various rheological properties of the solutions were measured using a cone and plate Rheometer (ARES Rheometer) provided by TA Instruments which is shown in Figure 3.10. The principle of operation and components of the equipment are discussed in the following section along with describing various tests that have been performed using this rheometer.

3.2.4.3.1 Description of the Equipment

ARES stands for Advanced Rheometric Expansion System, and it is a mechanical equipment capable of measuring the torque resulting from the application of dynamic or steady shear strains on a desired sample. Any rheometer consists of three major parts: motor, transducer, and control computer. The motor applies different shear rates. The transducer measures the resulting rotational or axial forces, and the control computer synchronizes all subsystems.

The motor used in ARES is a Low Shear (LS) type, in which, the shaft is supported by air bearing to provide a minimum axial runout and very small normal force data. This motor is also able to provide very small shear rates (less than 0.02 s^{-1}) for strain control tests, and it is capable to operate in two different modes depending on the type of the test.

Figure 3.10 ARES rheometer used for rheology measurements.

In steady mode, the motor can rotate at defined shear rates (rotational rates) and measures the resistance of sample to deformation, torque, as well as normal forces created by the liquid through a transducer.

In dynamic mode, the motor is not rotating but it is oscillating in the given frequency range. The maximum angular deflection of the motor is 0.5 radians from either side of motor when it is static. In this mode, only torque is measured. We have used both

steady and dynamic modes for separate rheological measurements for which the results are given in the next chapter.

ARES uses a Force Rebalance Transducer with Normal forces (FRTN1) that consists of torque and normal force (axial) servo control systems. The FFT shaft (Spindle) is in null position before and after every test. This is possible by using a position feedback system that creates an electrical current proportional to the amount of force applied for changing the position of the shaft by the sample.

ARES is connected to Orchestrator software as the user interface. All of the parameters for the test such as gap control, motor start/stop, transducer selection, test parameters edition, and etc. can be set using different menus in Orchestrator. The data obtained from the tests also can be graphed and displayed by this software along with doing some curve fittings with viscosity models, which has been extensively used in this study.

3.2.4.3.2 Viscosity and Normal Force Measurement

Obtaining the flow curves for each solution is essential for the calculation of the flow index, n, and the consistency index, m, (power law coefficients) and eventually the Reynolds number of bubbles moving through different solutions. For each working concentration of xanthan gum and CMC, a sample was used to do all the viscosity measurements by the ARES viscometer.

The required sample volume for each run of viscosity measurements was around 3 ml that had to be gently placed between the cone and plate (Figure 3.11a) in the viscometer to avoid small bubbles entrapment in the liquid. Then the cone had to be

adjusted at a distance of 0.241 mm from the plate and the excess of sample had to be cleaned from the edges of the cone and plate.

Attention must be taken that in all rheological measurements, the edges of the sample between the cone and plate must have a convexity when looking at the sample from a horizontal view (Figure 3.11b).

Long required time for performing the viscosity and frequency sweep measurements in a wide range of shear rates or frequencies, will make the amount of the sample to decrease because of evaporation. To keep the volume of the sample at the initial value, a humidity chamber, which contains some cotton pad inside, needs to be saturated by the sample (or water) and then mounted around the zone of the cone and plate. This chamber also helped to create a thermally isolated cover for the sample.

ARES Rheometer was also able to measure the First Normal Stress Difference (N1) or normal forces along with the viscosity measurements. N1 was measured as a function of shear rate in the steady shear mode. Allowing the sample to relax was the key point in getting accurate data for N1 measurements.

3.2.4.3.3 Strain Sweep Test

To perform the strain sweep test, successive dynamic strains were generated in ARES by a defined range of sinusoidal deformations at different angular frequencies and at a constant temperature of 22.5 $^{\circ}C$, which is maintained by a fluid bath and a circulator.

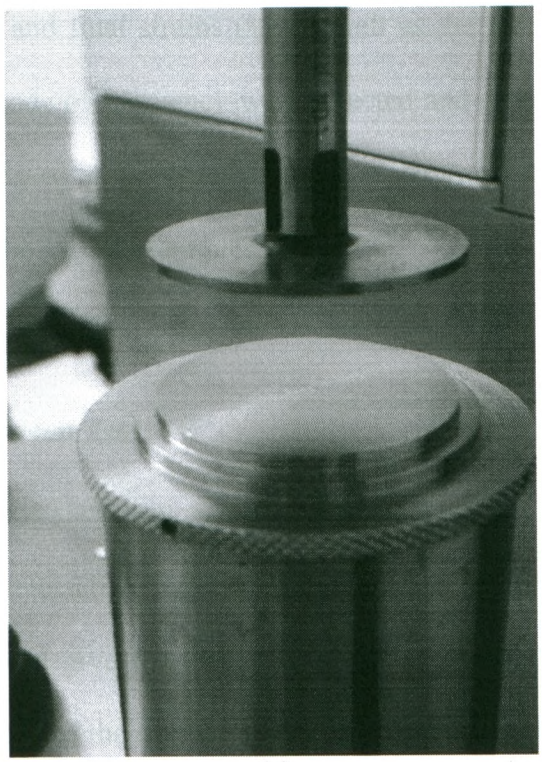

(a)

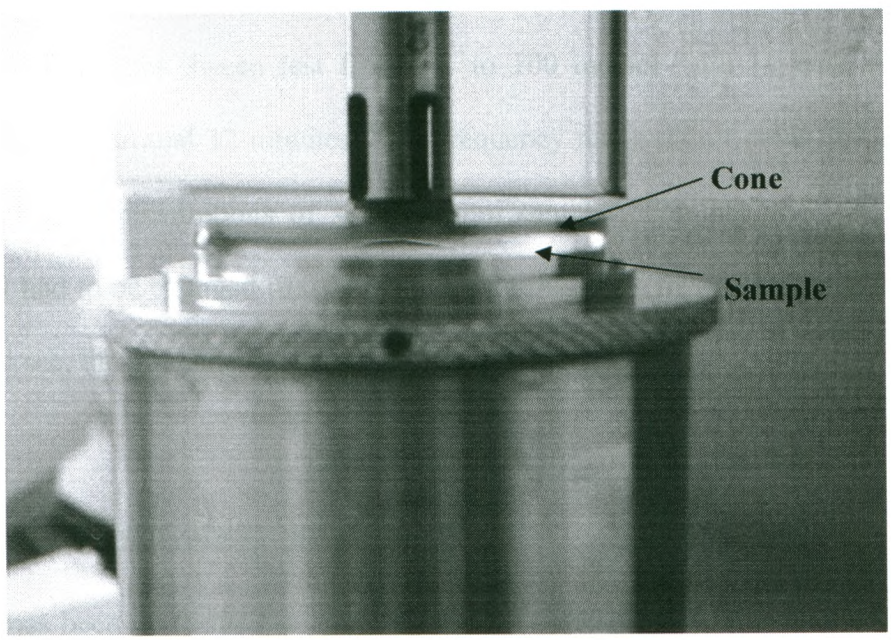

(b)

Figure 3.11 (a) Cone and plate in the ARES rheometer. The cone is connected to a moving shaft. (b) Convex edges of the sample between cone and plate.

Before the test, initial and final strains (%) as well as the number of equally spaced data points in each decade of frequency were selected and defined in ARES. The aim of doing this test was to obtain the amount of strain that is within the linear viscoelastic region of the xanthan samples.

3.2.4.3.4 Frequency Sweep Test

In this test, ARES takes successive G' (elastic modulus) and G'' (viscous modulus) measurements at the selectable frequencies at constant strain and temperature. The results of this test would give the elastic modulus and viscous modulus crossovers while the elastic property of the sample overcomes the viscous behavior or vice versa. This test is a time consuming one depending on the selected low frequency limit. For example, a frequency sweep test from 0.1 to 100 rad/sec with 10 data points per decade will take around 12 minutes. This frequency range didn't cover the crossover point for high concentrations of xanthan gum samples. For that, the low range of frequency had to be changed to 0.01 or lower. In this case, frequency range from 0.01 to 100 rad/sec, the test time increased to approximately 2 hours.

3.2.4.3.5 Normal Relaxation Time

This test has been performed to analyze the time dependant behaviour of the xanthan samples. For this purpose, a single transient deformation was applied to the sample and the relaxation of normal forces was monitored in the defined time period. This test was done to determine the relaxation time, or the time required for the sample to relax

after deformation. Before imposing the deformation, ARES had the option of applying a steady pre-shear prior to the normal relaxation test or other dynamic tests to help the sample relax after loading it to the rheometer.

4. Results and Discussion

To increase our understanding of the underlying fundamentals involved in bubble phenomena, it is essential to study the hydrodynamic behaviour of single bubbles rising in a liquid phase. As discussed earlier, bubble formation, rise velocity, trajectory, shape, and drag coefficient are the important hydrodynamic characteristics of single bubbles which need to be carefully determined to be able to extend the results for the design of multi-bubble operating systems. For instance, knowledge about the rise velocity of bubbles in a bioreactor helps to determine the mean residence time of gas bubbles in it, which finally leads to sizing of the equipment.

The continuous phase that we considered for this work was the aqueous solutions of xanthan gum as a typical non-Newtonian fluid. Subsequently, some experiments have also been conducted on CMC solutions to have a comparison between the results using a second non-Newtonian fluid.

Before studying the behaviour of air bubbles in xanthan gum aqueous solutions, it is essential to investigate the behaviour of the fluid as the continuous phase surrounding the bubbles. This investigation includes the determination of physical properties of xanthan gum and CMC solutions as well as the rheological measurements, which

cover the flow curves for all of the working concentrations, normal force measurements (first normal stress difference), normal force relaxation curves, strain sweep tests, and frequency sweep tests. The results of the rheological tests have been used in determination of the degree of shear-thinning and viscoelasticity of the solutions by means of flow curves and calculated relaxation times. Also, effect of presence of surfactants on the behaviour of the xanthan gum and CMC solutions have been studied through rheological measurements.

4.1 Fluid Behaviour for Xanthan Gum and CMC Aqueous Solutions

4.1.1 Physical Properties of the Solutions

The density of all solutions was measured by a constant volume pycnometer at $22.5^{\circ}C$. A Fischer tensiometer was used to measure the surface tension of the solutions based on the ring method. The results for all measurements are summarized in Table 4.1.

For density measurements, the volume of the pycnometer was corrected by the density of water at the same temperature from Perry's Handbook (1997, 7^{th} edition), for which the details described in chapter 3.

The surface tension of dilute solutions of xanthan gum at $22.5^{\circ}C$ is almost equal to surface tension of pure water at the same temperature. This value slightly decreases with increasing concentrations of xanthan gum up to 0.5% w/w (5000 ppm). Then, the surface tension reduces to 66.9mN/m by increasing the solution concentration to

1% w/w (10000 ppm). The same thing happened for CMC solutions, and adding CMC to distilled water up to 0.6% w/w did not change the surface tension of distilled water. When surfactant (SDS) was added to 0.5% xanthan solutions, surface tension decreased sharply depending on the concentration of the surfactant. For 200 ppm SDS, the surface tension of 0.5% xanthan dropped to 39mN/m., but, adding extra concentrations of surfactant did not change the value of the surface tension.

Table 4.1 Solution properties for xanthan gum and CMC at $22.5^{\circ}C$.

Solution	Concentration (ppm)	SDS Concentration (ppm)	**Density** (kg/m^3)	**Surface Tension** (mN/m)
Xanthan Gum	520	-	998.5	71.8
	780	-	998.6	71.9
	1050	-	998.7	71.7
	1280	-	998.8	71.8
	1530	-	998.9	71.5
	2100	-	999.1	71.0
	2580	-	999.4	70.5
	5000	-	999.9	69.9
	5000	50	999.9	51.0
	5000	200	999.9	39.0
	5000	1000	1000	38.9
	10000	-	1001.2	66.9
CMC	4000	-	999.7	71.8
	6000	-	1000.4	71.6
	6000	100	1000.4	54.0
Distilled Water	-	-	997.7	72.0

This shows that the concentration of surfactant in xanthan solutions reaches to the critical association concentration (CAC) between 200 ppm and 1000 ppm SDS concentration. A similar test has been done by Rodrigue and Blanchet (2002) on 0.5% polyacrylamide solution.

The results for affect concentration of solutions and addition of surface active agents on surface tension is consistent with the work of Tzounakos et al. (2004); Margaritis et al. (1999); and Prud'homme and Long (1983). There is only some discrepancy with the latter work for higher concentrations of xanthan gum. Prud'homme and Long (1983) have reported a sharp reduction for 1% xanthan gum solution, while we did not observe such a decrease that concentration. However, using ring the technique for surface tension measurements at high solution concentrations seems to be unsuitable due to the effect of viscous forces on the ring when moving up inside the liquid that can cause false readings.

4.1.2 Rheological Behaviour of Solutions

4.1.2.1 Shear Viscosity of Solutions

Flow curves (shear viscosity vs. shear rate) for different solutions of xanthan gum are plotted in Figure 4.1. The results show that all solutions have shear-thinning behaviour increasing with the concentration of xanthan gum. At small shear rates, all the curves tend to reach a constant value, the so-called zero shear viscosity (μ_0), in Newtonian region where viscosity does not vary with changes in shear rate.

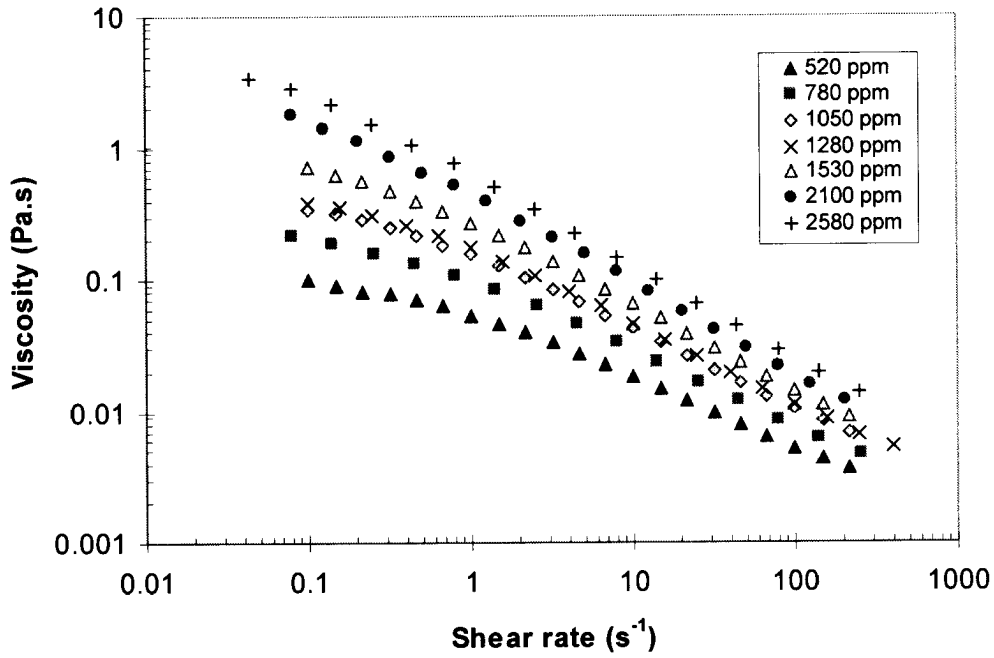

(a)

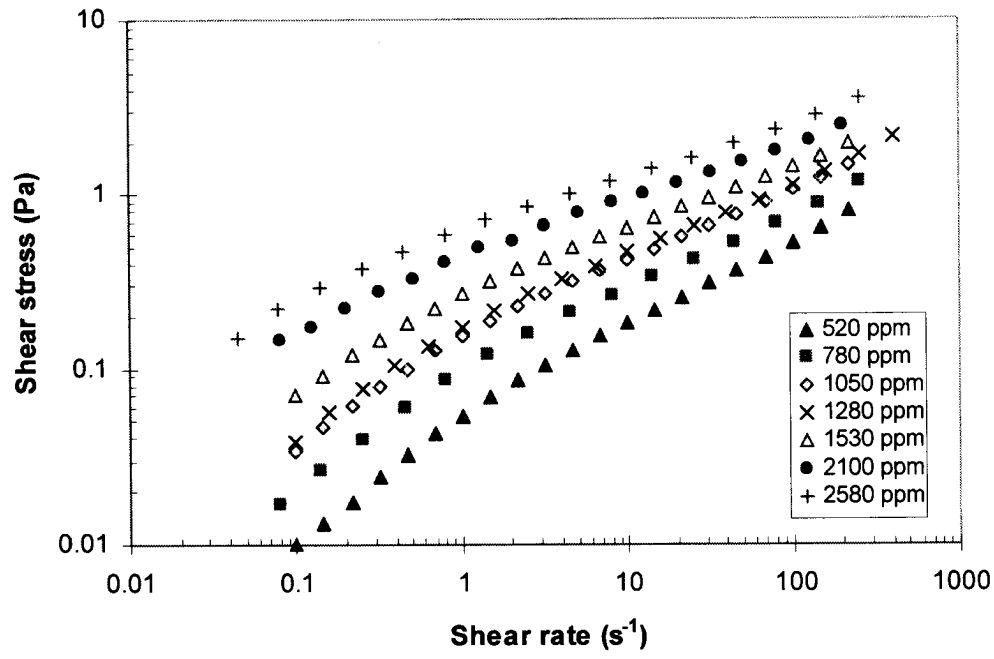

(b)

Figure 4.1(a), (b) Flow curves for various concentrations of xanthan gum.

As discussed in chapter 2, the estimation of shear-thinning behaviour by the power-law model is limited to a narrow range of shear rates, as selecting wider range of shear rates will lead to a poor approximation of fluid behaviour. In this study, the flow curves for xanthan solutions in Figure 4.1 are not linear for the entire range of shear rates. Therefore, the power-law model is not suitable to mathematically describe the behaviour of the solutions. However, this model will be used in calculations for the drag coefficient of bubbles rising in xanthan solutions.

Other viscosity models such as the Ellis or the Carreau models fit better in the flow curve data. The best fitting model can be found by the curve fitting abilities of the software provided by TA Instruments (Orchestrator). Figure 4.2 is an example of curve fitting for the flow curve data of a 520 ppm xanthan gum solution which is approximated by a four-constant Carreau model in the following form:

$$\mu = \mu_0[(1+\lambda\dot{\gamma})^m]^{(n-1)/m} \tag{4.1}$$

This model has been used in different forms by other researchers to fit the data for viscosity curves. For instance, Rodrigue and Blanchet (2002) have used a three-constant Carreau model similar to equation 4.1 with the fourth parameter, m, equal to 2 (m=2). Pilz and Berrn (2007) have used the Carreau model similar to equation 2.7 to approximate the flow curve data for polyacrylamide and polyethylene oxide solutions. The Carreau model (equation 4.1) has a good fit with viscosity data for the 520 ppm xanthan gum solution, and this model is a good approximation for the entire range of shear rates used in the flow curve. The Carreau model parameters have been obtained for the other concentrations of xanthan gum as well as for CMC solutions and the results have been summarized in Table 4.2. The flow curves with the Carreau model

curve fittings for the rest of the aqueous solutions of xanthan and CMC solutions can be found in Appendix A.

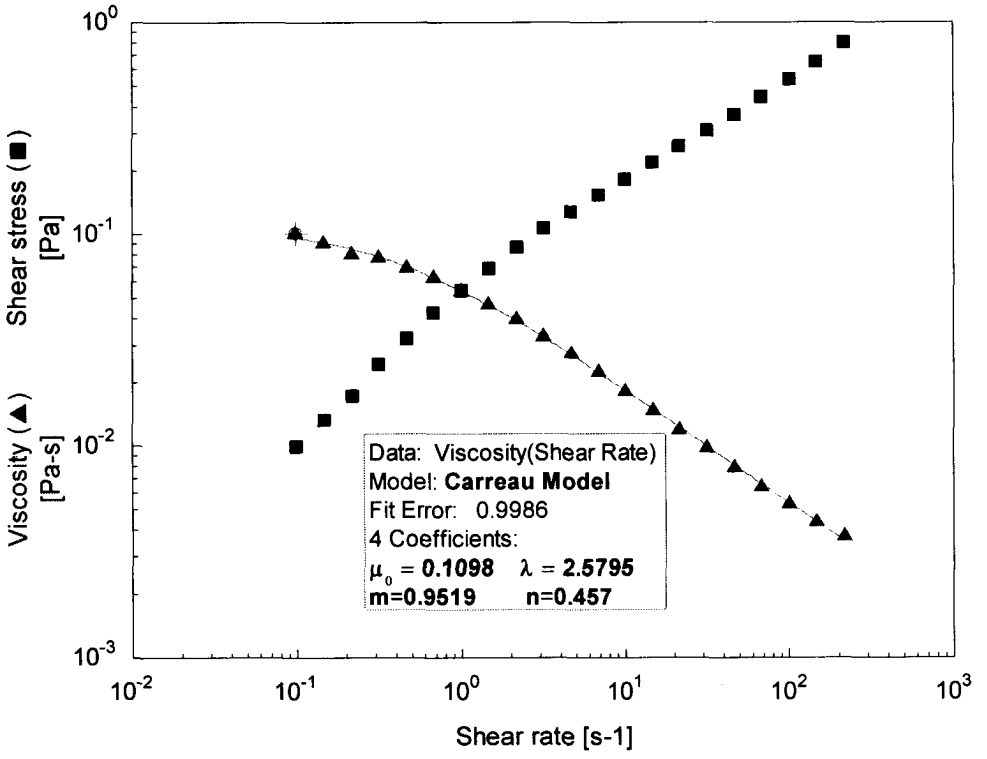

Figure 4.2 The Carreau model curve fitting for viscosity data of 520 ppm xanthan gum solution at 22.5 $^{\circ}C$. The values for zero shear viscosity (μ_0) and time constant (λ) have been calculated as the model's coefficients.

Flow curves for CMC solutions as the second non-Newtonian fluid in this study have been obtained by the ARES rheometer at the working temperature of 22.5 $^{\circ}C$ (Figure 4.3). The Newtonian region where the viscosity is constant at low shear rates is clearly shown in this figure.

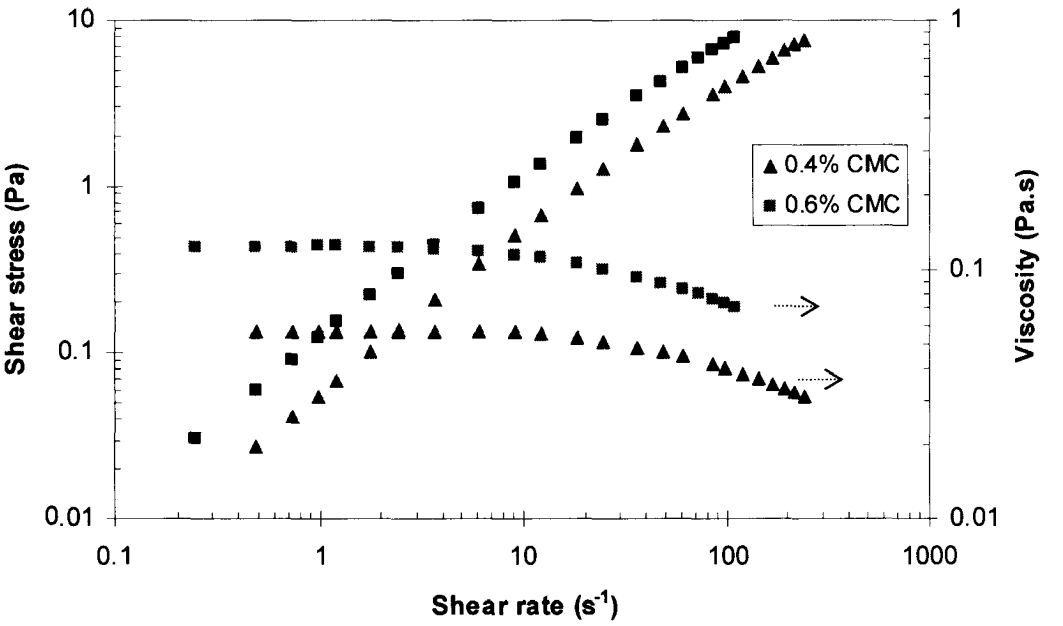

Figure 4.3 Flow curve for CMC solutions including shear stress and viscosity data.

Table 4.2 The Carreau model parameters for xanthan gum and CMC solutions.

Solution	Concentration (ppm)	μ_0 (Pa.s)	λ (s)
Xanthan Gum	520	0.1098	2.5795
	780	0.2994	4.2185
	1050	0.4209	4.1323
	1280	0.4555	4.2987
	1530	0.9429	5.8138
	2100	2.7365	12.7440
	2580	4.7943	16.9030
CMC	4000	0.0563	0.0287
	6000	0.1240	0.0535

4.1.2.2 Dynamic Strain Sweep Test

The purpose of doing the strain sweep test is to determine the limits of linear viscoelasticity for xanthan gum solutions. Figure 4.4 shows that for a 2100 ppm xanthan solution, the linear values start from below 1% strain and is on up to 100% strain. For this reason, a 10% strain has been selected as a constant value for all other dynamic measurements.

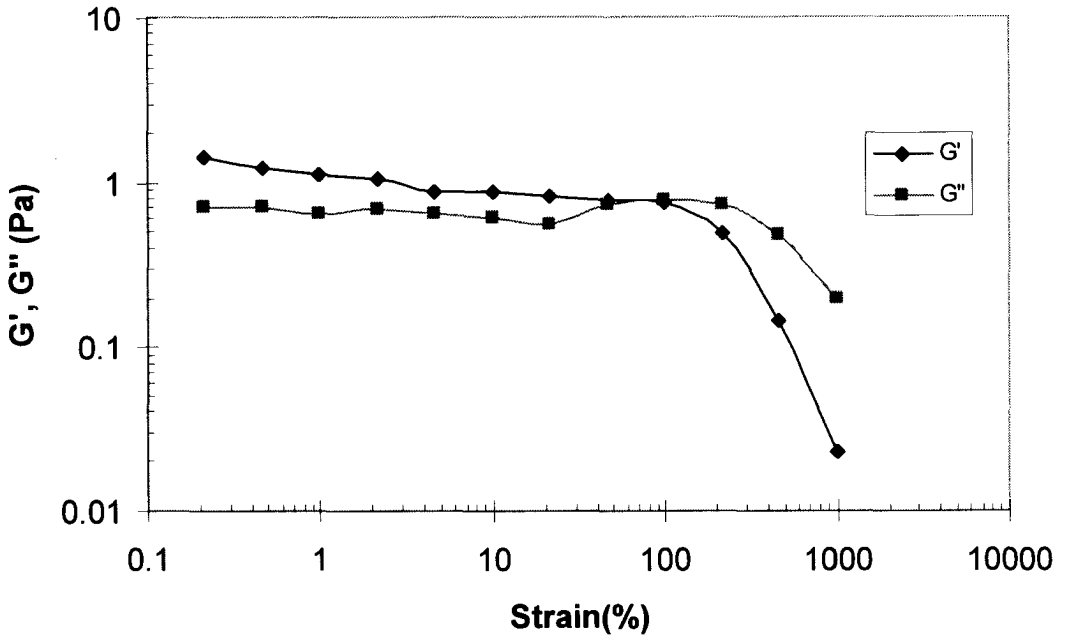

Figure 4.4 Strain sweep test for 2100 ppm xanthan gum solution to find the linear viscoelasticity limit.

4.1.2.3 Dynamic Frequency Sweep Test

In reality, all fluids exhibit elastic behaviour even pure Newtonian fluids. But, for practical purposes, it is convenient to neglect this behaviour and assume that viscous fluids have no elasticity. Most of polymers and biopolymers such as xanthan gum are typical material showing both viscous and elastic behaviours as a response to an applied force at the same time. This combined behaviour is termed viscoelasticity.

The effect of elastic forces on the bubbles rise velocity or the effect of the degree of viscoelasticity of the fluids is one of the main hypotheses in the literature for the existence of the jump discontinuity.

One of the ways to determine the degree of viscoelasticity of a material is to measure the elastic modulus (G') and the viscous modulus (G'') which are the ratio of the elastic stress to strain and of the viscous stress to strain, respectively. G' represents the ability of the material to store energy elastically, and G'' is the measure of the ability of the material to dissipate energy.

The frequency sweep test is a dynamic measurement method to determine the elastic and viscous moduli by analyzing time and frequency dependence of the material in oscillatory deformation. The crossover of the two moduli gives a time characteristics of the fluid where the elastic behaviour of the material overcomes the viscous behaviour. This can be called the fluid's relaxation time. The latter has been measured through the frequency sweep test for xanthan gum and CMC solutions. The results of the tests are given in Figure 4.5, as an example, and in Table 4.3, which is consistent with the work of Milas and Rinaudo (1990). The rest of the figures for this test can be found in Appendix C.

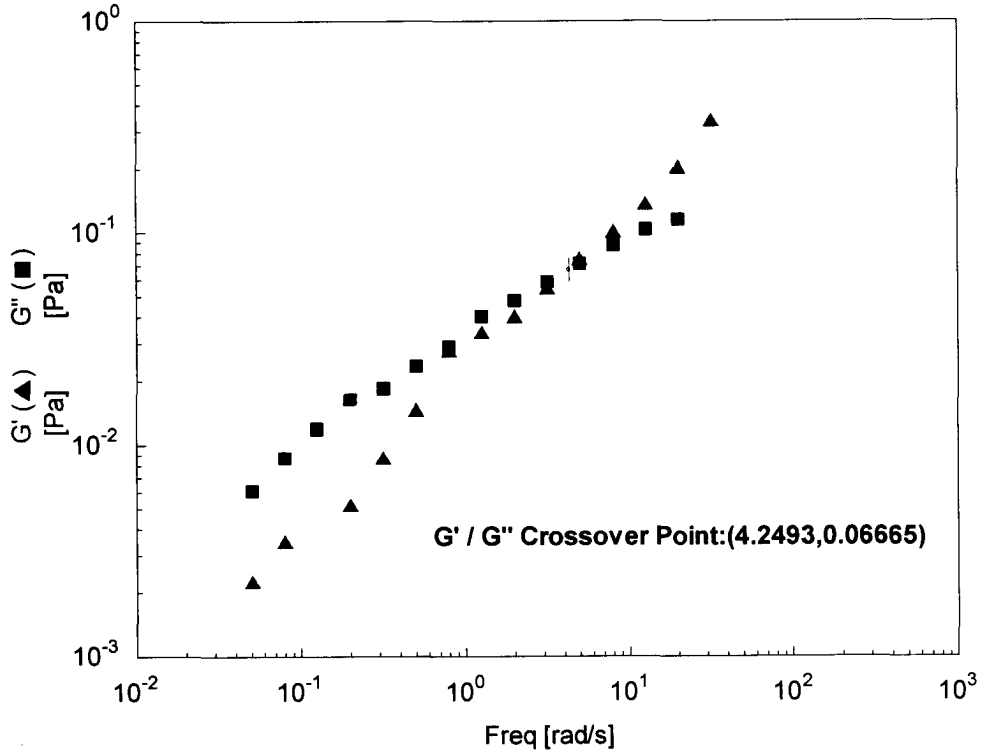

Figure 4.5 Frequency sweep test for 520 ppm xanthan gum aqueous solution. The crossover in the graph gives a time characteristics of the material, in which, elastic forces are acting more than viscous forces.

Table 4.3 Elastic modulus (G') and viscous modulus (G'') crossover results.

Solution	Concentration (ppm)	G', G" Crossover (rad/s)	G', G" Crossover (Hz)	**Relaxation Time** (s)
Xanthan Gum	520	4.2943	0.68365	1.46
	780	1.2836	0.20435	4.89
	1050	0.8795	0.14002	7.14
	1280	0.9558	0.15216	6.57
	1530	0.6369	0.10139	9.86
	2100	0.3121	0.04969	20.13
	2580	0.2436	0.03878	25.79
CMC	4000	33.466	5.32779	0.19
	6000	29.712	4.73015	0.21

4.1.2.4 First Normal Stress Difference Measurement

Normal forces are very small for low concentrations of xanthan gum and CMC. Measuring these forces at very low shear rates was outside the sensitivity of the rheometer. Therefore, all the measurements for first normal stress differences (N1) have been done at moderate shear rates ($\dot{\gamma} = 5 - 200 \ \ s^{-1}$) and the results have been extended to the entire working area through the power-law model (Rodrigue and De Kee, 1999) defined by:

$$N1 = a\dot{\gamma}^{b} \tag{4.2}$$

Figures 4.6 and 4.7 illustrate the first normal stress difference for xanthan gum and CMC solutions, respectively, represented by the power-law model.

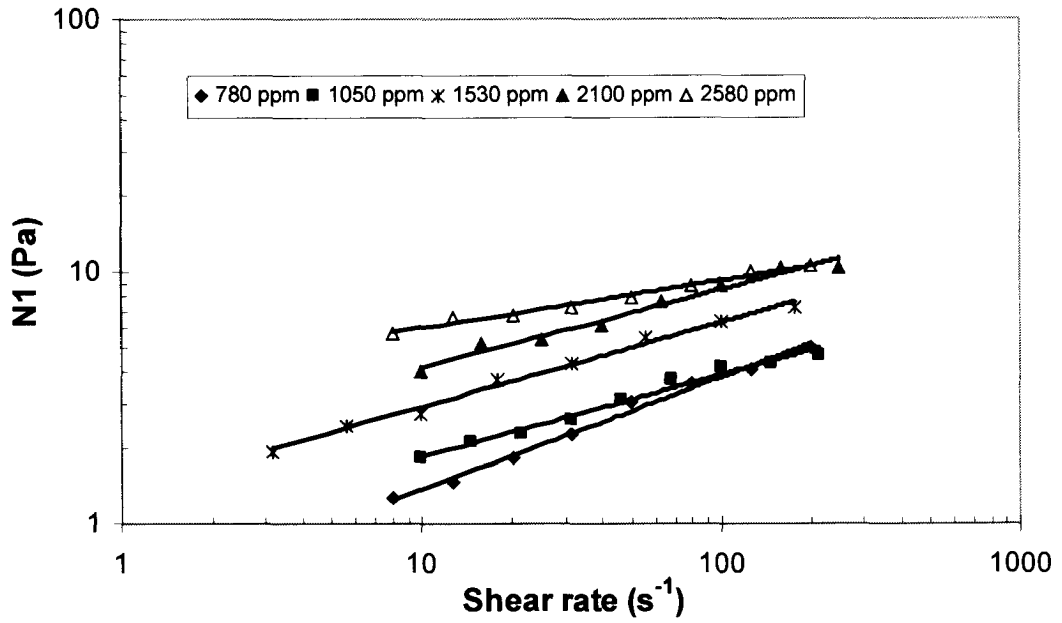

Figure 4.6 First normal stress difference data for different concentrations of xanthan gum at moderate shear rates.

Comparing the magnitude of normal forces in xanthan gum solutions and 0.5% PAA (polyacrylamide) in 20/80 glycerin/water solutions in the work of Rodrigue and Blanchet (2002), it is clear that normal forces are very small in xanthan solutions. In PAA solutions, N1 reaches up to a couple of thousands Pascal, while in the working xanthan gum solutions it does not exceed 15 Pa.

Macosko (1994) has measured the primary normal stress differences of 2% PAA and 3% xanthan gum solutions which have similar shear viscosities and has got bigger values for the PAA solution in comparison to xanthan gum. This is consistent with our results.

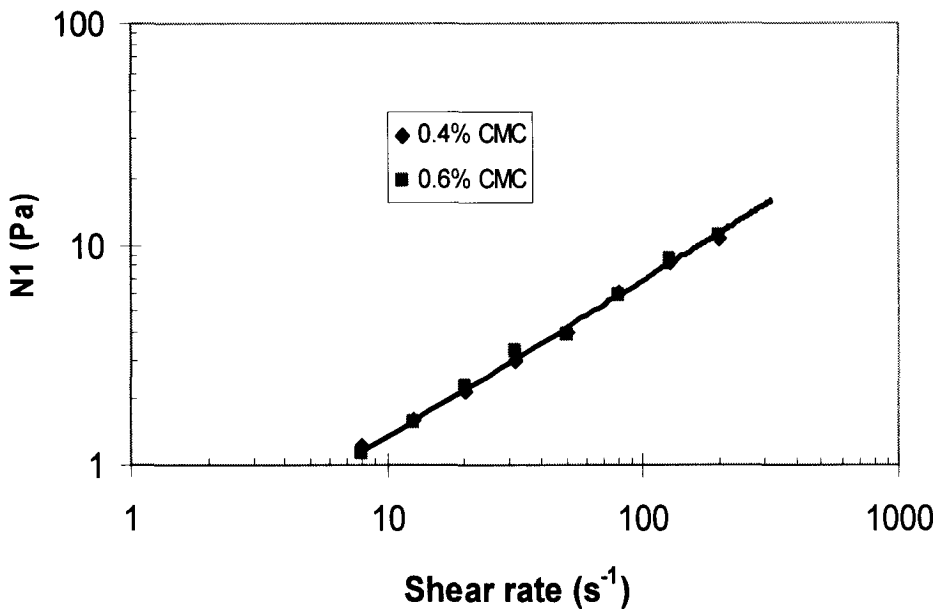

Figure 4.7 First normal stress difference (N1) data for CMC solutions represented by the power-law model

The results for power-law coefficients, a and b, representing the first normal stress differences for xanthan gum and CMC solutions are summarized in Table 4.4.

Table 4.4 N1 represented by Power-law model ($N1 = a\dot{\gamma}^b$).

Solution	Concentration (ppm)	a ($Pa.s^b$)	b -
Xanthan Gum	520	-	-
	780	0.4985	0.4413
	1050	0.8767	0.3239
	1530	1.3549	0.3334
	2100	2.0561	0.3082
	2580	3.8692	0.1889
CMC	4000	0.2825	0.6880
	6000	0.2637	0.7086

4.2 Bubbles Behaviour in Xanthan Gum and CMC Solutions

4.2.1 Formation of Bubbles in Xanthan and CMC Solutions

Photographs in Figure 4.8 display the bubble formation stages in an orifice in 100 ppm xanthan gum solution, which are observed by a high-speed image camera at 500 frames per second.

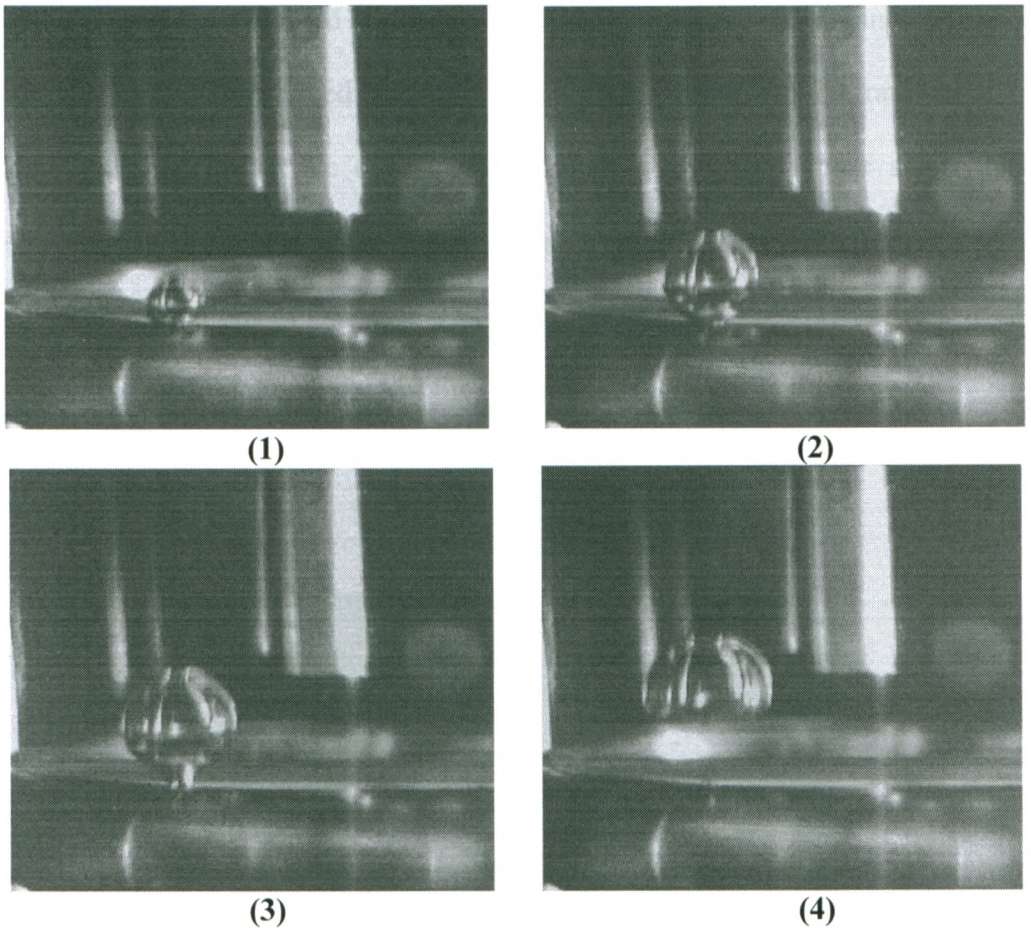

Figure 4.8 Bubble formation stages in an orifice of diameter 1.5 mm submerged in 100 ppm xanthan gum solution. Photographs have been taken by a high-speed camera at 500 frames per second.

The bubble formation stages in xanthan gum solutions are consistent with the theory of bubble formation in an orifice described in the previous chapters (Chhabra and De Kee, 1992). The expansion and detachment sequences for bubble formation are clearly shown in distinct slides in Figure 4.8.

Bubbles formed from an orifice with a constant flow rate of air, rise in a chain of same size bubbles in the surrounding fluid. The size of the bubbles depends on different parameters such as orifice diameter, surface tension of the continuous phase, and pressure difference of air through orifice.

In this study, we have applied the concept of bubble formation in making bubbles with known volumes. As described before, by maintaining very low flow rates of air with constant pressure inside the experimental column, constant-volume small bubbles were created and collected in the bubble release system (Figure 4.9). The time interval between the formations of two successive bubbles was adjusted by the pressure of the inlet air with respect to the height of the liquid in the column.

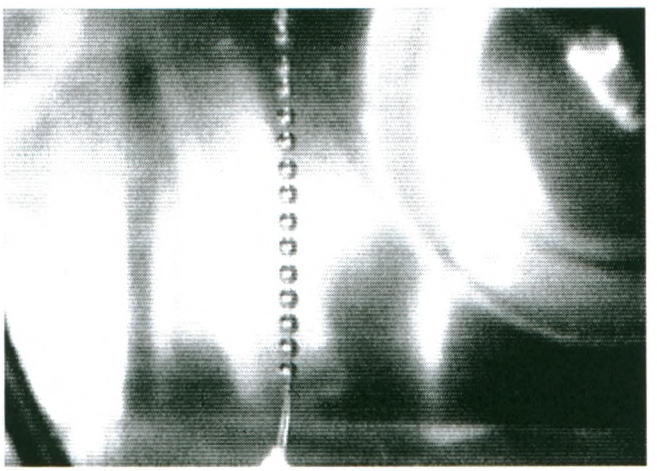

Figure 4.9 'Constant-Volume' method for creating bubbles with known volumes. Time interval between two successive bubbles in the experiments was around 10 seconds.

To our knowledge, this method has been used for the first time in this study for making bubbles with known multiples of a small constant-volume bubble. In this approach, even without knowing the real volume of bubbles, which depends on the

volume of created small single bubbles in the orifice, one can use the volume data to compare the results for rise velocity or any other hydrodynamic characteristic of the bubbles with each other for different multiples of unit volume.

The method of 'constant-volume' has been used in rise velocity measurements for 780 ppm xanthan gum and also for CMC solutions which are transparent and easy to apply this method by observing and counting the number of created constant-volume bubbles.

4.2.2 Rise Velocity of Bubbles

Basically, when talking about the rise velocity of bubbles, what all researchers consider is the vertical distance covered by the rising bubbles between two points over the time regardless of the trajectory of the bubbles. Rise velocity of the bubbles is dependent on a variety of parameters such as physical and rheological properties of the surrounding fluid, presence of surfactants, concentration of the continuous phase, volume of the bubbles, etc.

Generally, small bubbles with spherical shape have linear trajectories and big bubbles with moving boundaries have non-linear trajectories when rising in liquids. By changing the volume of the bubbles, their velocity also changes. Different trajectories for different sizes of bubbles lead to different vertical and instant velocities.

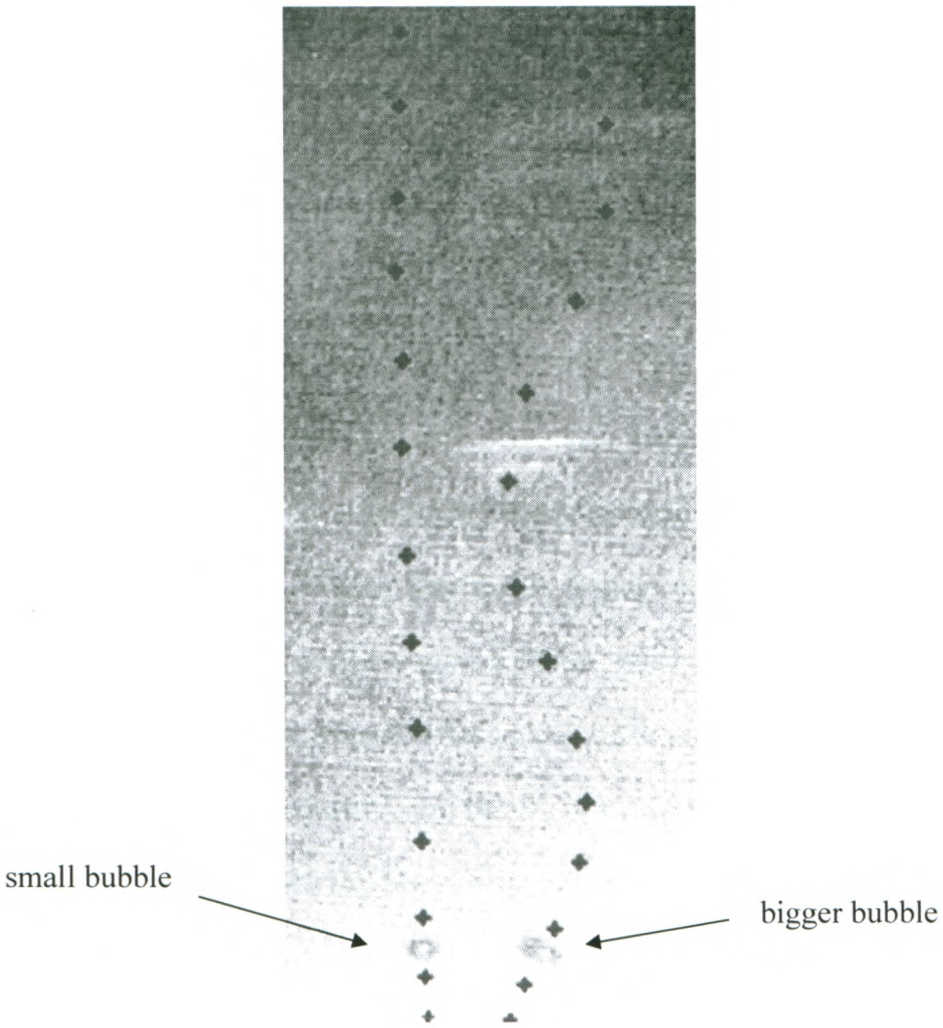

Figure 4.10 A comparison for the rise velocity of two bubbles with different volumes in a 520 ppm aqueous solution of xanthan gum with different trajectories. Considering the vertical velocity, these two bubbles have equal vertical velocities, while they have different instant velocities.

For instance, Figure 4.10 illustrates the trajectories of two bubbles with different sizes rising in a 500 ppm xanthan gum solution. The bigger bubble has a non-linear trajectory, while the small bubble has a vertical path. However, the rise velocities of both of them are equal when considering the vertical distance through which they have moved. This is the basis for all of the rise velocity measurements in this study.

4.2.2.1 Effect of Height on the Rise Velocity of Bubbles

The influence of height on rise velocity of bubbles was determined using two high speed cameras simultaneously at different heights to track the same bubble at different levels in the experimental column. The results (Figure 4.11) clearly proved that the rise velocity of bubbles in xanthan gum solutions reaches a velocity plateau at the height of 50 cm above the release point in our experimental set-up. Based on this result, for the rest of experiments, the camera was located at this height to ensure reaching the constant velocity that is termed 'terminal velocity'.

4.2.2.2 Effect of Injection Period

Using the 'constant volume' method for generating bubbles with desired volumes is a time consuming practice especially for big bubbles. This shortcoming for the bubble generation method in this study was kind of beneficial in maintaining enough time between two sets of rise velocity measurements. This ensured having a quiescent liquid in this study avoiding the history of movement of bubbles in non-Newtonian fluids (Rodrigue et al., 1996).

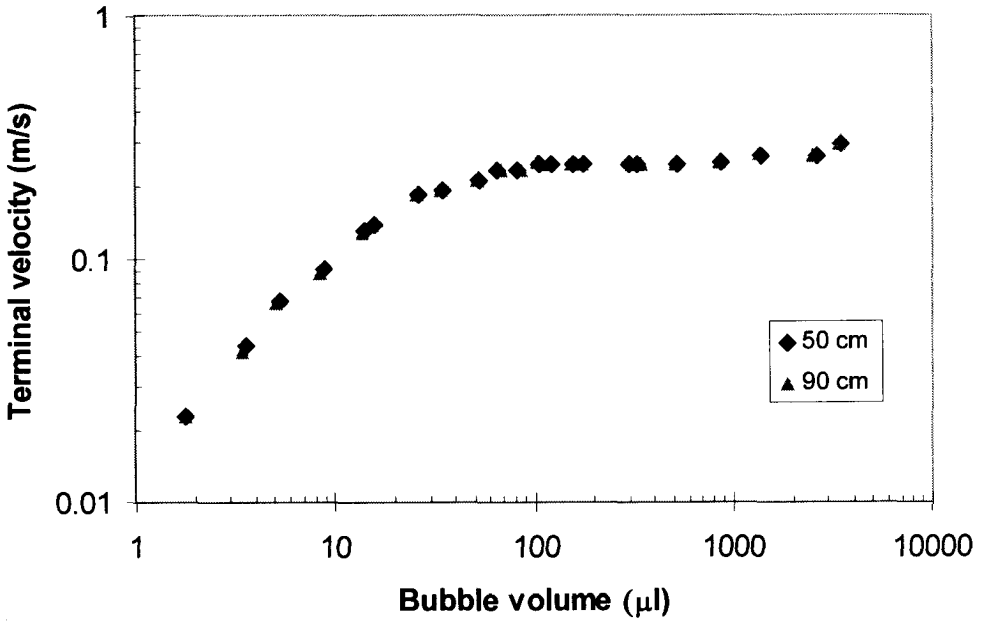

Figure 4.11 Effect of height on the rise of velocity of bubbles in 1530 ppm xanthan gum aqueous solution.

4.2.2.3 Bubbles Terminal Velocity versus Volume

Terminal velocities of single air bubbles in seven different xanthan gum solutions were measured. For each concentration, the velocity of bubbles had a sharp increase up to a certain level of bubble volume, and a very slight decrease afterwards, and then a slight increase at the higher volumes. However, no abrupt change was observed in all concentrations.

As the concentration of solutions was increasing, the terminal velocity of the same size small bubbles was decreasing because of the higher viscosities. For instance, a bubble with the volume of 8 microlitre has a terminal velocity around 28 cm/s in 520

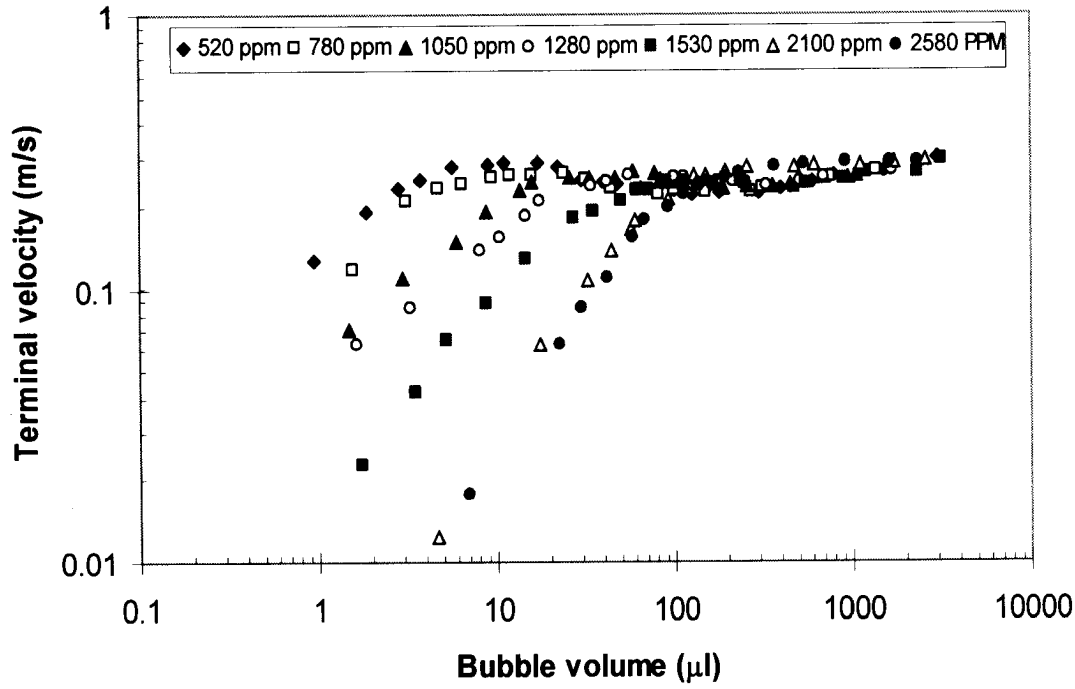

Figure 4.12 Rise velocity of different size bubbles in aqueous solutions of xanthan gum.

ppm xanthan gum, whereas at the highest working concentration of xanthan, which was 2580 ppm, the terminal velocity drops more than 90% to approximately 2 cm/s.

The dramatic decrease in the rise velocity for small bubble volumes at higher concentrations of xanthan gum is due to the increase in the viscous drag of the bubble with an increase in the concentration of the solutions. Comparing the results for zero shear viscosity in Table 4.2 that is given at low shear rates or low Reynolds numbers, the amount of zero shear viscosity at 2580 ppm xanthan gum solution is around 50 times more than the zero shear viscosity of the 520 ppm solution.

The rise velocity of the discussed bubble (8 microlitre) drops to 25 cm/s, 21cm/s, 14 cm/s, 9 cm/s, and 3 cm/s for 780 ppm, 1050 ppm, 1280 ppm, 1530 ppm, and 2100 ppm xanthan gum concentrations, respectively. As the volume of the bubbles increases, the velocities of the bubbles reach constant values between 25 to 30 cm/s for all concentrations of xanthan gum, which corresponds to the constant drag due to negative wake behind the big bubbles at Reynolds numbers between 30 and 135.

The results for the rise velocity-volume experiments for xanthan gum and CMC solutions are summarized in Figures 4.12 and 4.13, respectively.

No discontinuity was observed for the working concentrations of CMC solutions as well. The shape of the log-log rise velocity versus volume graph for the bubbles in CMC solutions was almost similar to the one for xanthan gum solutions. The only difference was that for xanthan solutions a slight decrease in the velocity of bubbles was observed for bubble volumes around 50 μl to 300 μl, but the velocity of bubbles was increasing in this range reaching a velocity plateau for the bigger bubbles at around 30 cm/s.

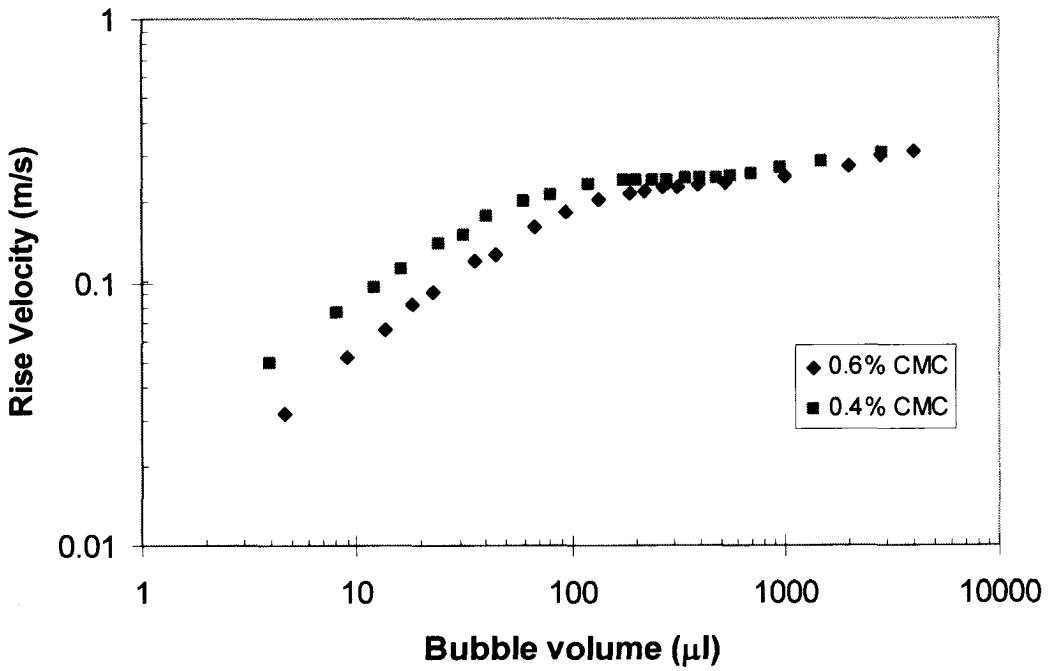

Figure 4.13 Rise velocity-Volume data for aqueous solutions of CMC.

4.2.2.4 No-jump Velocity for the Bubbles

As described earlier, there is no consensus of opinions among the researchers on the jump discontinuity in the volume-velocity curves of bubbles in non-Newtonian fluids. It is clear that bubbles are not meticulous in selecting the type of non-Newtonian fluid to make a jump in their rise velocity, and there must be a rule for bubble behaviour in all fluids. The only agreement between researchers is in the effect of elastic forces, or degree of viscoelasticity of the fluids that might affect the existence of the jump phenomenon.

Recently Pilz and Brenn (2007) connected the relaxation of stresses in elongational flow to the physics of the jump. They have suggested a dimensionless number based

on the rheological and physical properties of the solutions for the occurrence of the jump velocity in the following equation:

$$\Pi = \lambda_E (g^3 \rho_l / \sigma)^{1/4} \tag{4.3}$$

in which, $\Pi > 9.8938$ is required for the jump to occur.

For the xanthan gum and CMC solutions in this study, the part of equation 4.2 containing density (ρ_l) and surface tension (σ), is almost a constant number considering an average density of 999 kg/m^3 and surface tension of 71 mN/m using the data from Table 4.1:

$$(g^3 \rho_l / \sigma)^{1/4} \approx 60.3 \tag{4.4}$$

Therefore, to fulfill the jump condition, the relaxation time of the solutions in elongation (λ_E) needs to be more than 0.164 seconds in the latter hypothesis. Considering $\lambda < \lambda_E$ (relaxation time in elongation is bigger than relaxation time obtained from a viscometer (Stelter et al. (2002)) and using the relaxation time data obtained for the xanthan gum and CMC solutions in Table 4.3, the jump discontinuity should happen in both CMC and xanthan gum solutions having the relaxation times more than 0.164 seconds. This is not in agreement with the experimental results for the rise velocity of the bubbles in these solutions given in Figures 4.12 and 4.13. However, using the Carreau model relaxation time given in Table 4.2, the CMC solutions have smaller relaxation times than 0.164, and therefore, no discontinuity should occur in these solutions. For this case, the prediction of equation 4.3 is consistent with the experimental data. Thus, it can be concluded that the jump prediction by Equation 4.3 may vary depending on the type of the time characteristics of the material.

4.2.3 Drag Coefficient of Air Bubbles in Xanthan Gum Solutions

The drag coefficient-Reynolds number data have been calculated according to the approach offered by Karamanev (1994) and Margaritis et al. (1999) as described in the literature review section using equations 2.26 and 2.28.

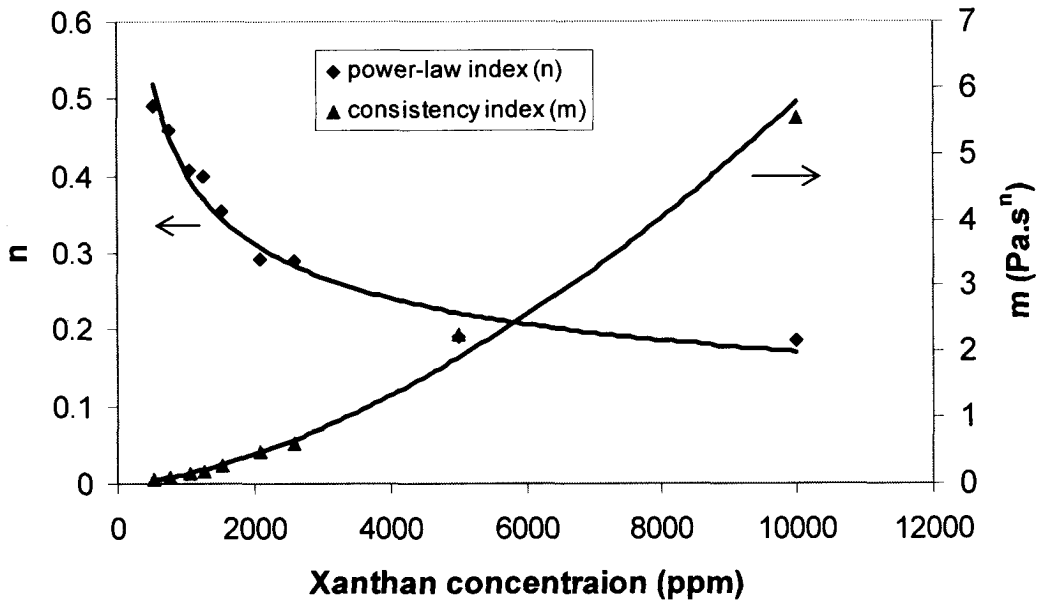

Figure 4.14 Power-law model coefficients, flow index (n) and consistency index (m), for xanthan gum solutions to be used in drag coefficient calculation.

To calculate the Reynolds number based on equation 2.22, the values of n and m have been obtained from flow curves at moderate shear rates. Figure 4.14 shows the changes in the power-law coefficients with the concentration of xanthan gum solutions. All of the flow curves along with the power-law model match of the shear

stress-shear rate data as well as the results for power-law constants are given in Appendix B.

The results show that the drag coefficients at different concentrations are almost in a single line at the Reynolds numbers below 60 (Re < 60). For the Reynolds numbers higher than 60, the drag coefficient data points are scattered around the constant value of 0.95 (Figure 4.15). For the CMC solutions, the drag coefficient results (Figure 4.16) have a good agreement with the bubble drag curve offered by Margaritis et al. (1999).

4.3 Effect of surfactants on the rheology of xanthan gum solutions

4.3.1 Effect of surfactant on viscosity

Sodium dodecyl sulfate (SDS) was used as a surfactant at concentrations between zero and 1000 ppm for 0.5% xanthan gum solution to study the effect of surface tension reduction on rheology and viscoelasticity of xanthan solutions.

Figure 4.17 shows that the addition of surfactants in xanthan gum solutions in the shear rate between $0.06\,s^{-1}$ and $300\,s^{-1}$ has no effect on the viscosity of the solutions. This result is consistent with the report of Rodrigue and Blanchet (2002) for 0.5% PAA solution at the same shear rates with the difference that at lower shear rates, a substantial decrease in zero shear viscosity was observed by them which is not covered in this study.

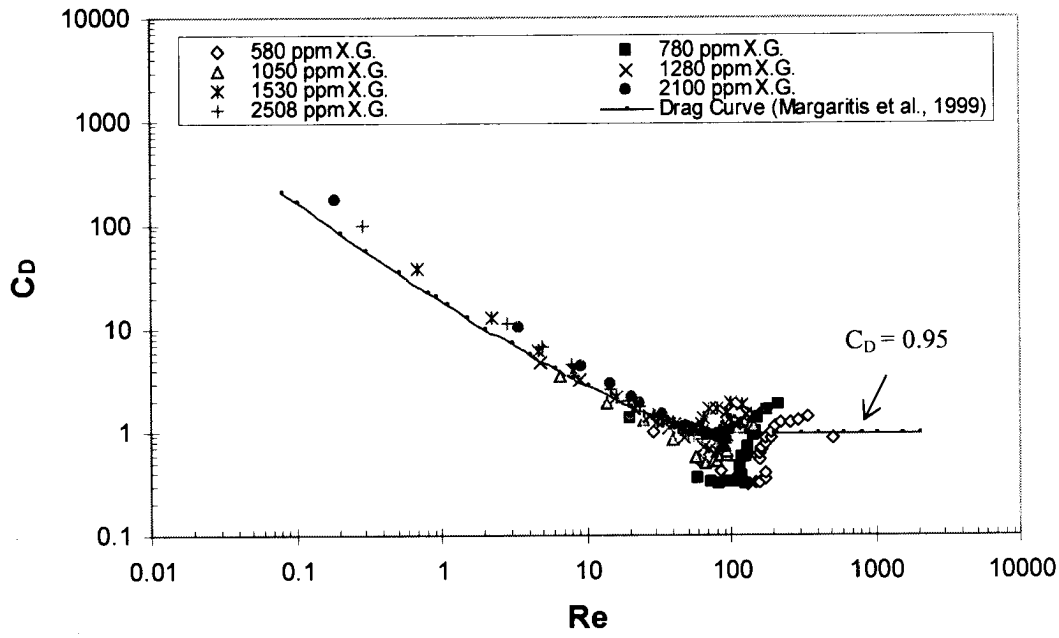

Figure 4.15 Drag coefficient-Reynolds number curve for xanthan gum solutions.

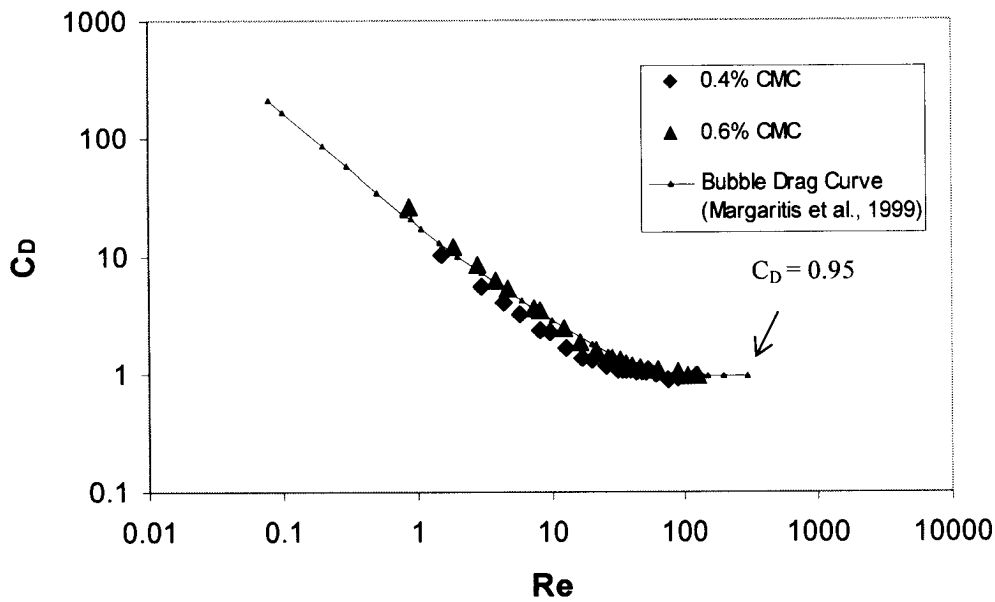

Figure 4.16 Drag coefficient vs. Reynolds number for the CMC solutions.

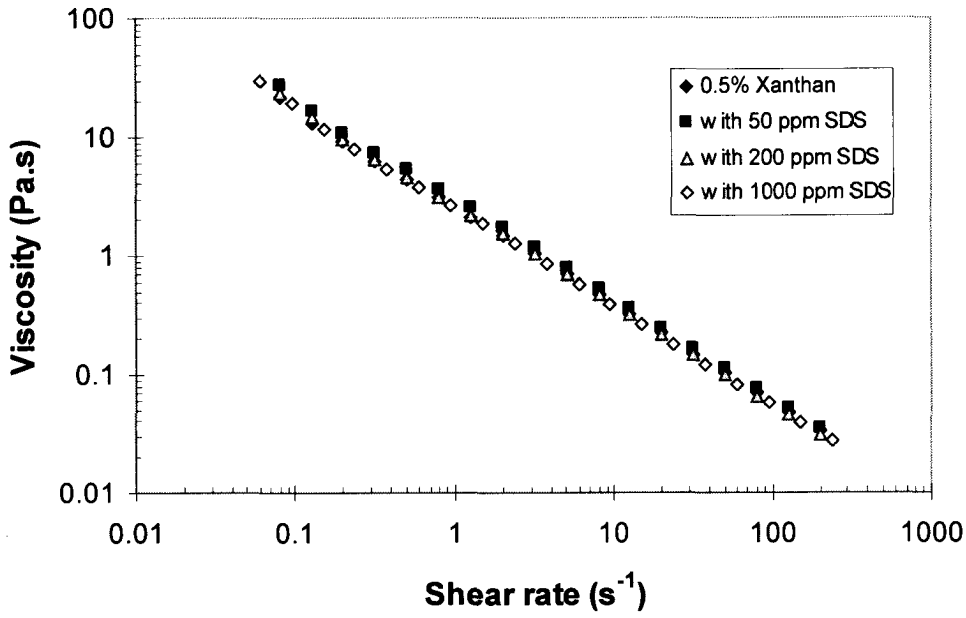

Figure 4.17 Effect of different concentrations of surfactant (SDS) on viscosity of 0.5% xanthan gum solution.

4.3.2 Effect of Surfactant on Normal Forces

Fig 4.18 shows that normal forces decreased by adding SDS to 0.5% solution of xanthan gum. However, the increase in the concentration of surfactant did not have a significant effect on the first normal stress differences (N1). The reduction of normal forces by adding surfactants is not completely consistent with the results of Rodrigue D. & Blanchet J. (2002) for 0.5% PAA/SDS solutions, in which a single set of data has been obtained for all PAA/SDS solutions.

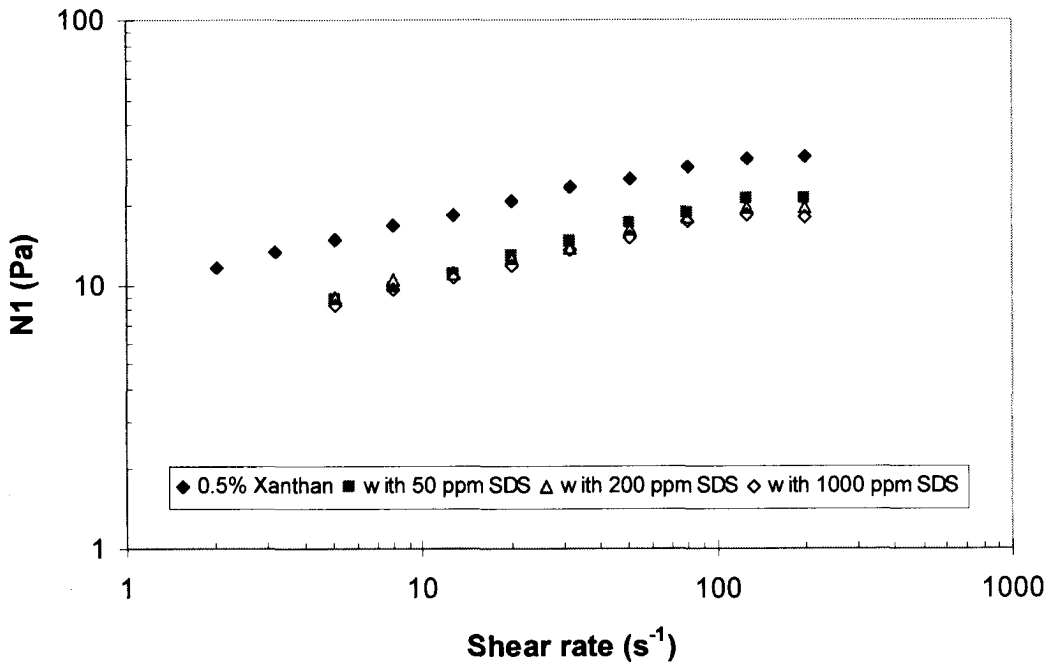

Figure 4.18 Effect of surfactant on the first normal stress difference for a 0.5% xanthan gum solution.

4.3.3 Effect of Surfactants on Relaxation Time

The time dependent behaviour of xanthan gum solutions by adding surfactants has been investigated by the normal force relaxation time test. As described in chapter 3, this test gives the time required for a material to relax after a deformation, and it is an alternate approach to the frequency sweep test giving the relaxation times for the solutions after a step strain applied to them.

The normal relaxation result for a 0.5% xanthan gum is given if Figure 4.19. The same test has been performed by adding different concentrations of SDS to this solution and the results are given in Appendix F. The relaxation time obtained had a slight decrease from 2.7 to around 2.1 seconds for 50 ppm SDS concentration, and then increased up to 4.5 seconds when 1000 ppm SDS added to the solution. The final results for this test can be seen in Table F.1 (Appendix F).

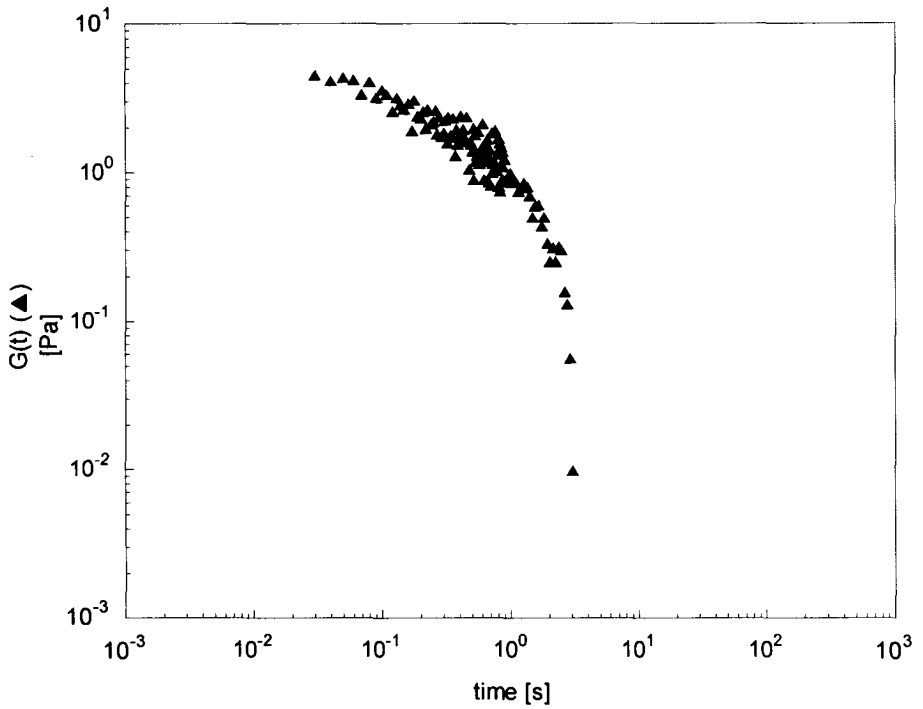

Figure 4.19 Normal relaxation test for a 0.5% xanthan gum solution.

4.4 Shape and Trajectory of Bubbles

The bubbles shape and trajectories varied for different xanthan gum and CMC solutions. Depending on the concentration of the solutions, the shape of the bubbles changed from spherical to ellipsoidal and spherical cap for different volumes of the bubbles. Figures 4.20 and 4.21 show the shapes of the bubbles encountered in this study at 1530 ppm xanthan gum and 0.6% CMC solutions, respectively.

The bubbles in CMC solutions had the typical shape change from spherical to spherical with cusp at the back end, and then to ellipsoidal and finally to spherical cap by increasing their volume. The same shape change regime was observed for the bubbles in xanthan gum solutions with the difference that the big bubbles did not have the exact spherical cap shapes as the same size bubbles in CMC solutions. This is discussed more in terms of an experimental parameter called 'aspect ratio' in the next section of this chapter. The trajectories of the bubbles were different depending on their size and the concentration of the solutions. For spherical bubbles whose boundaries with the continuous phase were like a rigid solid, the trajectories were in a straight (rectilinear) upward line. But, for the bigger bubbles with moving interfaces, the trajectories were non-linear with zigzag or spiraling path of movement (based on the top-view photographing). Figure 4.22 shows two bubbles rising in a 520 ppm xanthan gum solution with different trajectories. The deviation from rectilinear trajectory is more for the bigger bubble with ellipsoidal-like shapes in this figure. For the lower concentrations of xanthan gum solutions, non-spherical shapes with non-linear trajectories were started from smaller size bubbles in comparison to the higher concentrations.

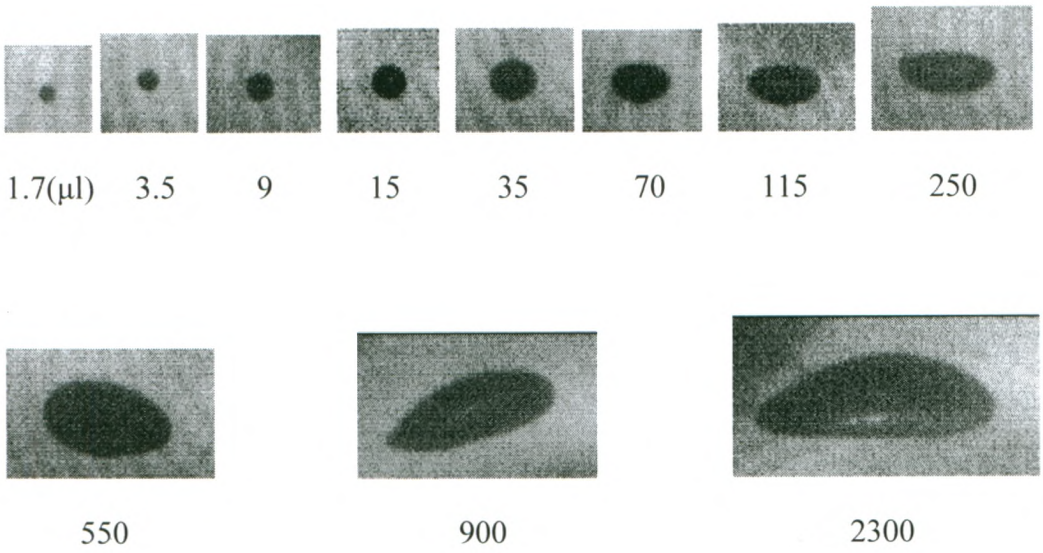

Figure 4.20 Shape of the bubbles encountered in 1530 ppm xanthan gum solution. Using the scale in the bottom of the figure, the approximate diameter of different size bubbles can be compared.

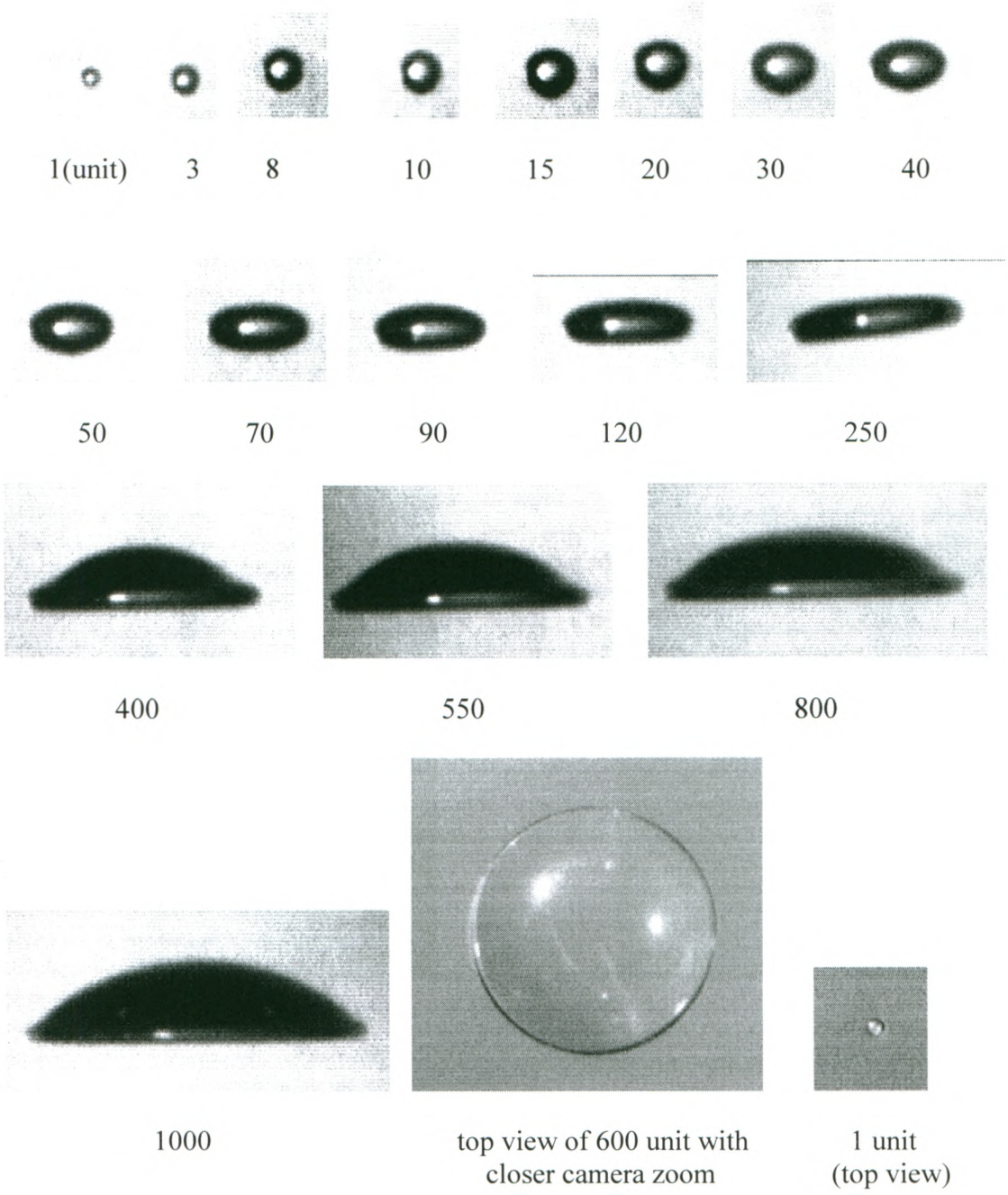

Figure 4.21 Shape of the bubbles encountered in 0.6% CMC aqueous solution. Volume of the bubbles are multiplies of the first bubble's volume which is the unit volume equal to 4.61 μl.

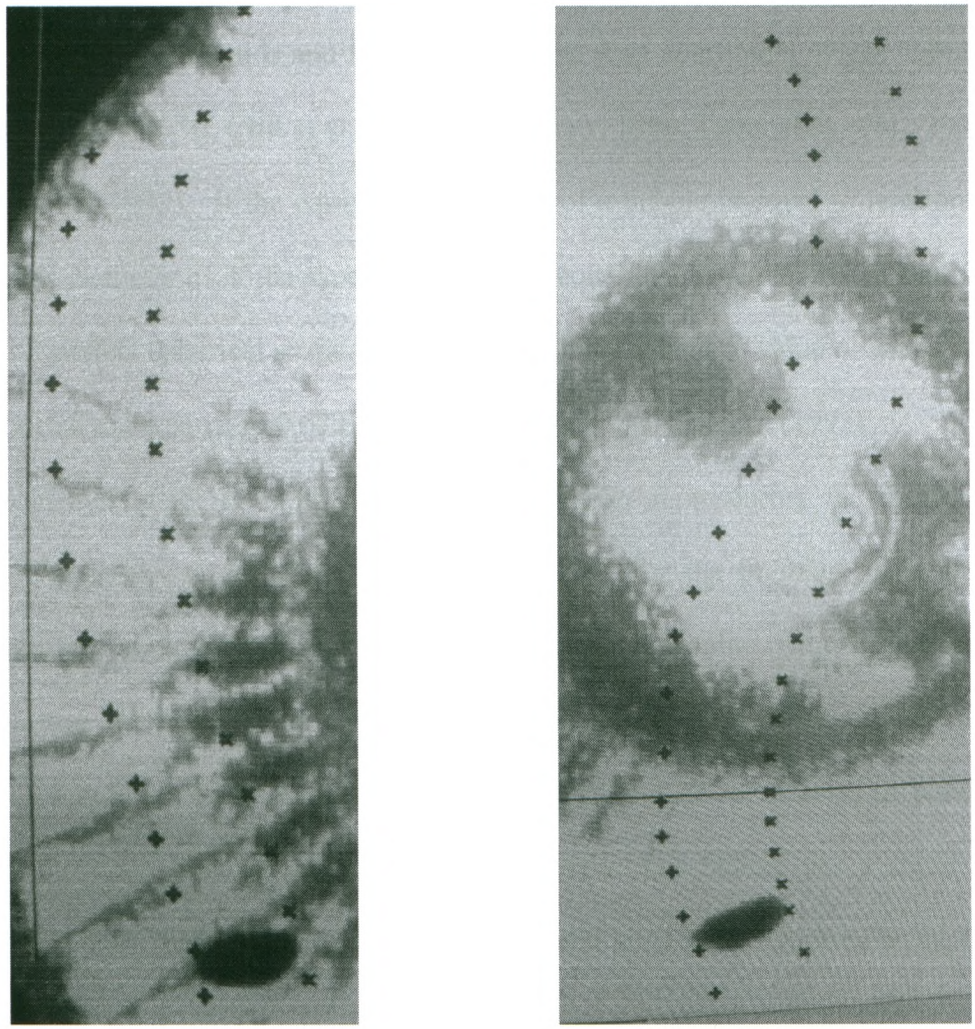

(a) (b)

Figure 4.22 Trajectory of bubbles in 520 ppm xanthan gum solution. (a)19 μl (b) 38 μl bubble volume (at a different camera zoom).

4.4.1 Aspect Ratio (d_e / d_h) versus Equivalent Diameter (d_e)

The experimental aspect ratio (d_e/d_h) is a criterion used by the researchers for studying the shape of bubbles in liquids and for calculating the drag coefficient of gas bubbles (Davies and Taylor, 1950; Clift et al., 1978; Karamanev, 1994; Tzounakos et al., 2004; Margaritis et al., 1999). If the equivalent diameter of a bubble is equal to horizontal (or projected) diameter of it, the aspect ratio will be equal to 1.0, which means that the bubble has a perfect spherical shape. For spherical cap bubbles, the value of the aspect ratio is reported to be equal to 0.62 by Clift et al. (1978) and Chhabra (1993).

The horizontal diameter is another important parameter representing the projected diameter of bubbles in liquids on a horizontal plane. For the bubbles rising in a straight path in liquids, the horizontal diameter is a constant value. But, for the non-linear-trajectory bubbles, the projected diameter is not constant with the upward motion of the bubble. This has been illustrated in Figure 4.23 for a 2000 μl bubble rising in a 0.6% CMC solution shown from top view. The bubble has a spiral 3-dimensional motion and its projection on a horizontal surface is not circular all the times.

Therefore, in the calculation of horizontal diameter for a non-spherical bubble with a non-linear trajectory, an average projected diameter ($\bar{d}_h$) of the bubble has been considered as the final horizontal diameter for the drag coefficient calculations. It is important to consider the entire repeating period of the trajectory of the bubble by having a wider field of focus of the camera to get more accurate results for the horizontal diameter.

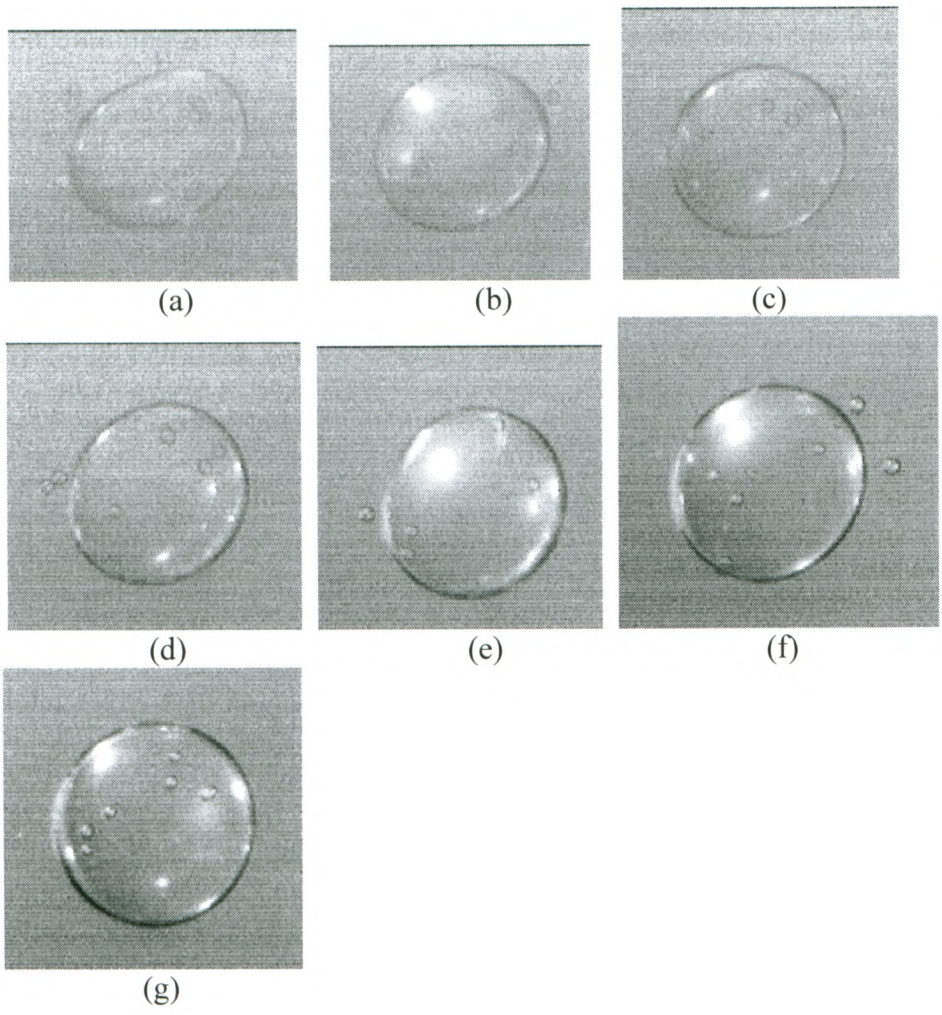

Figure 4.23 Top view of a 2000 µl bubble rising in 0.6% CMC solution. The projected diameter of the bubble varied with the upward movement of bubbles in a non-linear trajectory from (a) to (g).

Figure 4.24 shows the data points obtained for the aspect ratio ($d_e / \bar{d}_h$) versus equivalent diameter (d_e) for 2100 ppm and 2580 ppm xanthan gum solutions. The changes in the aspect ratio were almost constant for the both solutions. However, for lower concentrations of xanthan gum, the data did not math in a single line. This was due to the narrow region of vertical-trajectory bubbles in the lower concentration solutions as well as the trajectory-dependent average horizontal diameter ($\bar{d}_h$) of the studied bubbles.

The shape and trajectory changes for the bubbles are marked on Figure 4.24. The transition from spherical bubbles region to ellipsoidal bubbles region was from about 0.5 cm for the bubbles diameter (the equivalent diameter is equal to the real diameter for the spherical bubbles).

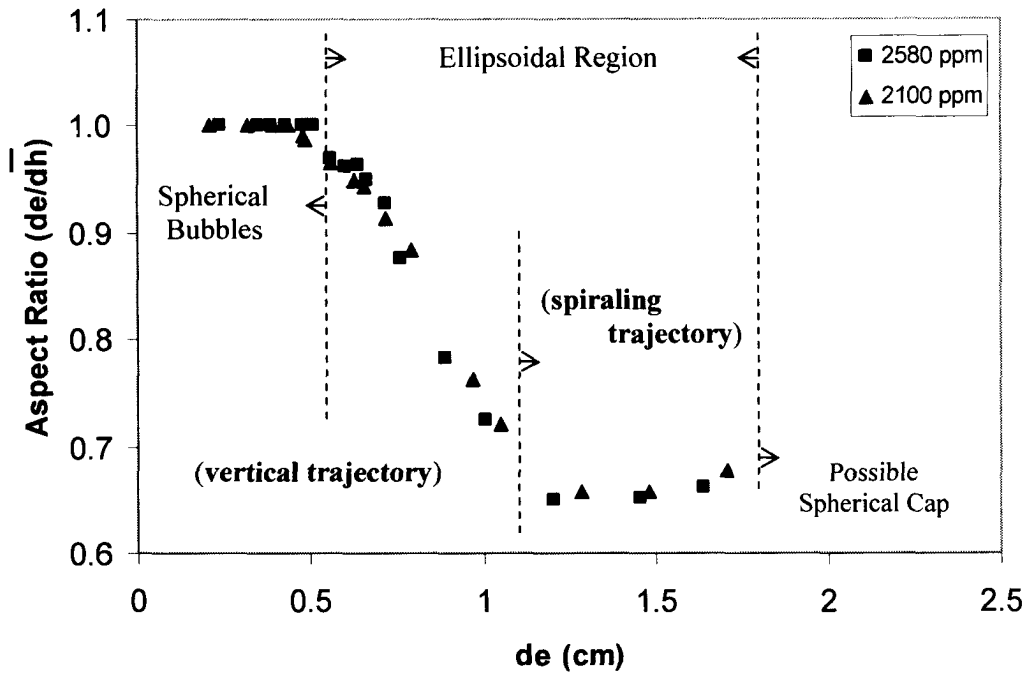

Figure 4.24 Aspect ratio vs. equivalent diameter for 2100 ppm and 2580 ppm xanthan gum solutions with the approximate regions for the bubble shapes and trajectories.

The ellipsoidal region starts for a d_e between 0.45-0.5, and the vertical trajectories for the bubbles continues up to around 1.1 cm of equivalent diameter. After this point, the trajectory of the bubbles becomes non-linear, however; the shapes of the bubbles are still ellipsoidal up to 1.7-1.8 cm.

For the ellipsoidal region, the aspect ratio reduces from 1.0 to around 0.65 by increasing equivalent diameter of the bubbles over 0.5 cm. But, the value d_e/d_h does not reach to 0.62 where the spherical cap bubbles are reported to appear (Clift et al, 1978). The spherical cap shape did not observed for xanthan gum solutions as clear as CMC solutions, for which, the aspect ratio of 0.62 is reached. There were only some temporary transitions to spherical cap shapes for the big bubbles (de>1.5) rising with non-linear trajectories and moving interfaces.

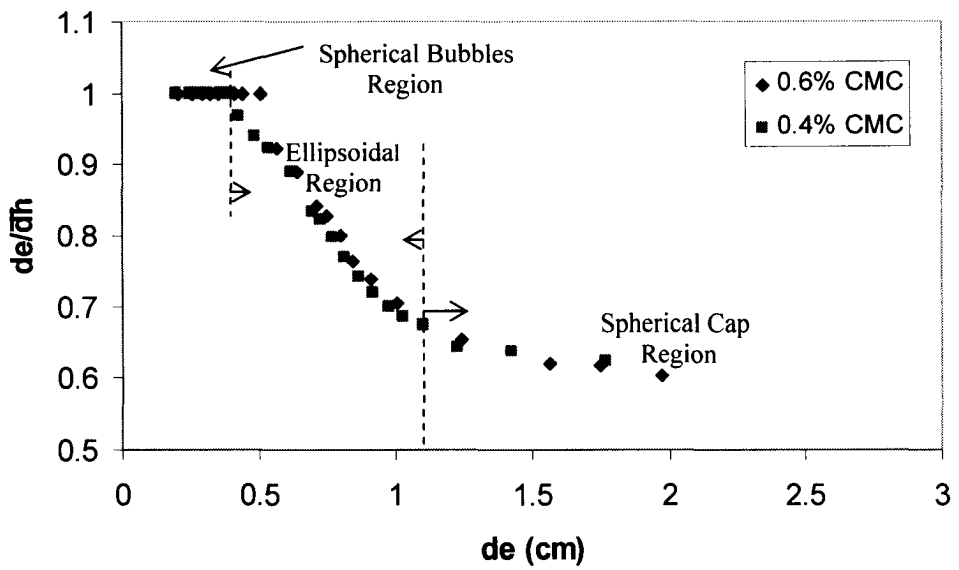

Figure 4.25 Aspect ration vs. equivalent diameter for the bubbles in CMC solutions.

According to Figure 4.24, it can be predicted that some possible distinct spherical cap shapes could appear at the bubble equivalent diameters more than 1.8 cm for higher concentrations of xanthan gum (>2580 ppm).

For the bubbles in CMC solutions, all the data points for the aspect ratio versus equivalent diameter are given in Figure 4.25. As described earlier, the shape of the bubbles in both working CMC solutions gradually changes through the three primary shapes – spherical, ellipsoidal, and spherical cap – as the volume of the bubbles increases. As it is shown in this figure (Figure 4.25), the aspect ratio reaches to around 0.62 for the CMC solutions at the equivalent diameter around 1.2 cm where the region of spherical cap bubbles begins.

5. Conclusions and Recommendations

The main conclusions drawn from this research are:

- No discontinuity was observed at the rise velocity versus volume curves for the air bubbles rising in the xanthan gum and CMC solutions.
- The terminal velocity of the small bubbles decreased as the concentration of the xanthan gum and CMC solutions increased up to a certain volume for each solution. A velocity plateau reached for the large bubbles.
- The "constant-volume" method proposed and used for creating bubbles with volumes which were multiples of a unit volume.
- The time characteristics (or relaxation times) were obtained for all the xanthan and CMC solutions using different methods, and the results used to determine the degree of viscoelasticity of the solutions.
- Rheological and dynamic properties of the xanthan gum and CMC solutions and the effect of the presence of surfactant on their rheology were thoroughly investigated.
- The aspect ratio-equivalent diameter relationship was almost constant for the CMC solutions and also for the high concentrations of xanthan gum.
- An average value considered for the projected diameter of the bubbles with non-linear trajectories (changing projected diameters), which obtained by the image analysis and used in the drag coefficient calculations ($\overline{d}_h$).

- The shape of the bubbles changed through the four primary shapes – spherical, ellipsoidal, cusp-ended, and spherical cap - as their volume increased. The spherical cap shapes were obvious for the CMC solutions reaching the aspect ratio of 0.62. But, the aspect ratio of 0.62 did not obtained for the xanthan gum solutions up to 2500 microlitre (volume).
- Appearance of a cusp-like shape of the rising bubbles in xanthan gum solutions did not coincide with any discontinuity in the terminal velocity of the bubbles.
- The drag coefficient-Reynolds number curves reached to a constant value for the xanthan gum and CMC solutions at $Re > 60$.
- Photographic evidence in this study showed that the motion of bubbles in non-Newtonian fluids at equivalent diameters higher than 1.1 cm is not linear. Also, the top view photographing of such bubbles indicated that they have three-dimensional zigzag or spiraling trajectories.

Recommendations

- In this research the hydrodynamic characteristics of air bubbles were determined in xanthan gum solutions. It is recommended that additional work be undertaken to determine the hydrodynamics of falling and rising solid particles in xanthan solutions, for which, to our knowledge, nothing has been reported in the literature.
- The smallest bubble covered by this study was around 1 mocrolitre. It would be interesting to investigate the behaviour of microbubbles or nanobubbles in xanthan gum solutions that are important for improving the production of this

material. The generation of such small size bubbles will be the challenging point for this type of research.

- It would be helpful to use some advanced image analysis software that can provide a three dimensional event capture and analysis of the bubbles along with the top view photographing to be able to track and quantify precisely the motion of the bubbles.
- To obtain more accurate values for rise velocity and average horizontal diameter of bubbles with non-linear trajectories using photographic techniques, it is recommended to do the image processing in a wider field of focus of camera covering at least a full period of bubble's motion. This was not possible in the case of xanthan gum solutions because of their poor transparency and the need for a narrower zoom of the applied camera.
- In addition to the rotational viscometer results for relaxation time and viscoelastic properties of the xanthan gum solutions, it would also be useful to characterize these solutions by means of elongational rheometry.
- This work was involved with rigid chemical structure xanthan gum aqueous solutions as well as semi-rigid CMC solutions. It is recommended to do the same work with some flexible structure polymers to be able compare the results for velocity-volume curves and evaluate the dependency of the probable jump discontinuity on chemical structure of polymers and biopolymers.

6. References

Astarita G., Apuzzo G., "Motion of gas bubbles in non-Newtonian liquids", *AIChE*, Vol. 11, No. 5, pg. 815 – 820, (1965).

Bangalore D.V., Bellmer D. D., "Micro-bubbles for Enhancement of Oxygen Transfer in Xanthan Gum Fermentation", *Chem. Eng. Comm*, 193, 1232–1252, (2006).

Belmonte A., "Self-oscillation of cusped bubble rising through a micellar solution", Rheol Acta, 39, 554-559, (2000).

Bird R. B., Armstrong R.C., Hassager, O., Dynamics of Polymeric Liquids, Vol. 1, 2nd ed., *Weily: New York*, pg. 171, (1987).

Bird R.B., Dai G.C., Yarusso B.J.," The rheology and flow of viscoplastic matrials", *Rev. Chem. Eng.*, 1, (1983).

Burns S.E., Yiacoumi S., Tsouris C., " Microbubble generation for environmental and industrial separation", *Separation and Purification Technology*, 11; 221-232, (1997).

Cadmus M. C., Jackson L. K., Kermit A. Burton, Plattner R. D., Slodki M. E., "Biodegradation of Xanthan Gum by *Bacillus sp.*", *Applied & Environmental Microbiology*, p. 5-11, (1982).

Calderbank P. H., Johnson D. S. L., Loudon J., "Mechanics and mass transfer of single bubbles in free rise through some Newtonian and non-Newtonian liquids", Chemical Engineering Science, Vol. 25, pp. 235-256, (1970).

Chhabra R.P., De Kee D., "Transport processes in bubbles, drops, and particles", *Hemisphere Publishing Corporation*, pg. 53-67, (1992).

Chhabra R.P., "Bubbles, drops, and particles in non-Newtonian fluids", CRC Press, Boca Raton, FL, (1993).

Chhabra R.P., Richardson J.F., "Non-Newtonian flow in the process industries, fundamentals and engineering applications", Butterworth Heinemann, (1999).

Chhabra R.P., "Bubbles, drops, and particles in non-Newtonian fluids", CRC Taylor & Francis, 2nd Edition, (2007).

Clift R., Grace J.R., Weber M.E., "Bubbles, drops, and particles", Academic press, New York, (1978).

Cross M. M., *J Colloid Sci.*, 20, 417, (1965).

Davies R.M., Taylor G.I., "The mechanics of large bubbles rising through extended liquids and through liquids in tubes", *Proc. Roy. Soc.*, A200, 357, (1950).

De Kee, D., Carreau P. J., Morfarski J., "Bubble velocity and coalescence in viscoelastic liquids", *Chemical Engineering Science*, Vol. 41. No. 9, pp. 2273-2283, (1986).

De Kee D., Chhabra R.P., Dajan, A., "Motion and coalescence of gas bubbles in non-Newtonian polymer solutions", *J. of Non-Newt. Fl. Mech.*, 37, 1-18, (1990).

De Kee D., Chhabra R.P., "Transport processes in bubbles, drops, and particles", *Taylor & Francis*, 2nd Edition, New York- London, (2002).

De Kee D., Chhabra R.P.,"A photographic study of shape of bubbles and coalescence in non-Newtonian polymer solutions", *Rheol. Acta*, 27, 656, (1988).

De Kee D., Chan Man Fong C.F., Yao J., "Bubble Shape in Non-Newtonian Fluids", *Journal of Applied Mechanics*, Vol. 69, 703-704, (2002).

Dewsbury K.H., "Rising particles and gas bubbles in non-Newtonian fluids", Master's Thesis, The University of Western Ontario, London, Canada, (2000).

Dewsbury K.H., Karamanev D., Margaritis A., "Hydrodynamic characteristics of free rise of light solids and gas bubbles in non-Newtonian liquids", *Chem. Eng. Sci.*, 54, 4825-4830, (1999).

Dhole S.D., Chhabra R.P., Eswaran V., "Drag of spherical bubble rising in intermediate Reynolds numbers", *Ind. Chem. Eng. Res.*, 46, 939-946, (2007).

Dziubinski, M., Orczykowska, M., Budzynski, P., "Comments on bubble rising velocity in non-Newtonian liquids", Chemical Engineering Science, 58, 2441–2443, (2003).

Funfschilling D., Li H.Z., "Effects of the injection period on the rise velocity and shape of a bubble in non-Newtonian fluid", *Chemical Engineering Research and Design*, 84(A10): 875–883, (2006).

Garcia-Ochoa F., Santos V.E., Casas J.A., Gomez E., "Xanthan gum: production, recovery, and properties", *Biotechnology advances*, 18, 549-579 (2000).

Hassager, O., "Negative wake behind bubbles in non-Newtonian liquids", *Nature*, 31, 402-403, (1979).

Herrera-Velarde J.R., Zenit R., Chehata D., Mena B., "The flow of non-Newtonian fluids around bubbles and its connection to the jump discontinuity", *J. Non-Newtonian Fluid Mech.*, 111, 199–209, (2003).

Karamnev D.G., "Rise of gas bubbles in quiescent liquids", *AIChE*, Vol.40, No.8, 1418-1421, (1994).

Karamnev D.G.. "Equations for calculation of the terminal velocity and drag coefficient of solid spheres and gas bubbles", *Chem. Eng. Comm.*, Vol 147, 75-84, (1996).

Karamanev D., Dewsbury K., Margaritis A., "Comments on the free rise of gas bubbles in non-Newtonian liquids: Letter to the editor", Chemical Engineering Science, 60, 4655 – 4657, (2005).
Kulkarni Amol A., Joshi Jyeshtharaj B., "Bubble Formation and Bubble Rise Velocity in Gas-Liquid Systems: A Review", *Ind. Eng. Chem. Res.*, 44, 5873-5931, (2005).

Leal L.G., Skoog J., Acrivos A.,"On the motion of gas bubbles in viscoelastic liquids", *Canadian Journal of Chemical Eng.*, 49, 5, pg. 569-575, (1971).

Leela J.K., Sharma G., "studies on xanthan production from *Xanthomonas campestris*", *Bioprocess Engineering*, 23, 687-689, (2000).

Leider P.J., Bird R.B., "Squeezing flow between parallel disks", *Ind. Eng. Chem. Fundam.* , 13, 336, (1974).

Lehr F., Millies M., Mewes D., "*Bubble* size distribution and flow fields in bubble column", *AIChE*, Vol. 48, No. 11, pp. 2426, (2002).

Liu Y.J. , Liao O T. Y., Joseph D. D., "A two-dimensional cusp at the trailing edge of an air bubble rising in a viscoelastic liquid", *J. Fluid Mech.*, vol. 304, *pp.* 321-342, (1995).

Margaritis A., Pace GW, "Microbial Polysaccharides, Principles and Applications", *Comprehensive Biotechnology, Oxford, UK: Pergamon Press*, Vol.3, 1005-1044, (1986).

Macosko CW, "Rheology principles, measurements and applications", WILEY-VCH Inc., p. 309, (1994).

Malaga C., Rallison J.M., "A rising bubble in a polymer solution", *J. Non-Newtonian Fluid Mech.* 141, 59–78, (2007).
Margaritis A., te Bokkel D.W., Karamanev D.G., "Bubble rise velocities and drag coefficient in non-Newtonian polysaccharide solutios", Biotechnology and Bioengineering, Vol.64, 3, 257-266, (1999).

Margaritis A., Zajic JE, "Mixing, mass transfer, and scale-up of polysaccharide fermentations", *Biotechnol. Bioeng.*, 20, 939-1001, (1978).

Milas M., Rinaudo M., "Flow and viscoelastic properties of xanthan gum solutions", *Macromolecules*, Vol. 23, 2506-2511, (1990).

Mouza A.A., Dalakoglou G.K., Paras S.V., "Effect of liquid properties on the performance of bubble column reactors with fine pore spargers", *Chemical Eng. Science*, Vol. 60, 1465 – 1475, (2005).

Pilz C., Brenn G., "On the critical bubble volume at the rise velocity jump discontinuity in viscoelastic liquids", *J. Non-Newtonian Fluid Mech.*, 145, 124–138, (2007).

Nussinovitch A., "Hydrocolloid application; gum technology in the food and other industries", *Blackie Academic & Professional*, 1st edition, (1997).
Perry R.H., Green D.W., "Perry's Chemical Engineers' Handbook", *McGraw-Hill*, 7th Edition, (1997).

Pillapakkam S.B., Singh P., Blackmore D., Aubry N., "Transient and steady state of a rising bubble in a viscoelastic fluid J. Fluid Mech., vol. 589, pp. 215–252, (2007).

Pons A., Dussap C.G., Gros J.B., "Xanthan batch fermentations: compared performance of a bubble column and stirred tank fermentor", *Bioprocess Engineering*, 5, 107-114, (1990).

Prince M.J., Blanch H.W., "Bubble Coalescence and Break-Up in Air-Sparged Bubble Columns", *AIChE*, Vol.36, 1485, (1990).

Prud'homme R., Long REJ, "Surface tension of concentrated xanthan and polyacrylamide solutions with added surfactants', *J. of Colloid and Interface Sci.*, Vol. 93, (1983).

Rodrigue D., De Kee D., "Bubble velocity jump discontinuity in polyacrylamide solutions: a photographic study", *Rheol Acta*, 38, 177-182, (1999).

Rodrigue D., Blanchet J., "Surface remobilization of gas bubbles in polymers containing surfactants", *J. of Colloid and Interface Sci.*, 256, 249-255 (2002).

Rodrigue D., De Kee D., Chan man Fong C.F., "An experimental study of the effect of surfactants on the free rise velocity of bubbles", *J. Non-Newtonian Fluid Mech.*, 66, 213-232, (1996).

Soto E., Goujon C. , Zenit R. , Manero O., "A study of velocity discontinuity for single air bubbles rising in an associative polymer", *Physics of Fluids*, 18, 121510, (2006).

Stelter M., Brenn G., Yarin A.L., Singh R.P., Durst F., "Investigation of the elongational behavior of polymer solutions by means of an elongational Rheometer", *J. Rheol.* 46, 507–527, (2002).

Tavlaridis L. L., Coulaloglou C.A., Zeitlin M.A, Klinzing G., Galo B., "*Bubble and Drop Phenomena*" Industrial and Engineering Chemistry, Vol. 62, (1970).

Tse K.L., Martinb T., McFarlane C. M., Nienowa A.W., "Small bubble formation via a coalescence dependent break-up mechanism", *Chemical Engineering Science*, Vol. 58, pp. 275 – 286, (2003).

Turton R., Levenspiel O., " A short note on the drag correlations for spheres", *Powder Technology*, 47, 83, (1986).

Tzounakos A., Karamanev D., Margaritis A., Bergougnou M.A., "Effect of the surfactant concentration on the rise of gas bubbles in power-law non-Newtonian liquids", *Ind. Eng. Chem. Res.*, 43, 5790-5795, (2004).

Tzounakos A. "Effect of surfactants on bubble rise non-Newtonian fluids", Master's Thesis, The University of Western Ontario, London, Canada, (2001).

APPENDIX A: Flow curves for xanthan gum and CMC solutions

The Carreau model curve fitting and related parameters are included for all concentrations of xanthan gum and CMC on related graphs.

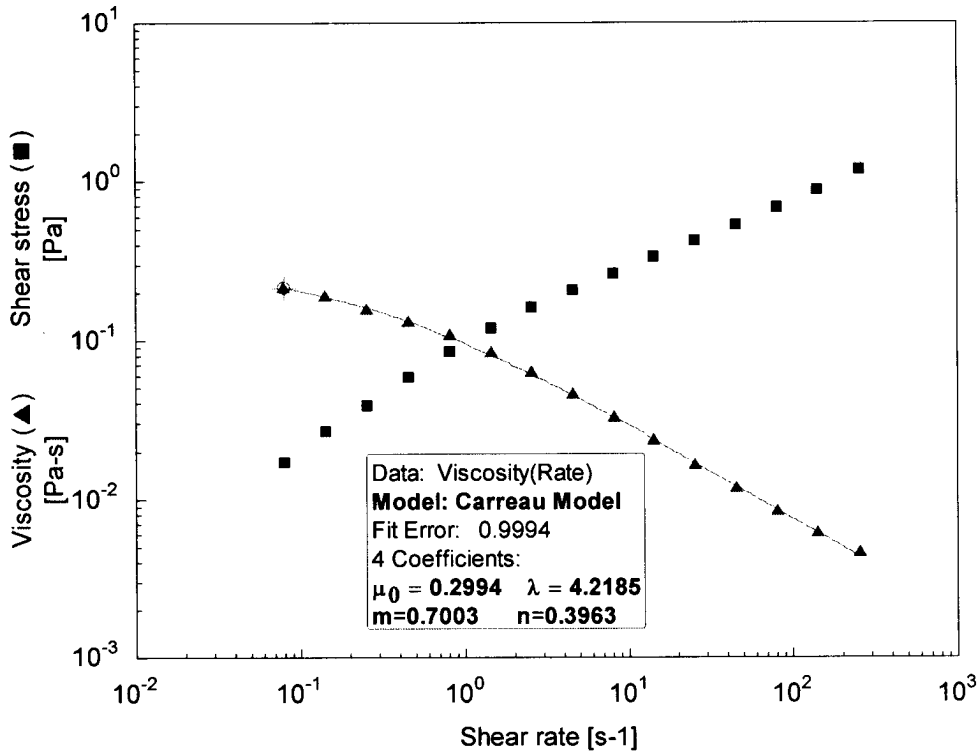

Figure A.1 Flow curve for the 780 ppm xanthan gum aqueous solution. The viscosity data have a good fit with the Carreau model.

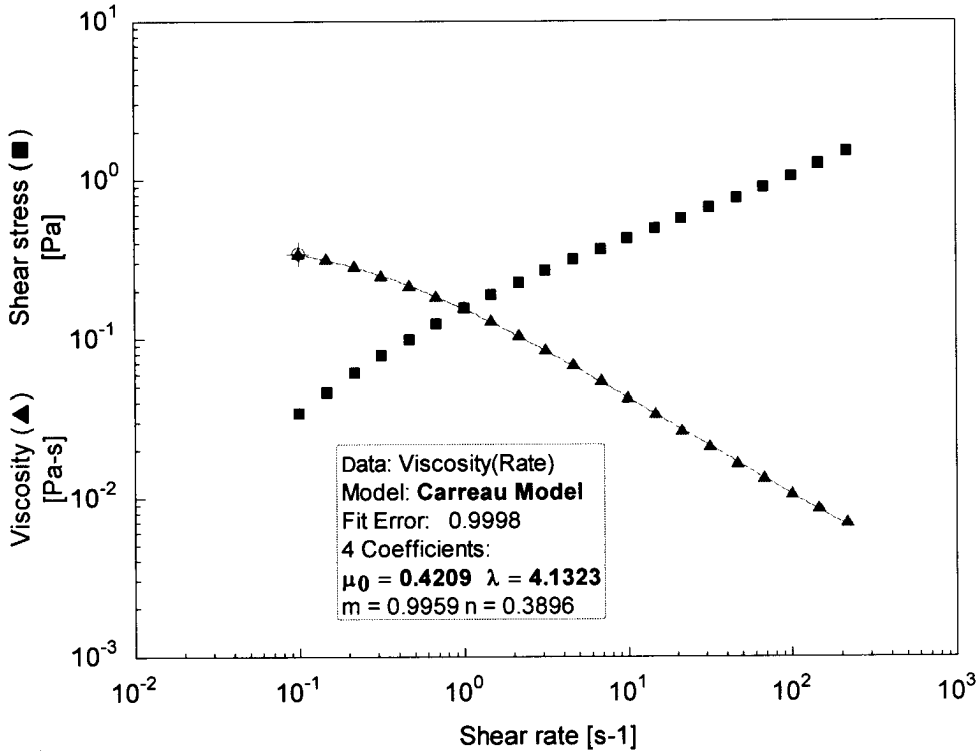

Figure A.2 Flow curve for the 1050 ppm xanthan gum solution with the Carreau model fitting the viscosity data.

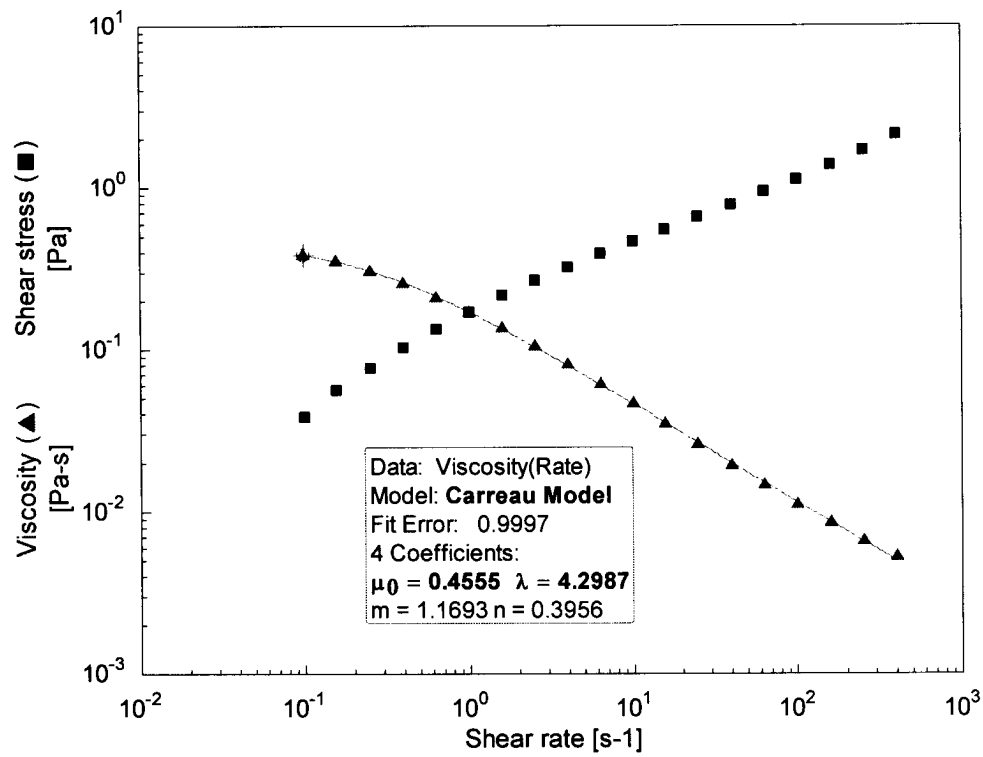

Figure A.3 Flow curve for the 1280 ppm xanthan gum solution with the Carreau model fitting the viscosity data.

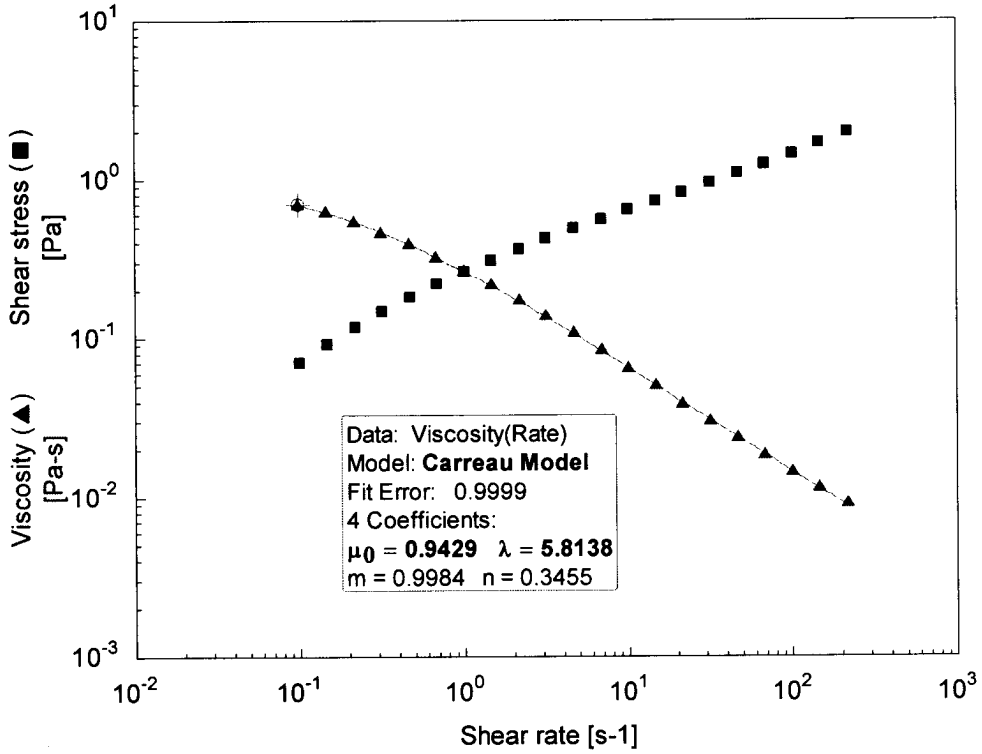

Figure A.4 Flow curve for the 1530 ppm xanthan gum solution with the Carreau model fitting the viscosity data.

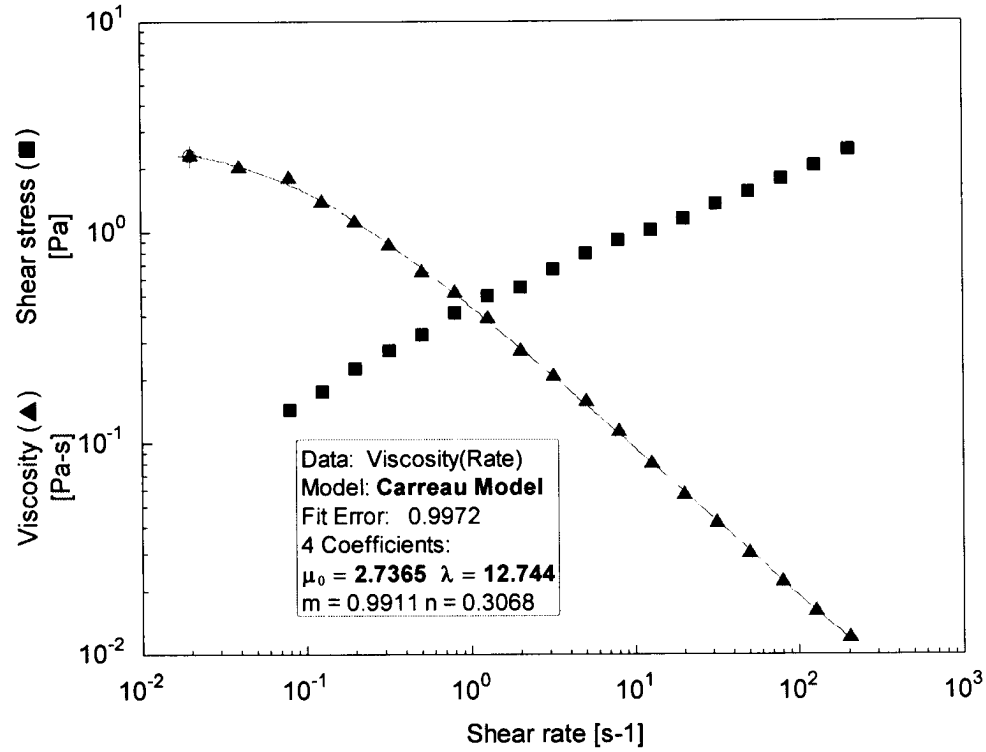

Figure A.5 Flow curve for the 2100 ppm xanthan gum solution with the Carreau model fitting the viscosity data.

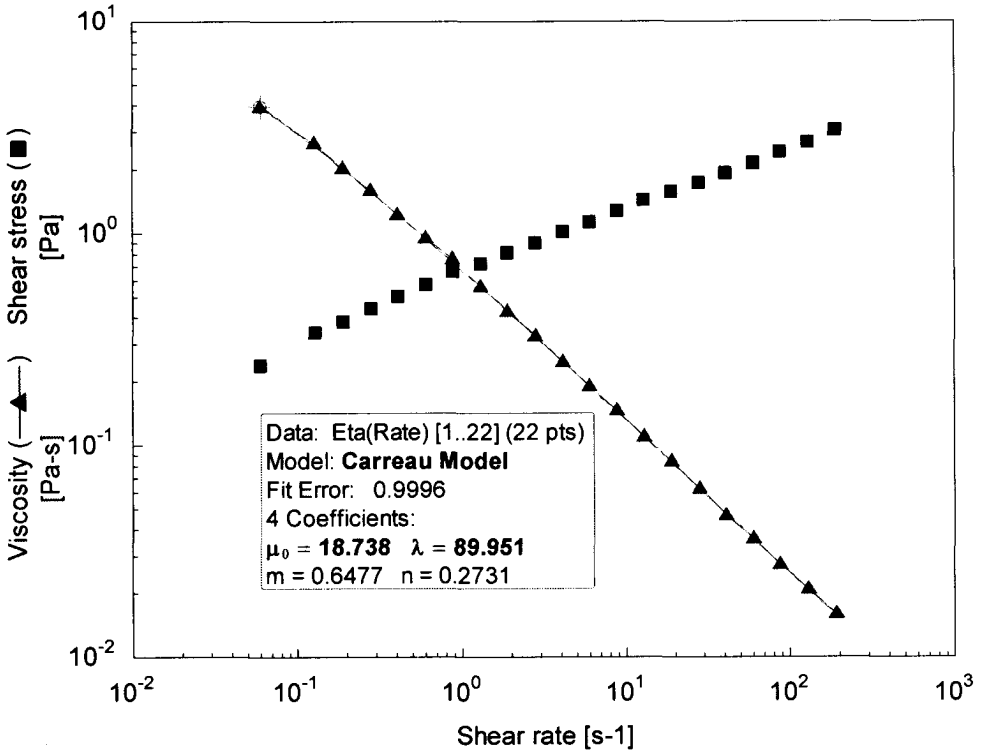

Figure A.6 Flow curve for the 2580 ppm xanthan gum solution with the Carreau model fitting the viscosity data.

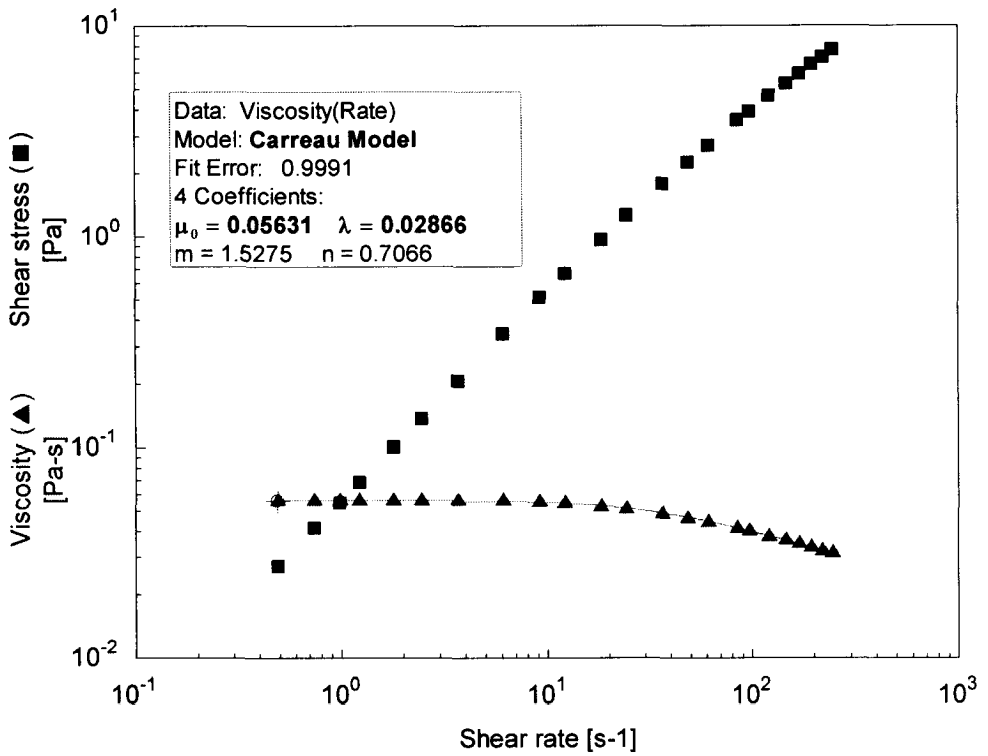

Figure A.7 Flow curve for the 0.4% w/w CMC solution with the Carreau model fitting the viscosity data.

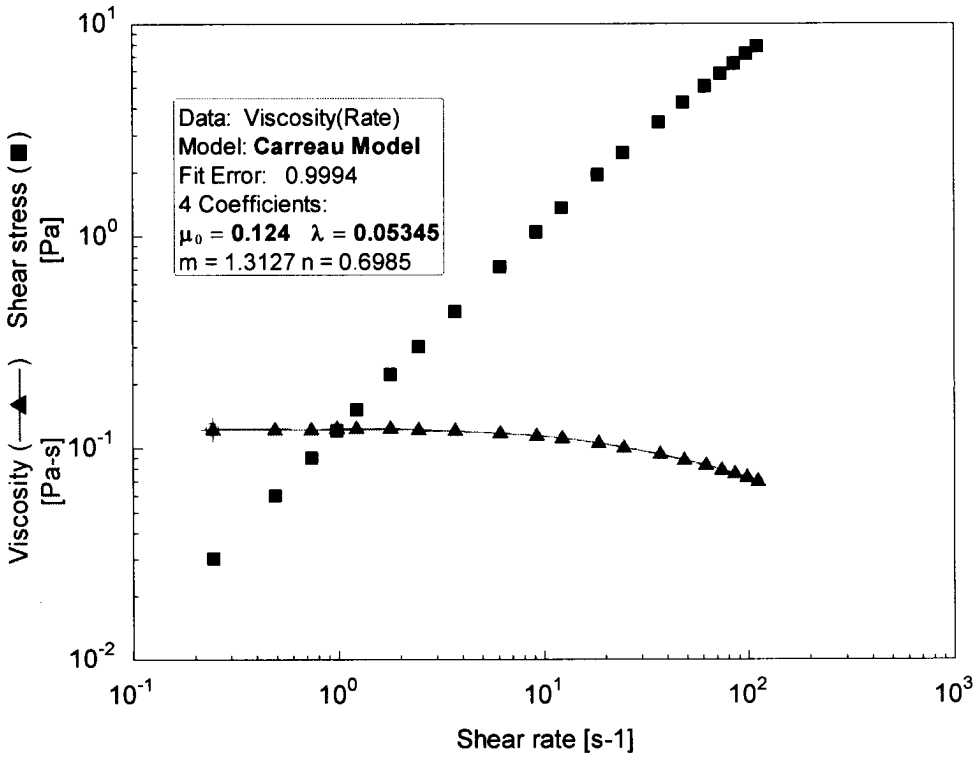

Figure A.8 Flow curve for the 0.6% w/w CMC solution with the Carreau model fitting the viscosity data.

Appendix B: Power-Law Coefficient

Power-law coefficient for xanthan gum and CMC solutions used in drag coefficient calculations.

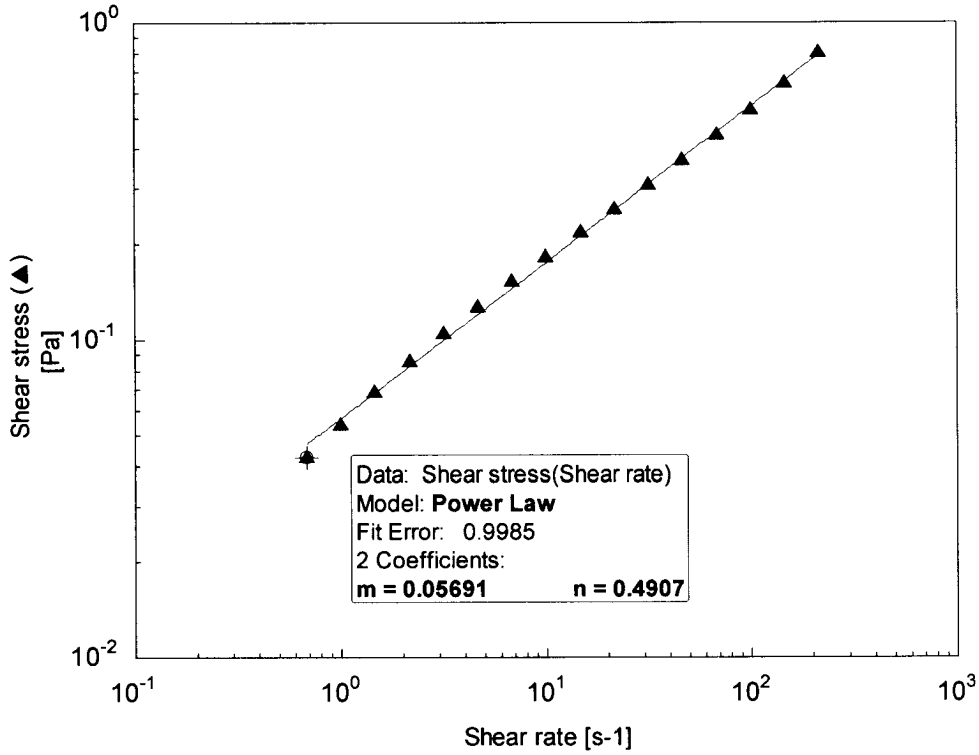

Figure B.1 Power-low index (n) and consistency index (m) for the 520 ppm xanthan gum aqueous solution.

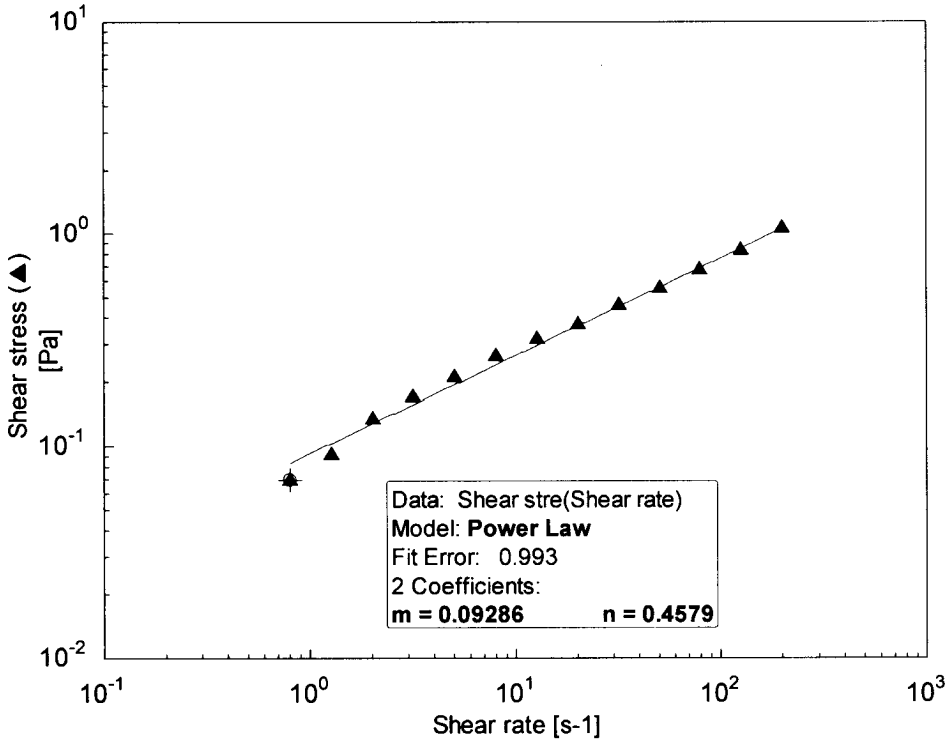

Figure B.2 Power-low index (n) and consistency index (m) for the 780 ppm xanthan gum aqueous solution.

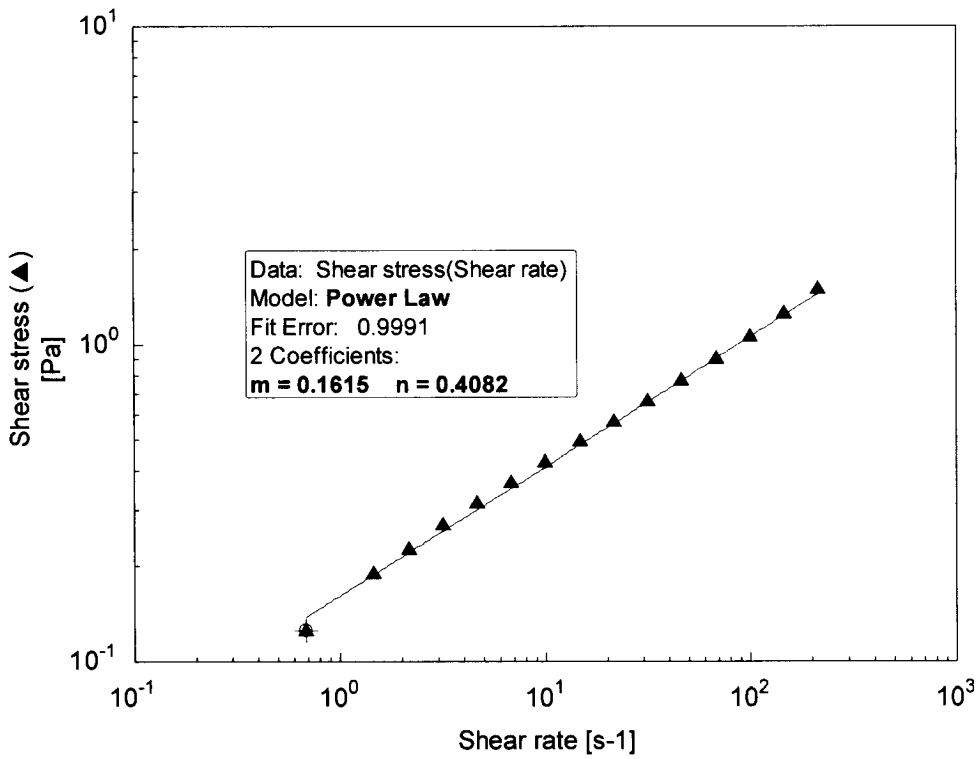

Figure B.3 Power-low index (n) and consistency index (m) for the 1050 ppm xanthan gum aqueous solution.

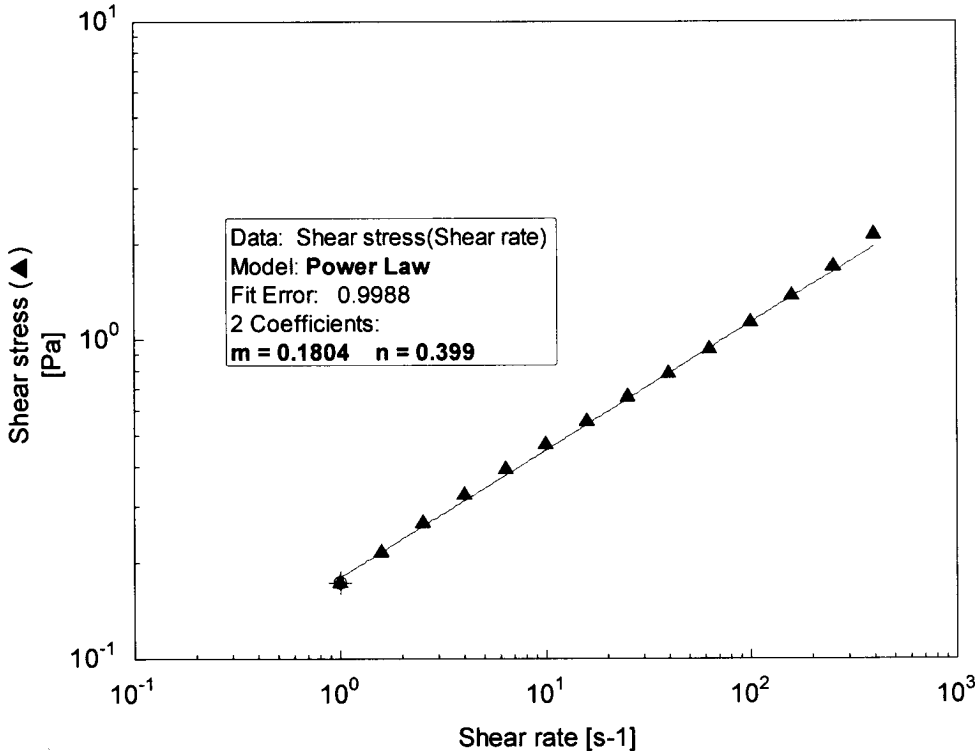

Figure B.4 Power-low index (n) and consistency index (m) for the 1280 ppm xanthan gum aqueous solution.

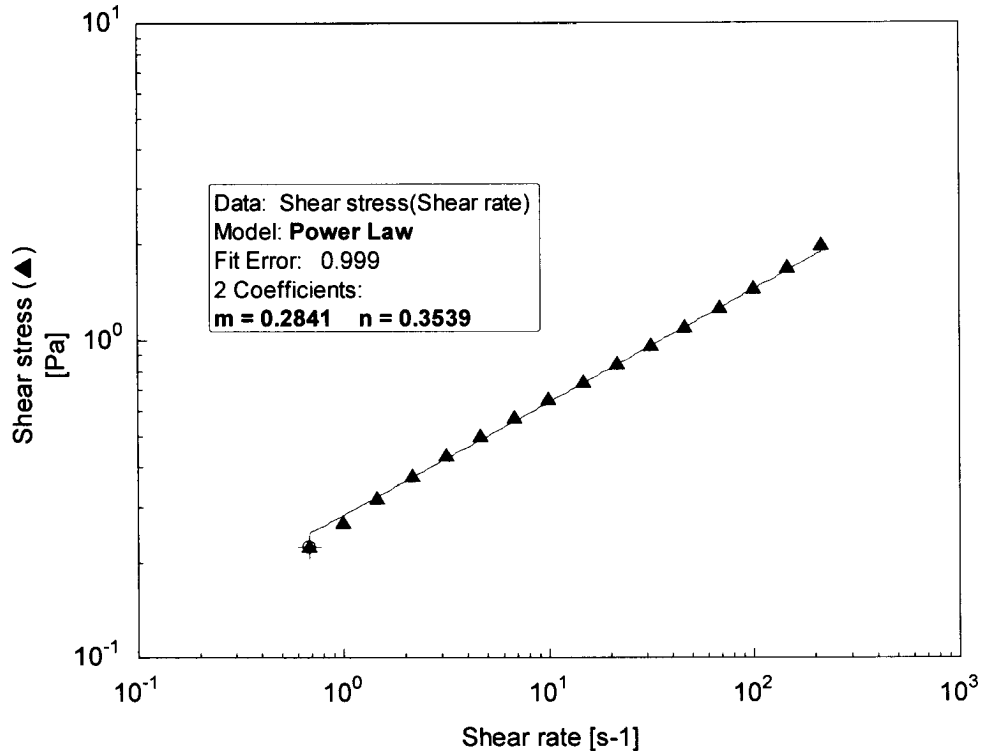

Figure B.5 Power-low index (n) and consistency index (m) for the 1530 ppm xanthan gum aqueous solution.

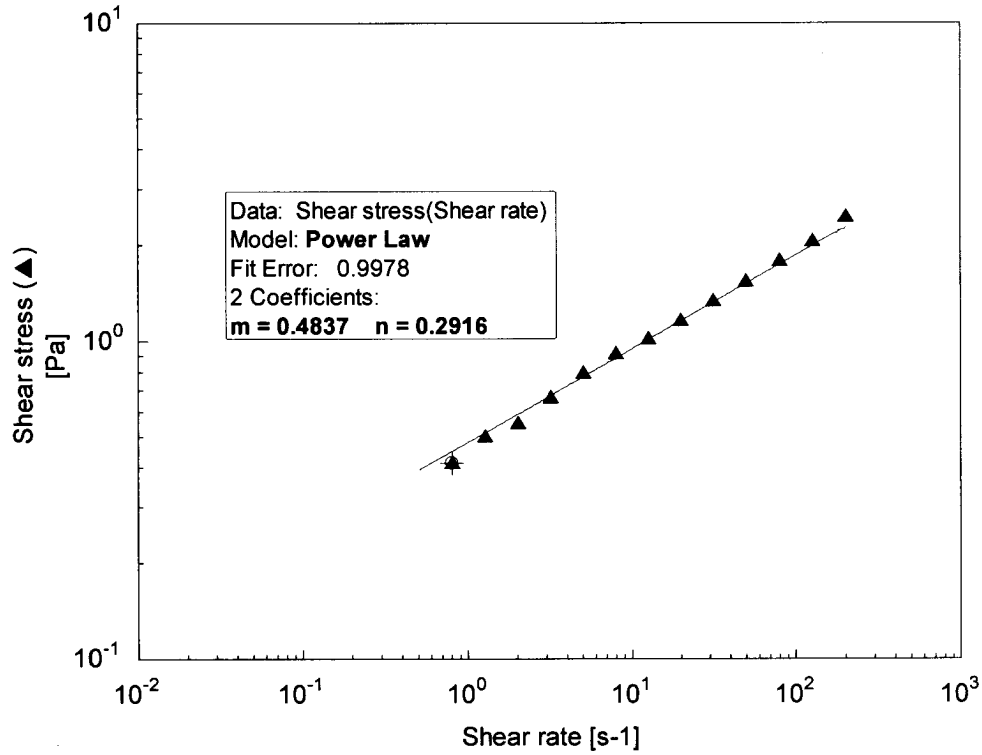

Figure B.6 Power-low index (n) and consistency index (m) for the 2100 ppm xanthan gum aqueous solution.

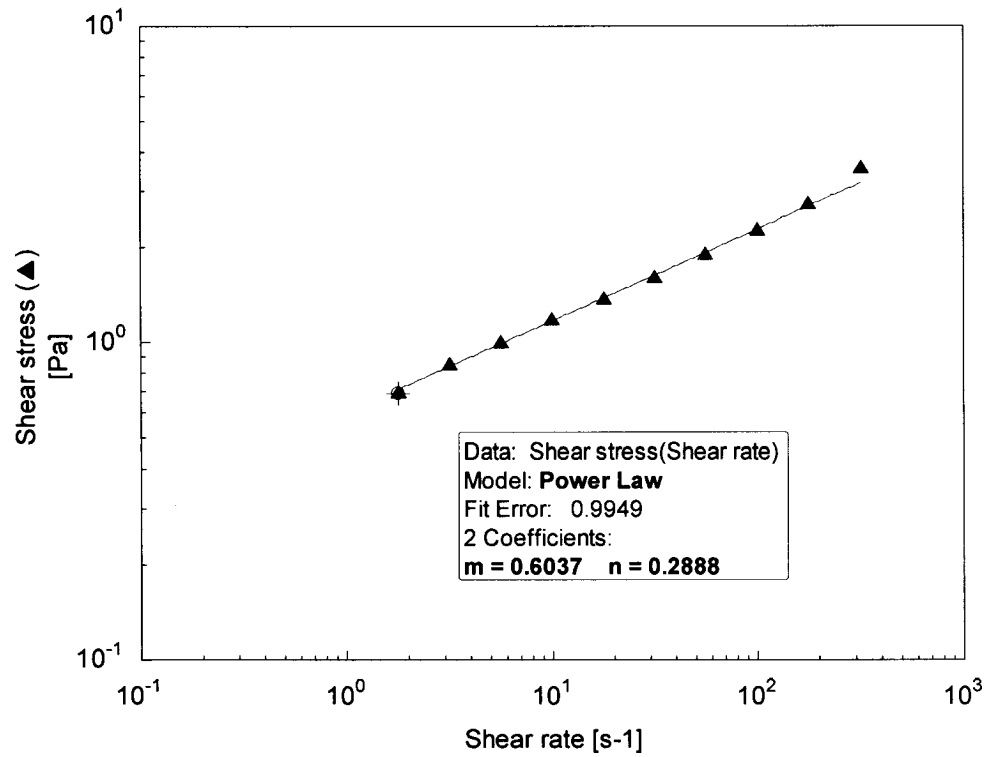

Figure B.7 Power-low index (n) and consistency index (m) for the 2580 ppm xanthan gum aqueous solution.

Table B.1 Power-law coefficients of solutions at low to moderate shear rates (5- 250 s^{-1}) at 22.5 °C .

Solution	Concentration (ppm)	SDS Concentration (ppm)	Flow index (n)	Consistancy index (m) ($Pa.s^n$)
Xanthan Gum	520	-	0.4907	0.0569
	780	-	0.4579	0.0929
	1050	-	0.4082	0.1615
	1280	-	0.3990	0.1804
	1530	-	0.3539	0.2841
	2100	-	0.2916	0.4837
	2580	-	0.2888	0.6037
	5000	-	0.1908	2.2519
	5000	50	0.1599	3.1093
	5000	200	0.1673	2.6940
	5000	1000	0.1720	2.5884
	10000	-	0.1863	5.5358
CMC	4000	-	0.8699	0.0976
	6000	-	0.8317	0.1184
	6000	100	0.8397	0.1123

Appendix C: Frequency Sweep Test Results

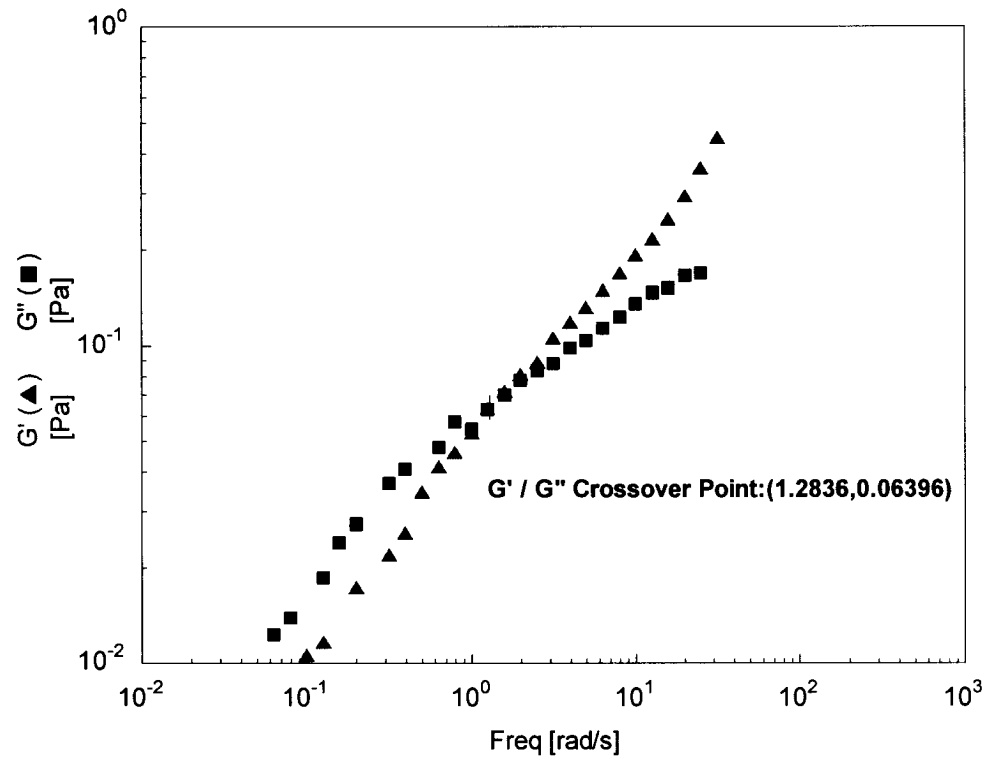

Figure C.1 Frequency sweep test for the 780 ppm xanthan gum aqueous solution.

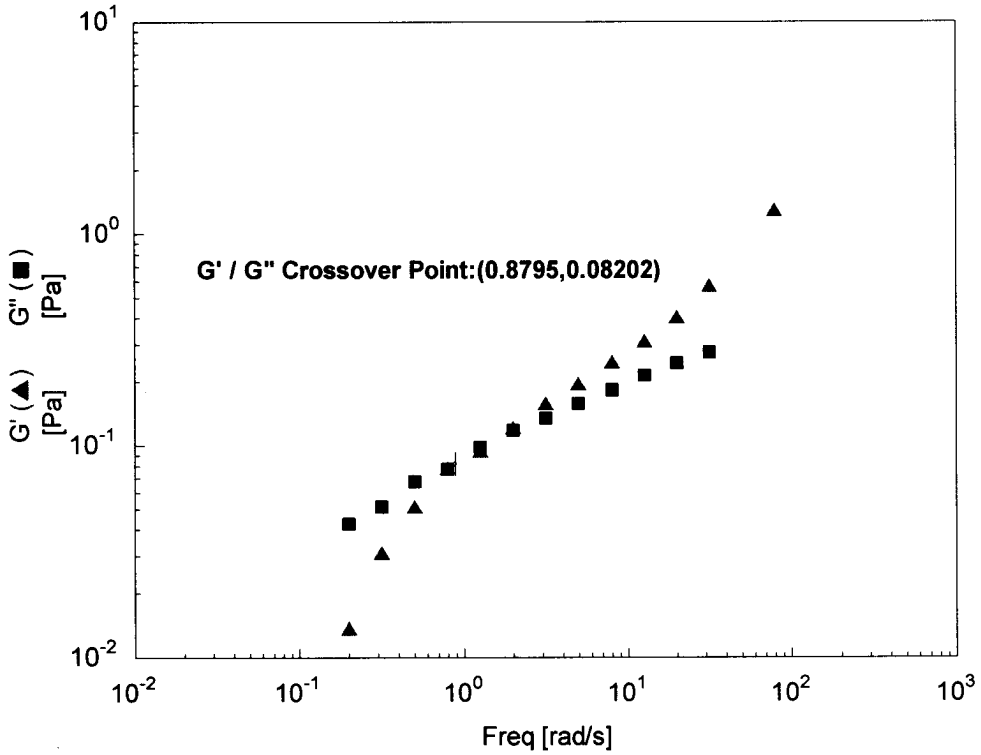

Figure C.2 Frequency sweep test for the 1050 ppm xanthan gum aqueous solution

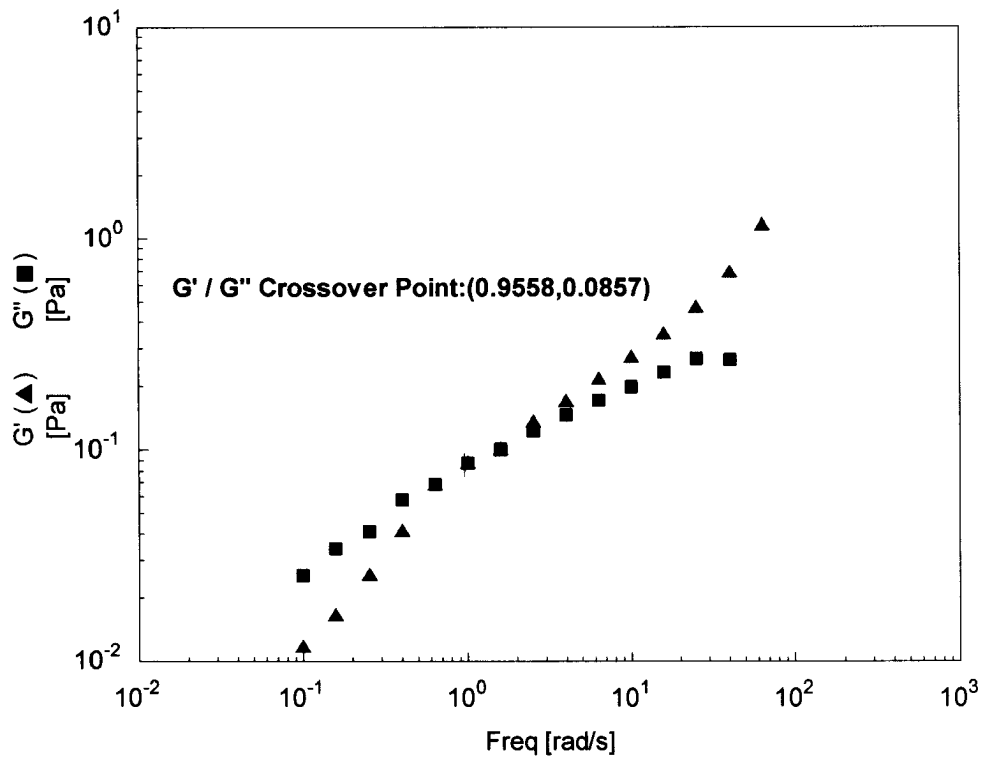

Figure C.3 Frequency sweep test for the 1280 ppm xanthan gum aqueous solution.

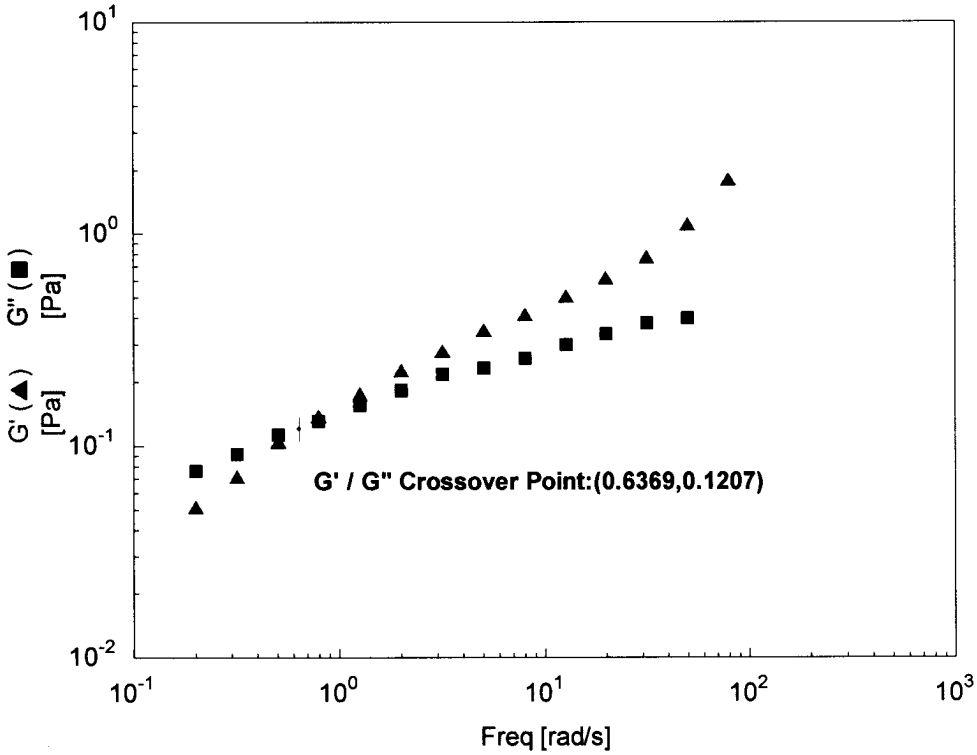

Figure C.4 Frequency sweep test for the 1530 ppm xanthan gum aqueous solution.

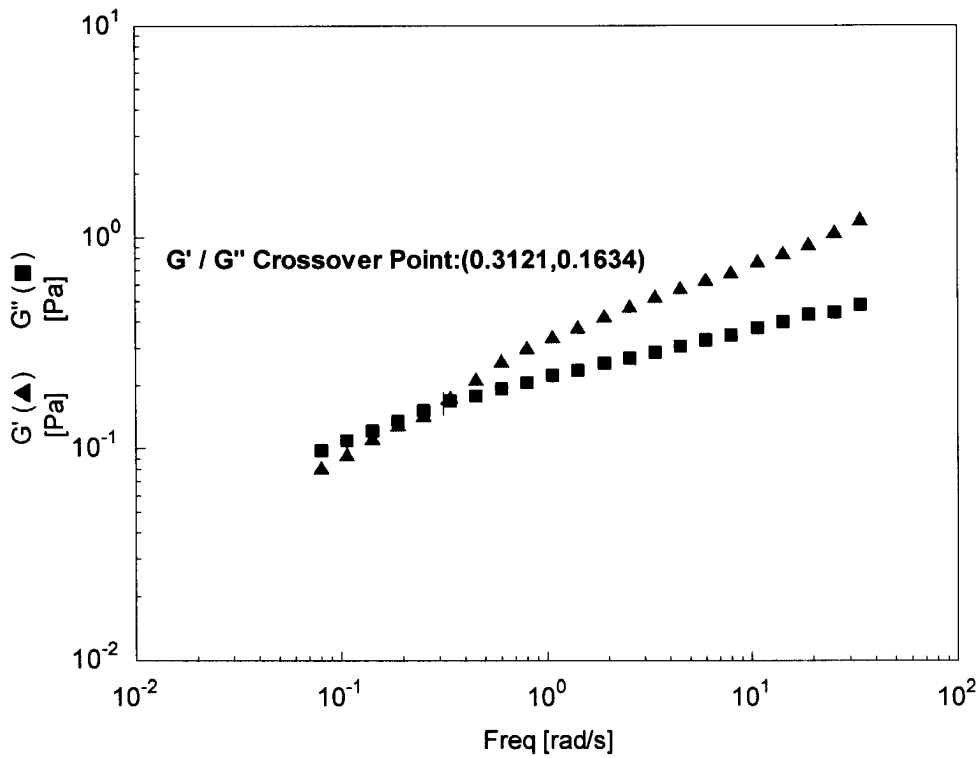

Figure C.5 Frequency sweep test for the 2100 ppm xanthan gum aqueous solution.

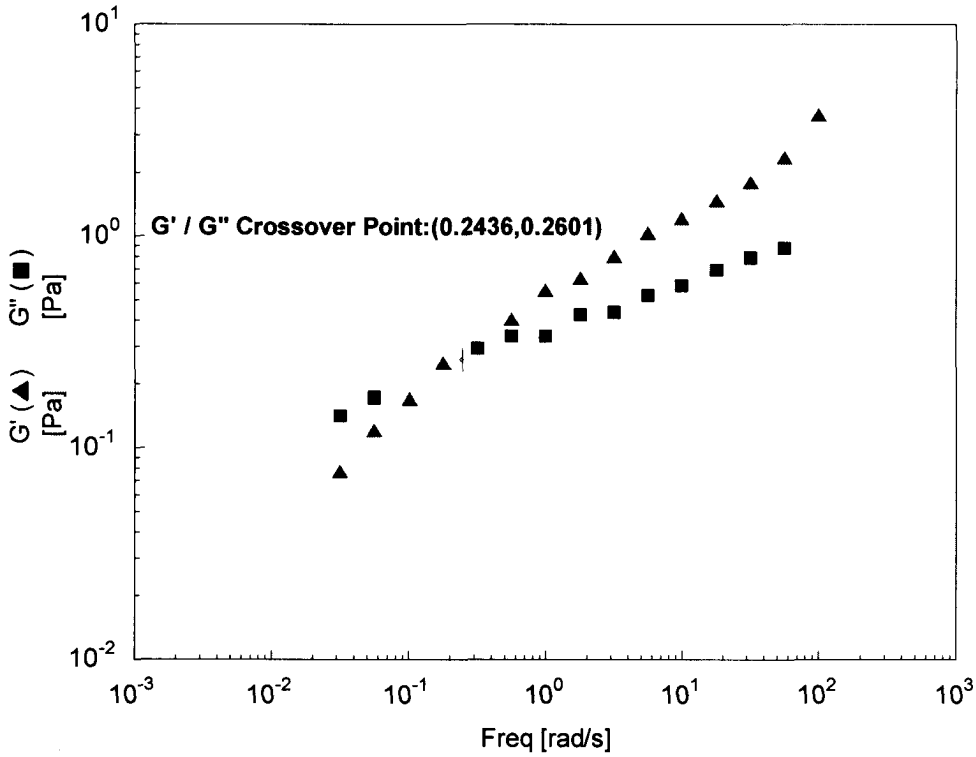

Figure C.6 Frequency sweep test for the 2580 ppm xanthan gum aqueous solution.

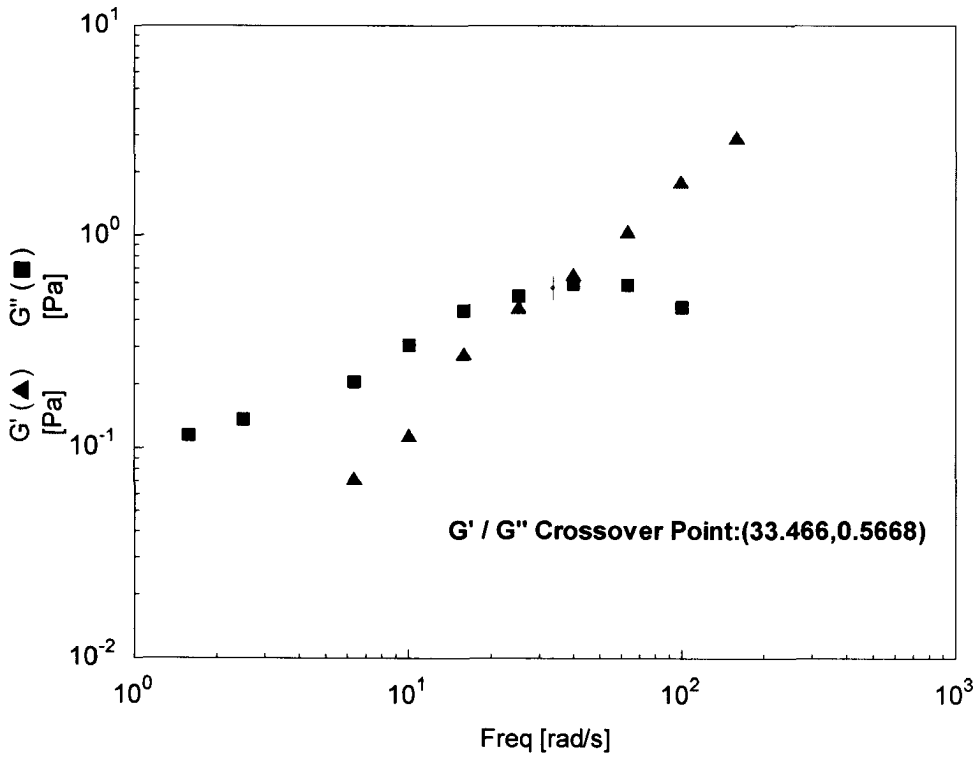

Figure C.7 Frequency sweep test for the 0.4% CMC aqueous solution.

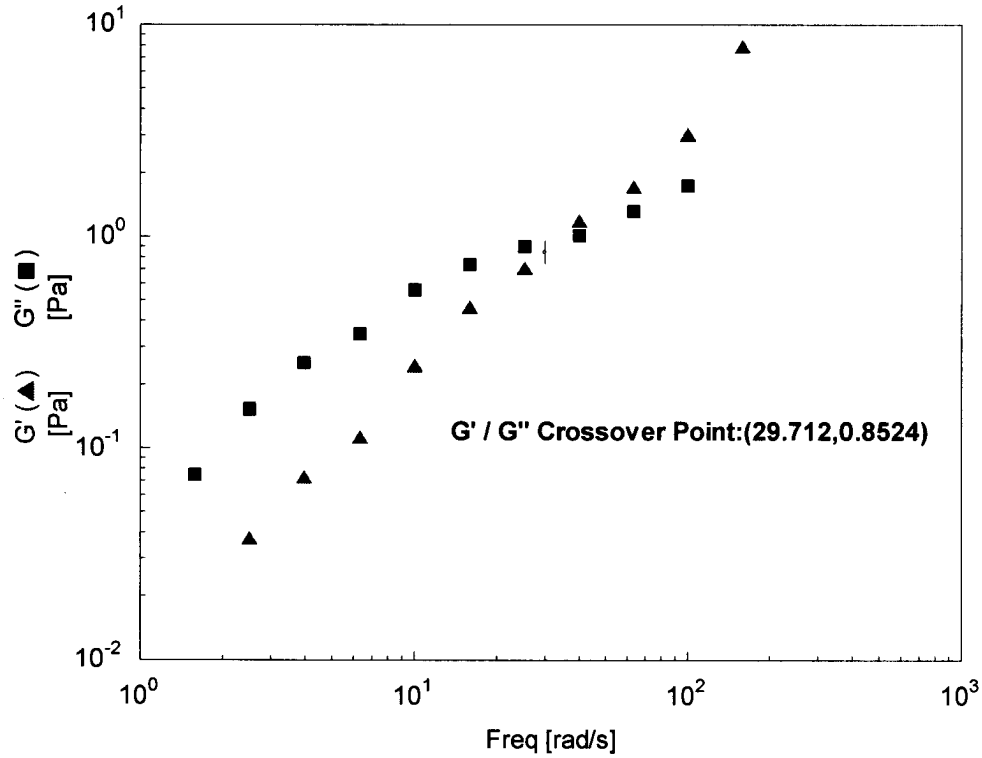

Figure C.8 Frequency sweep test for the 0.6% CMC aqueous solution.

Appendix D: Experimental Data

The experimental data used in the graphs in this study have been collected in this Appendix with related plot numbers.

Table D.1 Experimetal data used in Figure 4.12.

520 ppm **Bubble Volume** (microlitre)	**velocity** (m/s)	780 ppm **Bubble Volume** (microlitre)	**Velocity** (m/s)	1050 ppm **Bubble Volume** (microlitre)	**Velocity** (m/s)
0.95	0.1271	1.58	0.1183	1.52	0.0723
1.89	0.1914	3.20	0.2100	2.98	0.1106
2.84	0.2322	4.80	0.2328	5.97	0.1489
3.8	0.2528	6.4	0.2420	8.9	0.1914
5.7	0.2785	9.6	0.2556	13.5	0.2297
9	0.2838	12	0.2631	16	0.2467
11	0.2885	16	0.2631	26	0.2543
17	0.2925	24	0.2668	33	0.2572
22	0.2793	32	0.2497	47	0.2561
30	0.2530	44	0.2356	58	0.2684
40	0.2472	82	0.2228	77	0.2649
48	0.2443	100	0.2291	84	0.2536
65	0.2356	120	0.2303	94	0.2491
100	0.2305	150	0.2279	105	0.2471
125	0.2231	270	0.2276	115	0.2414
155	0.2325	320	0.2332	190	0.2339
180	0.2274	480	0.2334	260	0.2397
300	0.2248	750	0.2575	360	0.2384
400	0.2338	1350	0.2718	450	0.2429
600	0.2454			700	0.2556
800	0.2606			950	0.2582
1500	0.2691			1050	0.2624

Table D.1 (cont'd).

1280 ppm **Bubble Volume** (microlitre)	**Velocity** (m/s)	1530 ppm **Bubble Volume** (microlitre)	**Velocity** (m/s)	2100 ppm **Bubble Volume** (microlitre)	**Velocity** (m/s)
1.67	0.0630	1.77	0.0227	4.6	0.0125
3.35	0.0859	3.55	0.0419	17.4	0.0632
8.23	0.1393	5.28	0.0654	32.5	0.1080
11	0.1555	8.78	0.0883	44.3	0.1391
14.5	0.1845	15	0.1287	57	0.1669
18	0.2097	27	0.1832	60	0.1792
34	0.2386	35	0.1919	92	0.2158
42	0.2462	50	0.2093	130	0.2598
55	0.2605	61	0.2312	150	0.2601
99	0.2558	72	0.2311	195	0.2723
115	0.2556	91	0.2484	260	0.2806
138	0.2399	115	0.2465	500	0.2816
175	0.2478	165	0.2446	650	0.2835
215	0.2459	240	0.2454	1150	0.2848
255	0.2401	248	0.2431	1650	0.2922
329	0.2392	550	0.2424	2100	0.2950
520	0.2477	900	0.2514		
700	0.2577	1200	0.2666		
1200	0.2634	2300	0.2637		
1662	0.2718				

Table D.1 (cont'd).

2580 PPM **Bubble Volume** (microlitre)	**Velocity** (m/s)
7.05	0.0176
22.5	0.0629
30	0.086
41	0.1112
59	0.1552
68	0.1804
92	0.1993
115	0.2203
138	0.2407
154	0.2454
196	0.2577
230	0.2662
370	0.2786
540	0.2844
920	0.2887
1620	0.2885
2300	0.2919

Table D.2 Experimental data used in figure 4.13.

0.4% CMC		0.6% CMC	
Bubble Volume (microlitre)	**Velocity** (m/s)	**Bubble Volume** (microlitre)	**Velocity** (m/s)
3.99	0.04987	4.61	0.03191
8.12	0.07616	9	0.05235
12.2	0.09635	13.6	0.06664
16	0.11310	18	0.08187
24	0.13965	23	0.09254
32	0.15025	36	0.12119
40	0.17799	45	0.12825
60	0.20257	67	0.16299
81	0.21441	94	0.18242
121	0.23153	135	0.20430
175	0.23961	190	0.21811
202	0.24240	220	0.22107
242	0.24255	270	0.22699
282	0.24280	316	0.23084
343	0.24586	390	0.23430
403	0.24639	530	0.23926
484	0.24766	1000	0.25163
564	0.25123	2000	0.27676
700	0.25735	2800	0.29967
960	0.27128		
1500	0.28475		
2900	0.30702		

Table D.3 Experimental data used in Figure 4.15.

520 ppm X.G.		780 ppm X.G.		1050 ppm X.G.		1280 ppm X.G.	
Re	**C_D**	**Re**	**C_D**	**Re**	**C_D**	**Re**	**C_D**
28.97	0.9852	20.01	1.3512	6.51	3.5696	4.91	4.8436
60.82	0.5250	59.30	0.3601	14.04	1.9078	8.84	3.2874
86.57	0.4168	74.54	0.3240	24.77	1.3263	21.61	1.6880
105.49	0.3532	83.75	0.3122	39.64	0.8457	26.89	1.3984
133.10	0.3073	96.97	0.3198	58.07	0.5696	37.09	1.0779
150.59	0.3183	104.93	0.3248	67.14	0.5018	46.90	0.8689
159.60	0.3287	112.61	0.3181	76.36	0.5172	65.06	0.7127
176.85	0.3541	126.33	0.3085	80.88	0.5299	71.18	0.6777
173.65	0.4074	120.29	0.3723	84.54	0.5921	81.37	0.6378
157.79	0.5445	115.64	0.4618	93.57	0.5836	86.58	0.7537
160.03	0.6224	119.87	0.5646	95.26	0.6579	88.70	0.7719
162.00	0.6765	129.70	0.5569	89.97	0.7368	82.17	0.9274
166.16	0.7108	132.69	0.6202	88.63	0.8000	90.37	0.8873
177.04	0.7711	133.67	0.7145	88.79	0.8451	92.58	0.9222
175.80	0.8659	144.01	0.9229	86.65	0.9115	91.65	0.9965
192.88	0.8733	151.31	0.9888	88.64	1.1219	94.31	1.0890
189.17	1.0015	154.85	1.3461	96.74	1.1527	105.54	1.2085
204.56	1.1570	182.39	1.6389	100.68	1.2721	116.76	1.2446
224.56	1.2415	215.94	1.8224	107.68	1.2749	129.44	1.4517
260.92	1.2352			126.04	1.2321	142.68	1.4908
294.44	1.2914			137.70	1.1493		
346.29	1.4282			143.21	1.1510		
515.52	0.8861						

Table D.3 (cont'd)

1530 ppm X.G.		2100 ppm X.G.		2580 ppm X.G.	
Re	**C_D**	**Re**	**C_D**	**Re**	**C_D**
0.69	38.0622	0.19	172.7727	0.288	100.3538
2.24	12.7697	3.46	10.5297	2.844	11.5692
4.75	6.1791	9.19	4.4390	4.994	6.8089
8.17	4.0752	14.59	2.9639	7.996	4.5343
16.04	2.1999	20.47	2.1962	14.627	2.6131
30.75	1.2597	23.25	1.9262	19.205	2.0360
33.99	1.2616	33.52	1.4626	23.653	1.7296
41.09	1.1725	47.81	1.0975	28.751	1.5011
48.63	1.0454	48.67	1.1336	34.028	1.3416
49.54	1.1125	54.50	1.0590	35.697	1.3000
56.55	1.0467	59.56	1.0276	39.983	1.2184
59.26	1.0920	66.39	0.9714	43.634	1.0776
62.03	1.2117	69.92	0.9451	51.030	0.9674
64.37	1.3406	76.60	0.9351	56.027	0.9070
64.89	1.3554	83.54	0.9497	62.465	0.8425
71.40	1.6551	87.72	0.9489	65.846	0.9701
79.65	1.7034			69.192	1.0012
92.90	1.5693				
99.23	1.9178				
121.87	1.8647				

Appendix E: Shape of Bubbles

Shape of the Bubbles Encountered in Different Concentrations of Xanthan Gum Solutions.

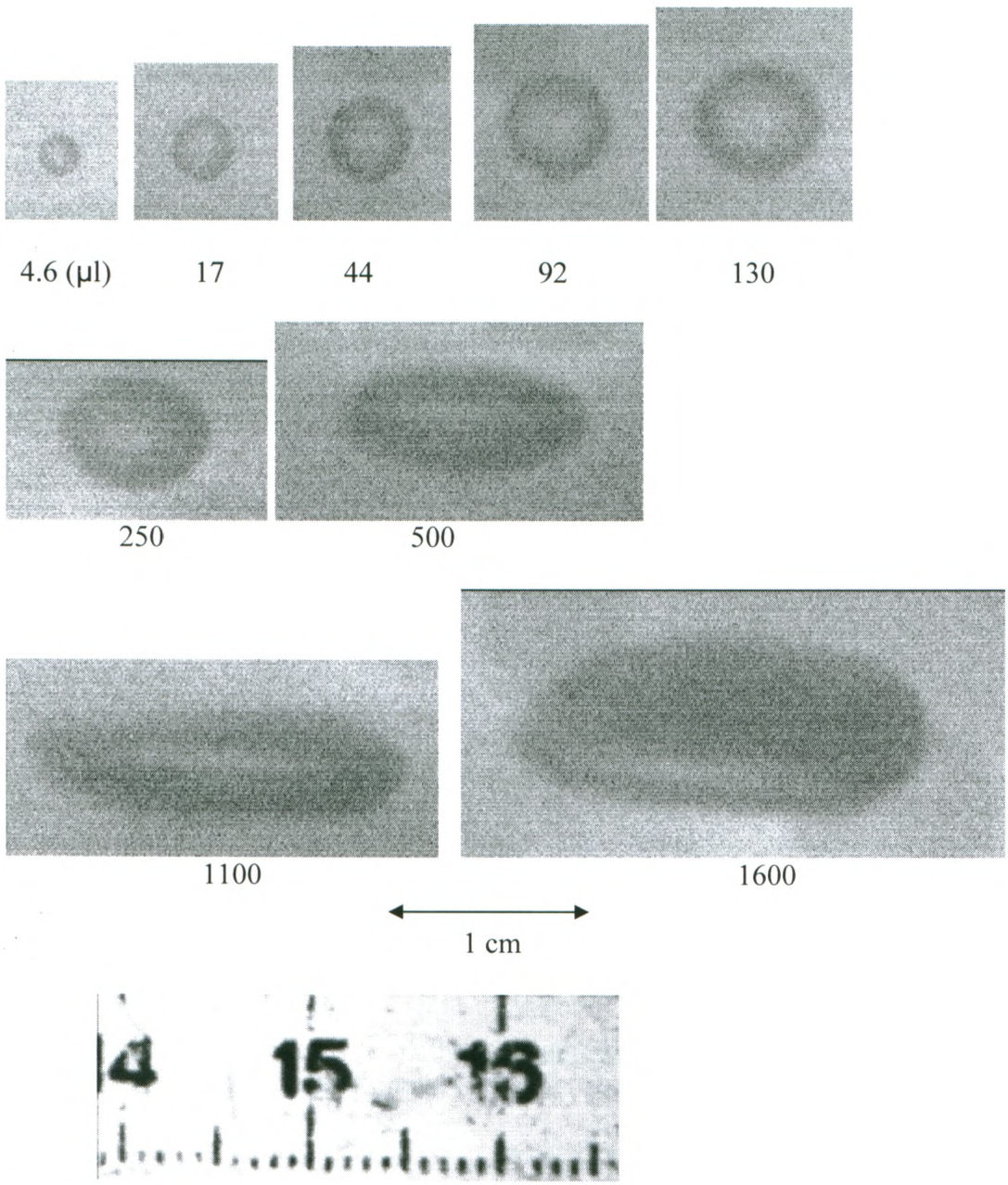

Figure E.1 Shape of the bubbles in the 2100 ppm xanthan gum solutions. The volume of each bubble is at the below of each shape in microlitre.

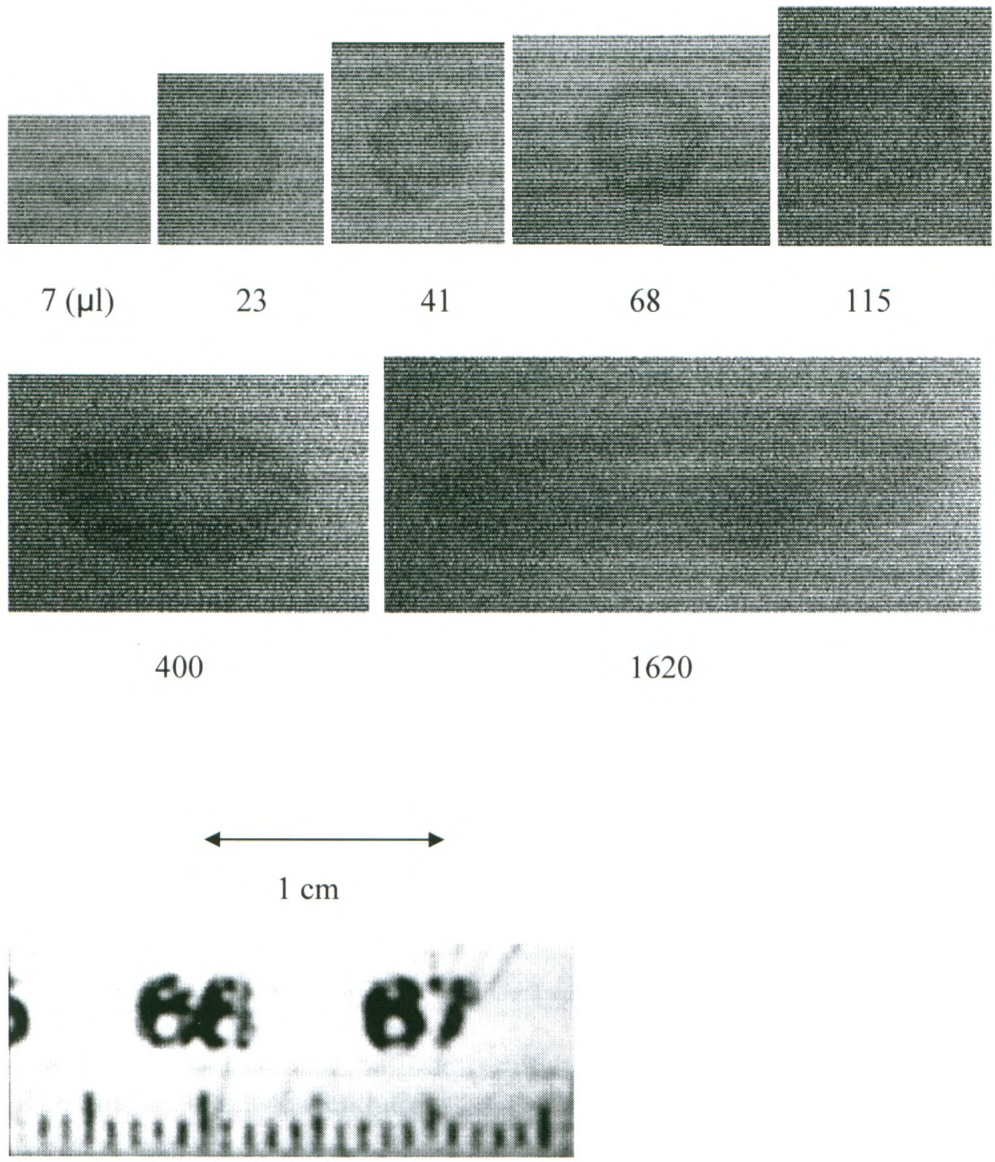

Figure E.2 Shape of the bubbles in the 2580 ppm xanthan gum solution (the highest working concentration in this study).

Appendix F: Normal Relaxation Time Results

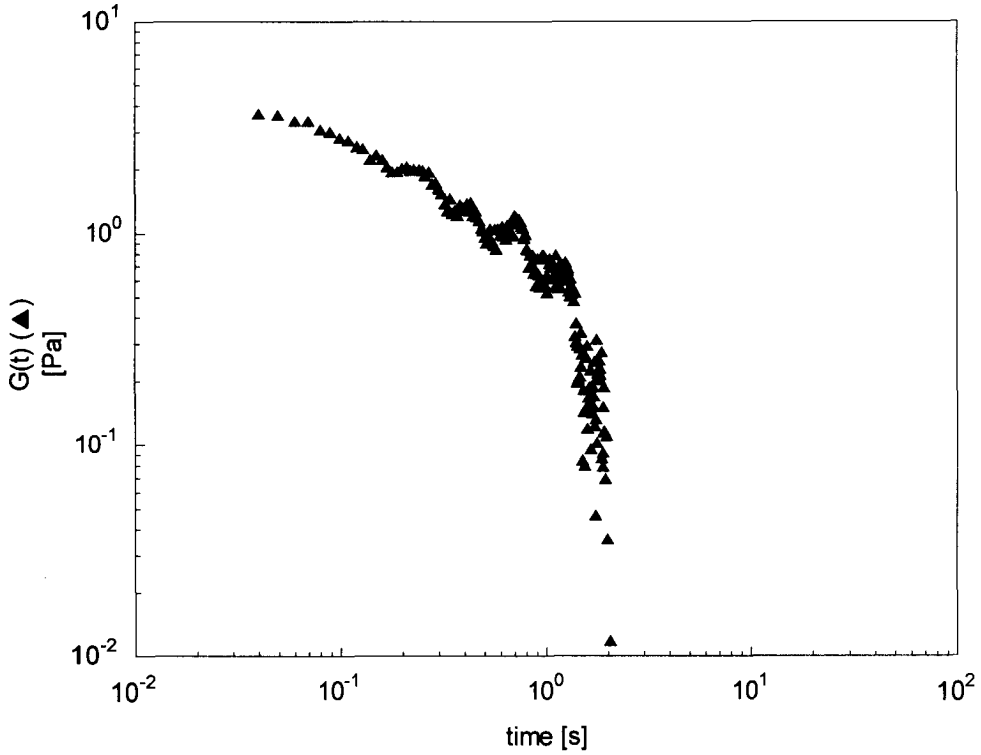

Figure F.1 Normal relaxation time test for a 0.5% xanthan gum solution with 50 ppm SDS concentration.

Table F.1 Normal relaxation time results for 0.5% xanthan gum solution with added different surfactant concentrations.

Solution	**Concentration** (%)	**SDS Concentration** (ppm)	**Normal Relaxation time** (s)
Xanthan Gum	0.5	-	2.7
	0.5	50	2.1
	0.5	200	4
	0.5	1000	4.6

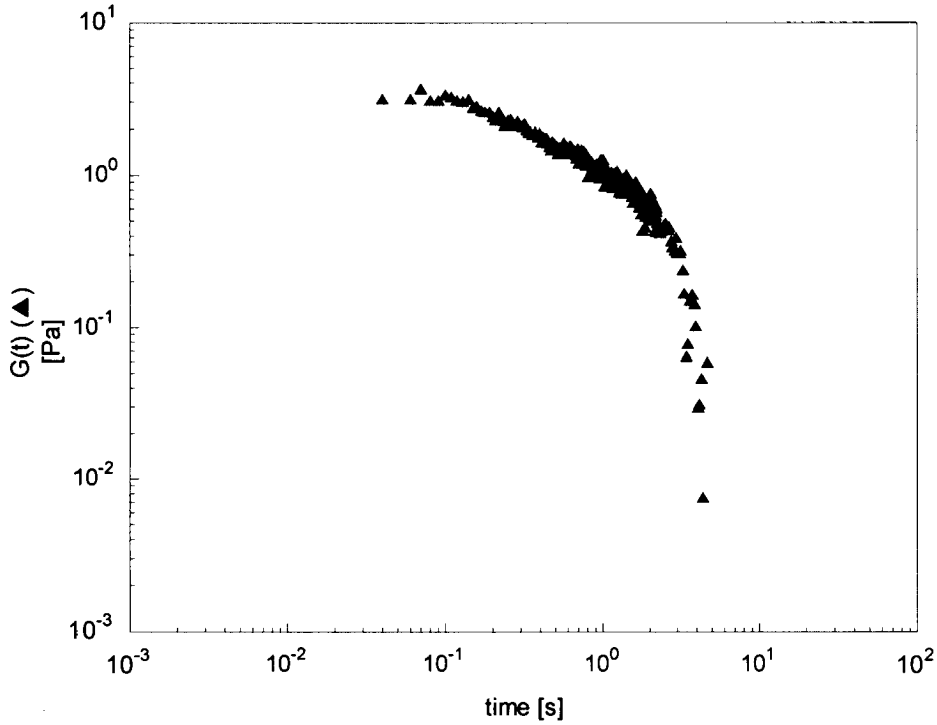

Figure F.2 Normal relaxation time test for a 0.5% xanthan gum solution with 200 ppm SDS concentration.

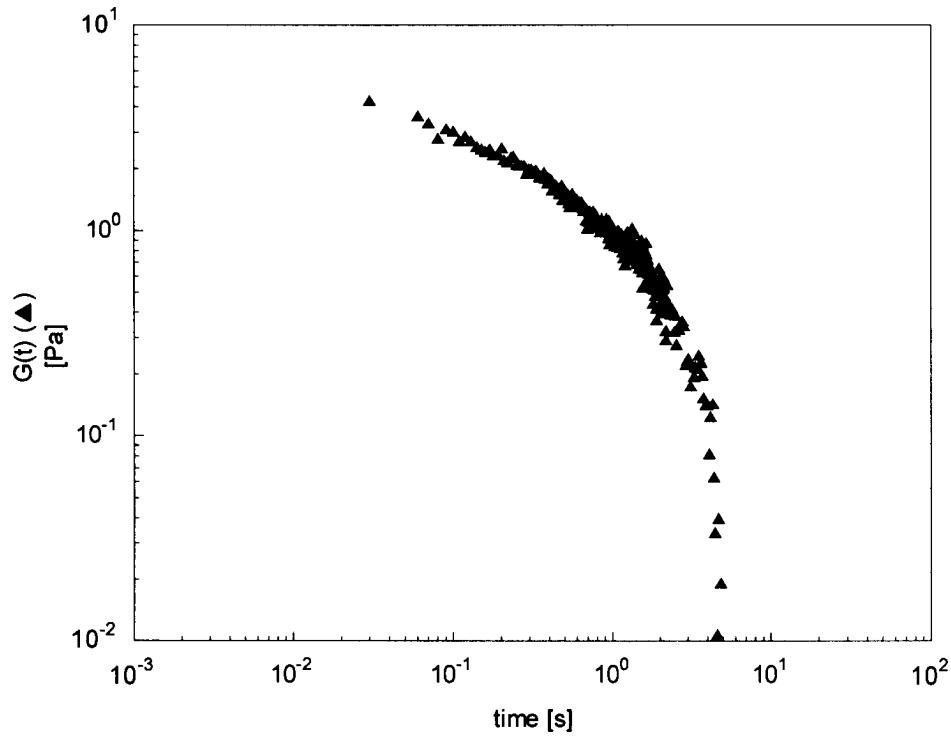

Figure F.3 Normal relaxation time test for a 0.5% xanthan gum solution with 1000 ppm SDS concentration.

Appendix G: Permission for the reproduced figures

RE: Permission
Raj P. Chhabra
Mon, Feb 25, 2008 at 11:31 PM
To: Shahram Amirnia

Permission is hereby granted to reproduce material from my books for scholarly, non-commercial use.
Good luck...RPC

PS: I would be grateful if you would please send me a copy of your thesis once it has been accepted.
Raj P Chhabra, Professor
Department of Chemical Engineering
Indian Institute of Technology, Kanpur, India

From: Shahram Amirnia
Sent: Monday, February 25, 2008 12:22 PM
To: Raj P Chhabra
Subject: Permission

Dear Professor Chhabra,
My name is Shahram Amirnia and I am a master's student in Chemical & Biochemical Engineering at the University of Western Ontario.
If you remember, I was one of your students in the course "Mechanics of non-Newtonian Fluids" that you offered in our department last summer (2007).
I am writing my thesis now which is about bubbles motion in xanthan gum aqueous solutions, and your books are as the main and the best references in all parts of my thesis.
I need your permission to be able to use some of the figures and tables in the textbook for the course that you offered at western (*Non-Newtonian flow in the process industries,* 1999) as well as your other books which are listed below.
I will enclose this e-mail along with your reply to my thesis to address as the permission from you for every part that I may cite from your books in my thesis.

- *Bubbles, Drops and Particles in Non-Newtonian Fluids* (1993, 2007).
- *Transport Processes in Bubbles, Drops, and Particles* (1992, 2002).

Best regards,
Shahram Amirnia

Appendix H: The log-sheet used for the bubble rise velocity measurement notes at work (in the lab).

Solution Concentration: Position of Camera:
Date: Focus Length: Temp:

Bubble Vol. (µl))	Travel Time (sec)	Bubble Vol. (µl)	Travel Time (sec)	Bubble Vol. (µl)	Travel Time (sec)	Bubble Vol. (µl)	Travel Time (sec)
1000		150		50		8	
1000		150		50		8	
1000		150		50		8	
800		120		40		6	
800		120		40		6	
800		120		40		6	
600		100		30		4	
600		100		30		4	
600		100		30		4	
400		85		20		3	
400		85		20		3	
400		85		20		3	
300		70		15		2	
300		70		15		2	
300		70		15		2	
200		60		10		1	
200		60		10		1	
200		60		10		1	